Well, Actuate(ly)...

Parametric Multi-Material 3D Printed Soft Robotics

A research portfolio submitted in partial fulfilment of the requirements for the degree of Master of Design Innovation.

Patrick Coulson

Supervised by Tim Miller

Victoria University of Wellington

School of Design

2020

Abstract

In recent years, soft robotics has gained wide interest in the research field and has also garnered some commercial success. This is because soft robots are comprised of soft materials that have inherent compliance which lends them to a wide variety of applications that are not suited to traditional hard-bodied robots.

Soft robots are generally created using a casting process, which comes with limitations to the geometry due to the removal of the cast body from the mould. This research seeks to enhance the capabilities of soft robotic limbs using multi-material Polyjet printing – a recently developed additive manufacturing technology – which allows for geometric freedom and variable materials within a singular soft 3D print which is not feasible using other fabrication methods.

This research draws inspiration from natural mechanisms such as muscular hydrostats, to enable the exploration of singular channel soft robots that exhibit bending, twisting, elongation, and expansion all in one 3D print. The geometric freedom and variable materiality of the Stratasys J750 produce actuation results for each motion that cannot be easily replicated using traditional fabrication techniques. The printable materials of the Stratasys J750 were found to have tendencies to tear upon inflation, however, a large array of prints with complex geometry were able to successfully actuate despite this. In some areas, results outperformed actuators made using other fabrication techniques, as was particularly evident in the twisting actuators. Through fine-tuned parametric control with equation driven modelling, this portfolio presents a method for soft robotic design and construction that can produce a limb with multiple motions and up to 5 axes of movement that can be tailored to specific pre-defined applications.

Acknowledgements

Table of Contents

INTRODUCTION

Soft robotics is a research field which has expanded rapidly over the last two decades, which utilises soft materials to manipulate irregularly shaped objects. Where conventional robotics are excellent for interacting with regular environments and defined geometries, soft robots thrive in the ability to adapt to their environment through their geometry and actuation method without reliance on digital sensors (Rus & Tolley, 2015). This gives them a wide range of possible applications that rely on compliance with irregular objects and environments. Many researchers have shown the dexterity of soft robots for gripping various organic objects, assistive stroke rehabilitation, and locomotion of unstructured terrain (Rus & Tolley, 2015). To further the wide range of potential applications for soft robots, research groups focus on optimising the motion of the actuators, and to increase the catalogue of possible motions.

Typically these robots are moulded and cast using silicone rubber. This research investigates the possibilities of using multi-material Polyjet 3D printing as an alternative fabrication method for soft robotic systems.

3D printing in soft robots has recently proven to introduce fine control over the motion of the actuator (Bartlett et al., 2015; Peele et al., 2015; Schaffner et al., 2018) which is difficult to replicate with a casting process. This fabrication technique is very new, and because of this, the current research only covers a small amount of what could be possible (Gul et al., 2018, p.258). Multi-material 3D printing offers new possibilities for programmable articulation in soft robots as it gives greater control over geometry and materiality than other fabrication processes.

This research encompasses a wide range of experiments that are all pneumatically actuated through one channel, all capable of vastly different motion. Through a number of iterations, this research demonstrates novel actuators capable of high-performance motion which have not been widely researched across the field of soft robots.

At a crucial stage in the research, this project was significantly impacted by Covid-19. This is mentioned in further detail in the limitations section of the discussion chapter.

Portfolio overview

Methodology
This chapter details the aims and objectives of this portfolio and the strategies used to achieve them.

Literature Review
This chapter gives context to the portfolio and assesses the gap in the literature that this research aims to fill. A history of soft robots, soft robots and 3D printing, and sequencing of motion in soft robots are all reviewed.

Biomimicry
Biomimicry has been used to ideate in the design stage of this portfolio. This chapter covers the relevance of adhesion and muscular structure in this portfolio.

Experimentation
The experimentation phase shows a wide range of Polyjet printed soft robots and how software and biomimicry have been used to inform the design.

Final Prints
This showcases the set of demonstrators with the most success as an output of the experimentation phase of the research.

Discussion
This chapter evaluates the success of using multi-material printing for soft robots, as well as discussing the limitations and possibilities for future research.

METHODOLOGY

Research Question

How can multi-material 3D printing be used to fabricate singular channel pneumatically actuated soft robots capable of complex actuation for advanced applications?

Aims & Objectives

1. *To investigate the nature and complexity of actuation currently achievable in soft robotic systems.*

   a. Analyse and critically assess the actuation achievable by soft robotic systems across the literature.
   b. Explore and identify biological precedents that present knowledge in variable materiality and geometry of movement, as well as any other areas that are determined as having the potential to improve the performance of soft robots.

2. *To establish and develop techniques for multi-material 3D printing as a method of fabrication for soft robots.*

   a. Explore and evolve a range of soft robotic concepts.
   b. Conduct a series of experiments exploring the opportunities and limitations of multi-material 3D printed soft robots.
   c. Evaluate and develop multi-material 3D printed soft robots to achieve complex actuation for determined applications.

This portfolio is structured and written with a research through design approach as defined by Frayling (1994, p. 5). Design research can be separated into three categories; research about design, research through design, and research for design (Frankel & Racine, 2010; Frayling, 1994; Hanington & Martin, 2012; Milton & Rodgers, 2013). Research through design follows a similar process to a conventional design process, however, research through design can be distinguished primarily through documentation; design experimentation along with reflection and contextualisation within the field are all written about in thorough detail (Milton & Rodgers, 2013) where typically the only evidence of design through process is in a final object produced (Frayling, 1994). This portfolio largely follows an iterative process of the creation of physical prototypes utilising a research through design approach. As described by Hanington & Martin (2012), research through design encompasses a process which begins with secondary research to contextualise the study as outlined by *Aim 1*. The past and present landscapes of soft robotic research have been assessed to gain an understanding of universal concepts and principles in soft robotics that can be applied to this research. Literature and precedent review are key research methods for determining the possible areas of influence or potential for the advancement of soft robotics through the utilisation of the geometric freedom and variable materiality through multi-material printing on the Stratasys J750. This background research is essential in focussing the scope of the project and obtaining knowledge which is then drawn upon during the primary research phase of the portfolio. Biological mechanisms have also been evaluated to gather knowledge about movement across natural structures, with the hope that this knowledge can be transferred across to inform geometry and variable materiality for soft robotic concepts. The second stage of this research, outlined by *Aim 2*, moves into the primary research of this portfolio. Primary research has been carried out to develop soft robotic concepts capable of a range of movements. This has been achieved through the following workflow:
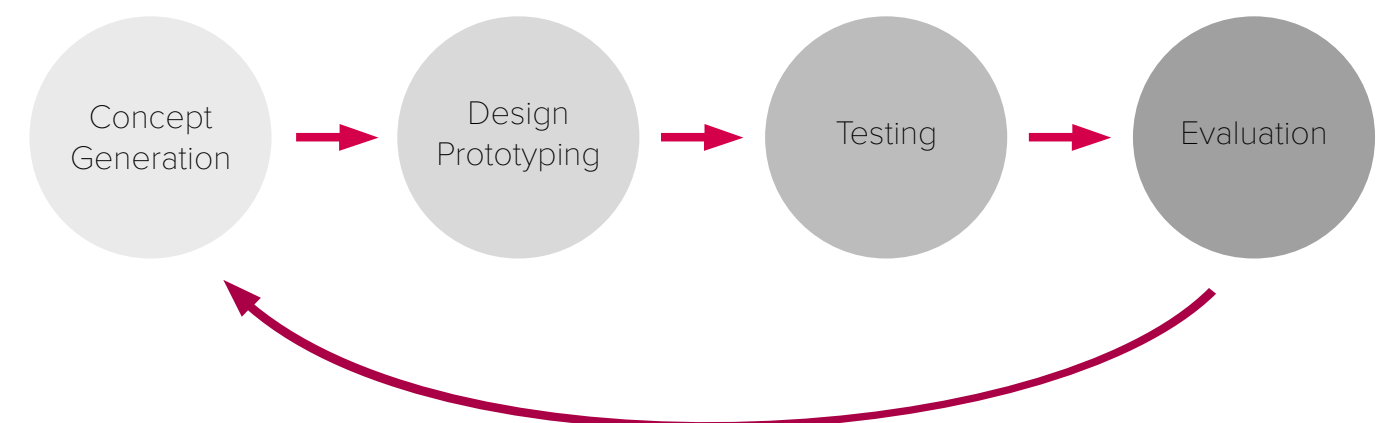

Figure 1. Workflow diagram.

This workflow has been created to explore the possibilities of soft robots that utilise the geometric freedom and variable materiality of printing on the Stratasys J750 in an efficient and deeply explorative manner as it prioritises a large number of iterations to be produced. Through the repetition of this workflow, concepts can easily be developed through the experimentation and evaluative research phases as these methods generate both comprehensive qualitative and quantitative data. ***Concept Generation*** is carried out through sketching and 3D modelling to produce soft robotic concepts that explore a variety of movements. Parametric modelling methods are employed to streamline an iterative design process where changes in geometry and materiality can easily be refined through fine-tuned parameter control. By employing these methods, improved control over geometry and materiality is obtained, and the iterative process is accelerated to produce a high quantity of iterations. ***Design***

Prototyping is carried out through fabrication using the Stratasys J750 3D printer to materialise the concepts into physical forms. A small amount of post-processing of the prints is required before the experimentation phase. ***Experimentation*** is used to gather quantitative data from the prototypes to obtain information about their success in achieving their respective motions. The experimentation covers the study of pressure, geometry, and variable materiality as functions of the soft robots' actuation. ***Evaluative Research*** (Hanington & Martin, 2012) is used to determine the points of success and failure in the prototypes, and what can be changed in future iterations. A set of soft robots capable of different motions that effectively exhibit the advantages of using the Stratasys J750 as a fabrication method are then combined to complete objective ***2c***. This final complex soft robot is a demonstrator for the precision, optimisation, and range of motions that can be printed using multi-material Polyjet 3D printing.

LITERATURE REVIEW

Introduction

When we think 'robot' we probably think of an autonomous steel machine with intricate componentry that operates using sensors or predefined actions through motors - a machine that offers movement at higher speeds and higher accuracies than in their biological counterparts. This idea has been challenged in recent years as a field of robotics labelled 'soft robotics' has surfaced. The field encompasses the use of soft or extensible bodies with inherent compliance (Trivedi et al., 2008) which are used to traverse or manipulate their surrounding environment (Rus & Tolley, 2015). Unlike hard-bodied robots, soft robots move in a way that seems organic, which is achieved through their adaptation and compliance. Soft robots offer certain advantages over conventional hard-bodied robots, and in turn are better suited to specific applications (Trivedi et al., 2008).

History

Soft robotic applications can be split into three main categories: locomotion, biomedicine, and gripping.

Locomotion has been studied in many different scenarios, from navigating under small gaps to swimming. A paper published in PNAS demonstrating a multi-gait soft robot capable of crawling through a small gap (Shepherd et al., 2011) is one of the most widely known soft robotics papers. The soft robot was cast using a silicone elastomer and it contained five separate actuation channels. The authors were able to achieve locomotion of their robot by sequencing the actuation of each channel to create a gait similar to crawling. They proved the dexterity of the finely controlled soft robot by optimising its gait to navigate under a glass sheet. George Whitesides, a prominent figure in the soft robotic field, believes that this technology could be utilised to navigate through hazardous or inhabitable terrain such as nuclear disaster sites (Whitesides, 2016) as a significantly cheaper and easier to manufacture alternative to conventional hard-bodied reconnaissance robots. The design of the robot shown by Shepherd et al. (2011) has since been expanded upon by other researchers. A notable example is Tolley et al. (2014) who were able to scale up the design and bring the pneumatic system on board so that it would be completely untethered. This paper is significant as it shows that scaling a pneumatic actuator up will affect either the material density of the robot or the pneumatic input pressure in order to achieve the same level of movement as its smaller counterpart. This paper also details the moulding and casting process used to fabricate their robot. Multiple materials and fabrication processes were required for the creation of the mould.

The mould was assembled from multiple sheets of both laser cut and water jet cut materials, the rubber composite used for the main body was degassed, and it was then poured into the mould. In contrast to the locomotion achieved by both Shepherd et al. (2011) and Tolley et al. (2014), Marchese, Onal, & Rus (2014) demonstrated a soft robotic fish capable of swimming and performing rapid escape manoeuvres. This robot included an onboard gas CO_2 gas cylinder for actuation, meaning that, like the soft robot created by Tolley et al. (2014), the soft robot could move unconstrained by any tether. The robot actuated through internal inflation chambers on either side of the fish, which allowed it to bend in both directions and propel the fish. Although the swimming gait was determined to be suboptimal (p.82), this research demonstrates the possibilities of soft robotic locomotion in a vastly different environment to what had been previously researched.

Many research groups have been studying the possibility of using soft robots for biomedicine. This is a field of significant interest for soft robots because their compliance allows for interaction with human tissue without damage (Cianchetti et al., 2018). Although soft robotic systems have been developed for the assistance of a range of body parts, hand rehabilitation has attracted the most attention (Cianchetti et al., 2018, p. 147). Yap, Jeong Hoon Lim, Nasrallah, Goh, & Yeow (2015) show a rehabilitation glove comprised of cast silicone elastomer soft robotic actuators with localised bending. The bending is located over the knuckles of the fingers which, when pressurised, assist in the bending of the fingers. The localisation of the bending was achieved by having bellows in the chamber geometry only in the regions

Soft robotics and 3D printing

where bending was required. With this, Yap et al. (2015) were able to generate a force output of 3.59N for gripping. Polygerinos, Wang, Galloway, Wood, & Walsh (2015) were able to achieve an output force of approximately 8N for a similar rehabilitative glove, however, the method for localising the bending around the knuckles was less precise than that demonstrated by Yap et al. (2015). Outside of hand rehabilitation, Ranzani et al. (2015) were able to create a bioinspired manipulator for minimally invasive surgery which was able to manoeuvre through the use of segments along the robot which each generated its own motion. This was done in order to navigate through the human abdomen with precision. A braided sheath with bellows geometry was fitted around the system in order to constrain it from excessive radial expansion (Cianchetti et al., 2013). This paper also identified that scaling soft robots is a big issue for biomedical applications as it often requires a radical change in the fabrication process as well as redimensioning of the geometry.

The most documented and widely researched application for soft robots revolves around gripping. Soft robotic grippers are used to pick up irregularly shaped or organic objects by having actuators conform around the surface of the object. Early examples show simple bending actuation of grippers to pick up delicate objects such as eggs demonstrated by Ilievski et al. (2011). This research helped to pave the way for future soft robotic research as it comprehensively demonstrated how the distribution of material and changing geometry altered the performance of the actuators and implemented these findings into a versatile soft robotic gripper with a textured surface which increased the grip performance. This research

quickly developed into soft robots capable of bending in 3 dimensions rather by increasing the number of pneumatic inputs and creating separate controllable regions of inflation to grasp objects with delicate features (Martinez et al., 2013; Ranzani et al., 2015). Martinez et al. (2013) also used this technique to demonstrate how 3-dimensional movement could be used for biomedical applications with fine-tuned, precise navigation. As demonstrated by Galloway et al. (2016), gripping of delicate features can extend to deep-sea reef sampling, as shown by their soft gripper. To be able to use hard-bodied robots for deep-sea sampling, sophisticated force feedback is required to minimize damage when grabbing (Galloway et al., 2016) - so the compliance of soft robots is an ideal replacement. In order to minimise damage, tests were done to assess the pressure distribution of the soft robot across the surface that they were gripping. Galloway et al. (2016) determined that adding a layer of memory foam to the gripping surface of the soft robot created a more even pressure distribution across the surface (p. 30), which would, in turn, lower the risk of damaging a reef sample.

Soft Robotics Inc has commercialised soft robotic grippers for packaging applications (MGrip, n.d.). These soft robots work as end effectors for a hard robot. The hard-bodied robot is used to position the robot over the object is trying to grab, and the soft robotic end effectors grab the object and put it down.

In the last five years, the use of 3D printing technologies has become increasingly more prominent for the fabrication of soft robots. 3D printing offers advantages over a moulding and casting process in the accuracy and complexity of the output actuation (Drotman et al., 2017, p.5532; Hong Kai Yap et al., 2016, p. 145), however, each 3D printing process comes with its own advantages and limitations.

As outlined by Ngo et al. (2018), there are many different methods for 3D printing. One of the most inexpensive and accessible 3D printing methods, Fusion Deposition Modelling, extrudes a heated layer of filament onto a print bed which is then built up layer by layer on top of itself. This method is good for prototyping, however, it is limited by its accuracy and anisotropic properties (Ngo et al., 2018). This method was demonstrated to have capabilities in the soft robotic field by Yap et al., (2016), which used a commercially available filament to fabricate a dual-channel actuator capable of bi-directional bending. The filament used exhibited repeatable actuation; however, high pressure was needed for actuation as the material had a much lower elasticity than elastomers commonly used for soft robotic fabrication with a moulding and casting process.

Paste printing follows a very similar process to Fusion Deposition Modelling but without heating the material before extrusion. Paste printed materials often harden after extrusion for the next print layer to be extruded on top of it to build up a structure. Yirmibesoglu et al. (2018) developed a silicone elastomer paste printer for soft robots to overcome the limitations of commercially available 3D printer materials. They were able to produce soft

robots that had a similar performance to cast silicone soft robots. However, the extrusion process has inherent limitations with the complexity of the soft robot, as it is not suited to overhanging geometries.

Stereolithography was the first developed 3D printing technology and it can achieve a much higher print resolution than with Fusion Deposition Modelling. Stereolithography works by curing resin from a bath with an Ultra-Violet laser layer by layer as the object is being drawn out of the bath to create 3-dimensional forms (Ngo et al., 2018). This method was used for soft robotics by Peele et al. (2015) in which detailed air chambers allowed for complex movements. Although Martinez et al. (2013) achieved similar multi-chamber actuation by casting silicone rubber, the tentacle could not manoeuvre at the same level of precision because of the inherent geometrical restrictions on the chamber complexity in the moulding and casting process which can impact the actuation accuracy. The main drawbacks of this printing method include its high cost and long print times (Ngo et al., 2018). This is why Peele et al. (2015) were only able to create small scale soft robots. Peele et al. (2015) also found that the photopolymerisable resin used was prone to tearing which created air leaks.

Digital Light Projector printing is similar to Stereolithography where a resin is cured from a bath when exposed to Ultra-Violet light. However, a digital projector is used to flash an image across the entire layer rather than using a laser that needs to be directed at a specific region of a layer to cure it (SLA vs. DLP, n.d.). This allows for faster build times than Stereolithography and no disruption

to build times with higher density models. Ge et al. (2018) used Digital Light Projector printing to fabricate a soft robotic gripper at a high resolution compared to other examples of 3D printed soft robots. This allowed for a very small gripper to be fabricated without compromising its functionality. The material used for this gripper has a 170% - 220% elongation at break (Ge et al., 2018) which is poor compared to the 900% elongation at break of the silicone elastomers used with cast soft robots (EcoflexTM 00-30 Product Information, n.d.). Patel et al. (2017) developed a photopolymerisable elastomer for Digital Light Projector printing which exhibits a 1100% elongation at break, although this is not commercially available.

Inkjet printing works by depositing drops of Ultra-Violet curable resin onto a print bed and curing it once a full layer has been deposited. The drops of resin are deposited from a nozzle into their specific locations unlike Stereolithography and Digital Light Projection which draws material from a bath (Barclift & Williams, 2012). As a result, some Inkjet printers are capable of depositing multiple materials of varying flexibility and softness into the same print. Bartlett et al. (2015) utilise this technology to create a soft robot capable of jumping using on-board combustion. Complex geometry was able to be created using multiple printed materials to maximise performance. More recently, this technology is starting to be used for air pressurised soft robots. Zhu et al. (2019) illustrated how an Inkjet fabrication process significantly decreases the fabrication time and streamlines the process (p. 509). This is then proven through the creation of a soft robotic gripper using Inkjet printing that is used as an end effector on a robotic arm

to grasp objects (Zhu et al., 2019). Soft robots have also been created using this technology exploring embedded Shape Memory Polymers (Zhang et al., 2019) and resistive sensors (Shih et al., 2019). Fabrication of soft robots through Inkjet printing allows for geometric freedom and multi-material capabilities, however, this is yet to be thoroughly explored. The soft robot designs using this technology primarily still present designs similar to those which were created to suit a moulding and casting process (Shih et al., 2019; Zhang et al., 2019; Zhu et al., 2019). This is no longer necessary as the main advantage of Inkjet printing is that it allows for vast freedom of design and is not at all restricted by the same limitations as a casting process. Schaffner et al. (2018) present multi-material 3D printed soft robots that exhibit geometry dissimilar to that used in a casting process by using silicone inks with tunable elasticity. The soft robots presented exhibit individual examples of contraction, bending, grabbing, and twisting motions by creating an anisotropic strain achieved through sections of variable material stiffness (p.2).

Sequencing of motion in soft robotics

Sequencing of motion refers to the configuration of an array of different motions within a single soft body.

The sequencing of motion in soft robotics is very commonly used to create locomotion. Tolley et al. (2014) demonstrated how the sequencing of different segments of a soft robot can be used to achieve different gaits. Both an undulating and an ambulating gait are demonstrated in this paper. This was achieved by the individual control of a pneumatic channel for each segment. This technique was demonstrated as early as Shepherd et al. (2011), however, Tolley et al. (2014) were able to further expand on the variation in gait patterns that were possible through the individual control of each segment of inflation.

Sequencing of motion is less commonly used in soft robotics for grippers. Peele et al. (2015) show a Stereolithography printed soft tentacle with four controllable pneumatic channels that allow for 3-dimensional motion. Peele et al. (2015) utilise 3D printing in order to achieve much finer control over their soft robot than previous examples of 3-dimensional motion in soft robotics.

Sequencing of a range of motions (e.g. twisting, bending, and extension in one soft body) is not widely documented, however, the examples of this are usually directed toward applications in biomedicine. Ranzani et al. (2015) utilise sequencing of bending and elongation as well as stiffening and softening for minimally invasive surgery. Sequencing was utilised for the specified purpose of grabbing an organ, and the individual motions were sequenced in accordance with this. Polygerinos et al. (2015) show bending, twisting, and extension

motions for a stroke rehabilitation glove. These motions are sequenced by localising the strain restricting layer which in this case is a fibre, along an otherwise uniform actuator to comply with the different movements that occur when grasping with fingers.

The example of sequencing with the most extensive research and experimentation was carried out by Connolly et al. (2015) where the impact of fibre placement in soft robots was examined to create a soft robot that exhibited localised bending, extension, expansion, and twisting to perform a defined task. This robot was used as a proof of concept for the principles determined to create each motion with fibre reinforcement. It exhibited a sequence of extension and expansion to achieve peristaltic locomotion inside a tube, and further exhibited bending and twisting to perform its specified task. This research was expanded on to focus on matching the path of actuation to a pre-defined trajectory using mathematical models (Connolly et al., 2017). This research demonstrates the importance of the configuration of the strain restricting regions in soft robotics, and it presents a streamlined method for sequencing different motions. However, it is limited in the performance of the actuators as the change in the type of motion is achieved purely through the placement of the strain restricting regions and not by altering the actuator geometry which could further enhance the performance of each segment. This is particularly evident in the extending and twisting motions.

Synthesis of the literature

The primary advantages that soft robots have over hard-bodied robots are:

Compliance: Soft robots have inherent compliance because of the soft materials they are made from, and this lends them to applications where interaction with irregular or organic environments and objects is crucial. Hard-bodied robots would need a number of assembled hard components and carefully considered geometry to pick up a delicate object such as an egg. A pneumatically actuated soft robot can achieve this with simple geometry and a singular pneumatic input (Ilievski et al., 2011, p.50).

Safety: Conventional robots and humans are typically in separate workspaces in an assembly line because the robots operate at high speeds and forces which can be very dangerous to humans (Krüger et al., 2009). Soft robots typically operate with considerably lower force outputs and are constructed with soft material which lends itself to working alongside humans in a safe environment.

Minimal assembly needed: Soft robots are typically fabricated with a moulding and casting process meaning that they are operational once the material has cured.

The process for creating a soft robot varies greatly from that of a hard robot. Hard-bodied robots consist of a vast number of hard components which are carefully assembled along with sensors, servo motors, and various other electronic components which need to be configured to make the robot move in the desired way. Soft robots rely on their geometry and materiality to determine the way in which they move. Soft robots are conventionally

fabricated by pouring a silicone elastomer into a mould. Once the elastomer has set and the robot is taken out of the mould it is fully functional, and it needs only to be connected to an actuation system.

Soft robots are typically actuated in one of two ways; pneumatically or electrically (Trivedi et al., 2008). A pneumatic system works through the expansion or contraction of internal channels which force the robots' geometry to move in a designed way (*Figure 2*). The electrical alternative is through the use of electroactive polymers which contract when a certain voltage is passed through them. Using a pneumatic input is often preferable as these are commonplace (i.e. a bike pump) and are safer as there is no risk of electrocution.

Figure 2. Pneumatic inflation.

For pneumatically actuated soft robots, the geometry used for actuation can be separated into two categories; bellows-type and what can be described as 'boa-type' (Galloway et al., 2016). A boa-type soft robot consists of a singular air channel and movement is achieved by using a strain restricting layer. The placement of this restricting layer will change the inflated form of the robot. A bellows-type soft robot has air chambers which, when inflated, apply a force on one another, aiding the expansion in a specified direction. These two types of actuators are most documented in bending actuators, as shown in *Figure 3*.

Although the type chosen will impact factors such as repeatability of actuation, required input air pressure, and output force of the soft robots' actuation, there are no definitive trends between the two types that can be found across the literature as the geometries are very case-specific.

Biomimicry

In design, inspiration is commonly taken from certain aspects of our natural world such as forms, behaviours, and mechanisms. The method of incorporating this technique into design research is commonly referred to as 'biomimicry' or 'biomimetics'. According to Benyus (1997), biomimicry can be implemented on three levels; mimicking of natural form, process, and systems. By analysing biological examples, new knowledge can be gained to aid and optimise designs throughout the design process. Schaffner et al. (2018) show a successful example of this in the field of soft robotics at a research level where multi-material robots were fabricated to mimic the motion created by an elephant's trunk. Festo has also successfully shown the possibilities of soft robotic biomimetic design at a commercial level with their Bionic Handling Assistant (Festo, 2012) and more recently their Bionic Soft Arm (Festo, 2019). Biomimicry, however, has no universal set of guidelines for implementation, therefore it must be used in a carefully considered way. Where design and engineering can be aided by referring to theory, biomimicry is case-specific and each project must employ biomimicry with a fresh
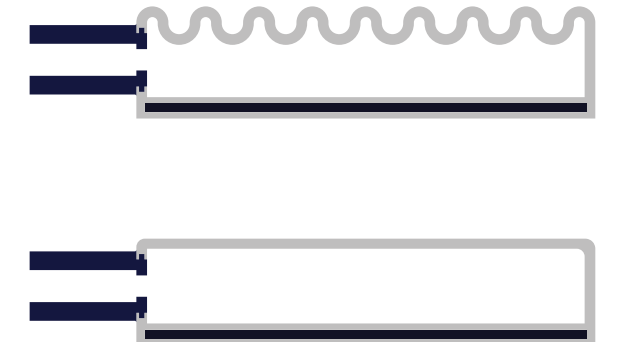

Figure 3. Bellows and boa-type actuators.

approach (Vincent et al., 2006).

For the purpose of this portfolio, biomimicry has been studied to analyse how materiality and geometry are utilised. To separate the areas of biology to determine their relevance to this portfolio, they have been categorised in accordance with the physical scale at which they function. At the smallest size, surface adhesion in nature is the way in which animals grip to surfaces. Next is muscular structure, which dictates how the muscles of an organism facilitate movement. Gait looks at the resultant movement that is generated through the organism's muscular structure. At the largest scale, locomotion is defined as how the movement of the organism can allow for travel from place to place.

Adhesion

For soft robots to interact with their surroundings, good grip strength can significantly increase their performance (Glick et al., 2018) which makes surface adhesion an area of significant interest for soft robotics. Surface adhesion also typically occurs at a
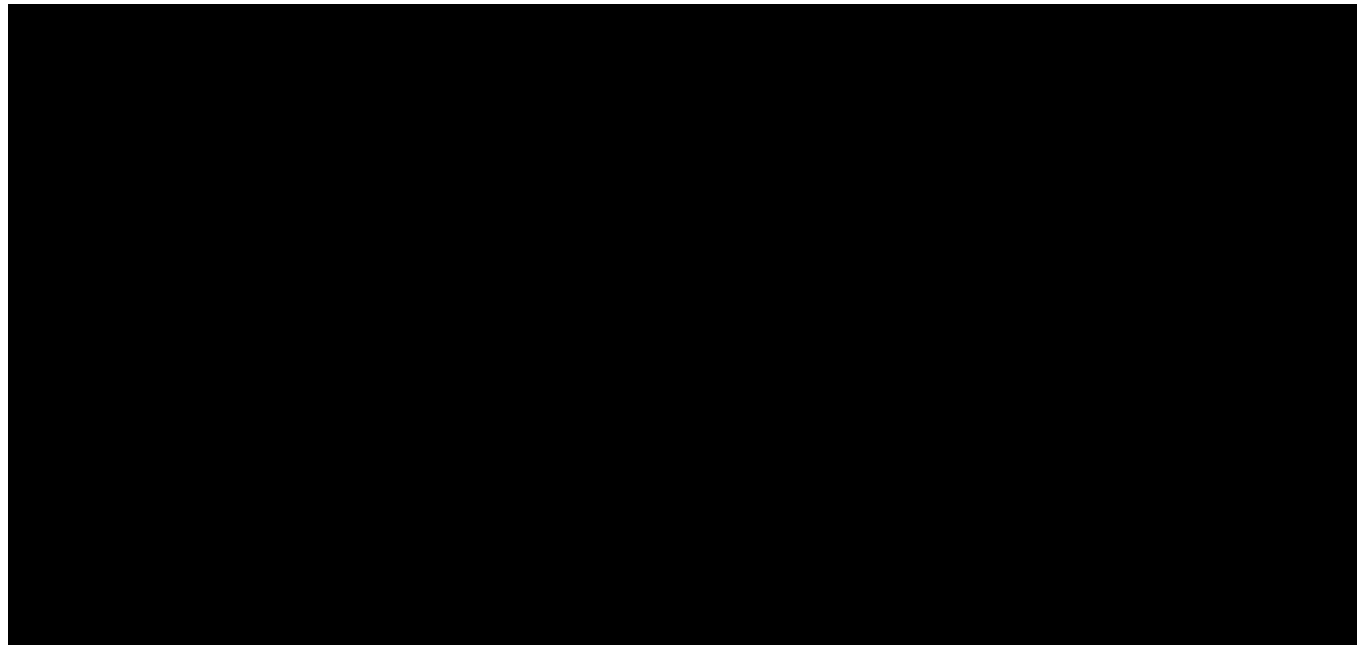
Figure 4. Description of different types and characteristics of main adhesive interactions: Adapted from Heepe & Gorb (2014).

scale where the resolution of the Stratasys J750 3D printer is capable of printing which makes it of particular interest when exploring the capabilities of this machine for the purpose of this portfolio.

Adhesion in nature is defined as an interaction between two surfaces in which one of the surfaces has a system to create attachment (Arzt et al., 2003; Gu et al., 2016). Adhesive forces can be split into four main categories (Gu et al., 2016); surface and field forces more commonly known as 'dry adhesion' (Autumn et al., 2002; Bhushan, 2009), material bridges or 'wet adhesion' (Federle et al., 2002; Hanna et al., 1991; Vogel et al., 2010), mechanical interlocking, and suction forces.

Dry adhesion often operates using van der Waals forces such as can be found in geckos (Autumn et al., 2002; Rizzo et al., 2006). Geckos have toepads comprised of 'setae' which are stalk-like geometries which split off repeatedly into nano-scale geometries. The microscopic size of these setae creates intermolecular forces in the interaction of atoms between them and the surfaces they touch. The adhesion force between a singular seta and

the adhesion surface is minuscule. However, there are approximately 14,400 setae per square millimetre on the toepads of the Tokay gecko - allowing it to support its body weight with ease (Autumn, 2006). Recently, synthetic replications of the dry adhesion of geckos have been successfully created (Glick et al., 2018; Li et al., 2019; Peressadko & Gorb, 2004). Glick et al. (2018) showed how this can be used in harmony with soft robotics, by fabricating a soft robotic gripper with adhesive pads which increase the robot's gripping performance.

Wet adhesion utilises the surface tension of a liquid to stick to surfaces through static friction (Federle et al., 2002) and/or viscous forces (Hanna et al., 1991). A common example of this can be found in the Torrent frog, which secretes mucus from in between spongey toepads to allow for adhesion even on wet surfaces (Hanna et al., 1991). This has also been reproduced synthetically. Vogel et al. (2010) take inspiration from the wet adhesion of the leaf beetle to create a capillarity based switchable adhesion system which can pick up and drop substrates.

Mechanical interlocking is the interaction

between solids to connect surfaces. A classic example of this can be found in Velcro (de Mestral, 1955) which was inspired by the hooks on burdock burrs which stuck to the clothes of de Mestral. Evidence for mechanical interlocking has been found in snakes in order to increase their grip when climbing trees (Hamidreza & Hu, 2012). The scales on the underside of the snake's belly lock onto imperfections in the tree's bark, creating security if the muscular grip of the snake is to slip.

Suction forces create adhesion through a pressure differential between the internal cavity of the suction cup and the surrounding environment (Gu et al., 2016). In nature, this can be found in octopuses (Kier & Smith, 2002) but suction cups have also been widely replicated synthetically for household and industrial applications.

Muscular structure

Muscular structure is a common source of biological inspiration for soft robots. A muscular hydrostat is a biological actuator primarily comprised of muscle tissue with no need for a supporting skeletal structure (Kier & Smith, 1985). Muscular hydrostats are used by animals to interact with or manipulate elements in their surrounding environment. Muscular hydrostats are a commonly referenced form of biomimicry found in the field of soft robotics (Peele et al., 2015; Schaffner et al., 2018). This is because muscular hydrostats, like soft robots, can conform to their surroundings using only soft material. They are able to extend, twist, and bend by shortening and extending muscle fibres in specified directions or configurations to achieve their desired movement. This is

reminiscent of the strain restriction in certain areas of soft robotic geometry which dictates the movement of the actuator. An important distinction between muscular hydrostats and pneumatically actuated soft robots is that muscular hydrostats maintain a constant volume during actuation, and soft robots do not.

EXPERIMENTATION

Introduction

In response to **Aim 2**, this chapter demonstrates a range of soft robotic concepts that utilise the Stratasys J750 3D printer to explore the opportunities and limitations that it presents. Adhesion testing was carried out to assess how Polyjet printed textures can enhance the capabilities of subsequent soft robotic concepts. They were first tested separately from the soft robotic prints to understand the success of the primary mechanisms of adhesion.

Biological inspiration, Software, Measurement, and Balloon Testing are all discussed prior to any pneumatically actuated soft robotic experiments performed on the Stratasys J750. This is used to detail the early design process; initial inspiration, CAD design, experimentation setup, testing fundamental concepts of actuation.

The soft robotic inflation tests use the prior information covered in this chapter to directly tackle **Aim 2**. This details the range of concepts that were tested, all presented in chronological order. These were tested with a small air pump with a maximum capacity of 10psi. A pressure sensor was used to relay data back to an Arduino, which displayed this data on a connected laptop.

The naming convention used to identify the prints is as follows:

1.01 – 1.14: Extension geometry actuators

2.01 – 2.10: Bending geometry actuators

3.01 – 3.17: Twisting geometry actuators

4.01 – 4.08: Expansion geometry actuators

5.01 – 5.07: Complex motion actuators

Stratasys J750

The Stratasys J750 is the printer that was used for the primary testing of this portfolio. The printer has a build size of 490 x 390 x 200mm and a horizontal build layer thickness of 14 microns. The materials that were used are AgilusClear and Vero. AgilusClear (Agilus) is the soft material resin loaded in the printer, and it has a minimum shore hardness SH of 30 (30SH). The Vero material resin came in four colour variations; cyan, yellow, magenta, and black – all with 95SH. These can be combined in different ratios to support a range of possible shore hardness, shown in *Figure 5*. This was fully utilised throughout the experimentation to explore a range of material shore hardness combinations.

The Stratasys J750 uses a support material, called SUP706, to build models with overhanging geometry. After printing, this needs to be removed. A chemical solution bath was used to remove the support material which could not be manually removed with tools. This solution consisted of 2% sodium hydroxide and 1% sodium metasilicate, and a pump which circulates the solution. The prints in this portfolio were kept in this bath for 2-4 hours, before being removed from the bath and rinsed off.

AgilusClear (Shore-A 30)

Shore-A 35

Shore-A 40

Shore-A 50

Shore-A 60

Shore-A 70

Shore-A 80

Shore-A 95

Vero (Shore-A 100)
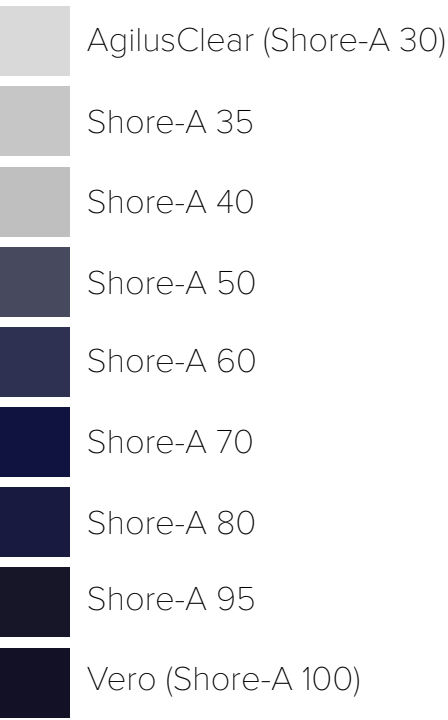
Figure 5. Stratasys J750 Shore A Hardness printable materials.

Adhesion testing

Goals
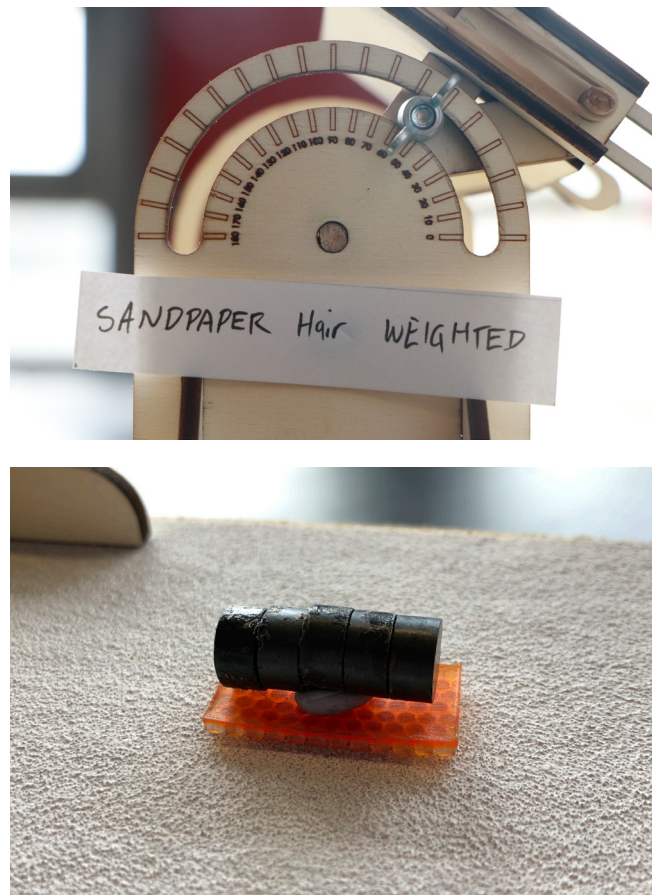
Figure 6. Adhesion testing setup.

A selection of natural adhesion mechanisms were mimicked and printed on the Stratasys J750. These included:

- Gecko toepads
- Frog toepads
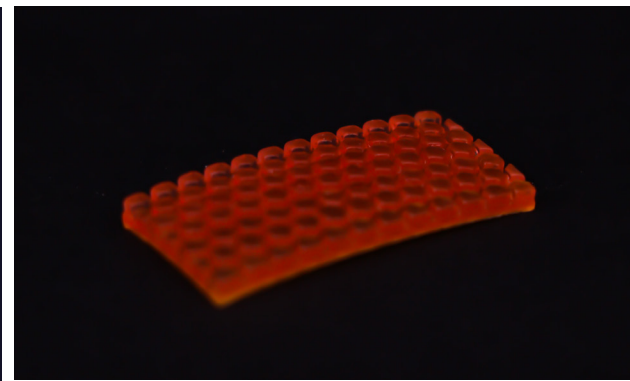- Adhesive hairs
- Suction cups
- Snake scales

These prints all focused on either dry adhesion, mechanical interlocking, or suction. Wet adhesion was not focused on because it would require an additional human intervention to implement the adhesive liquid. To test the effectiveness of these prints, a rig was assembled in which a material plate could be secured, and its angle changed. The materials that were tested were:

- MDF (smooth)
- Sandpaper (coarse)
- Felt (soft)

To test the angle of failure of each texture, the angle of the material plate was gradually increased from 0° until the texture fell off the material plate where the value was recorded. Each texture was also tested with a small weight added, to see if that would impact the performance of each texture. As a control, a smooth pad of the 30SH Agilus material was printed. Each pad was 30mm x 15mm in size.

Frog toepad (mechanical interlocking)
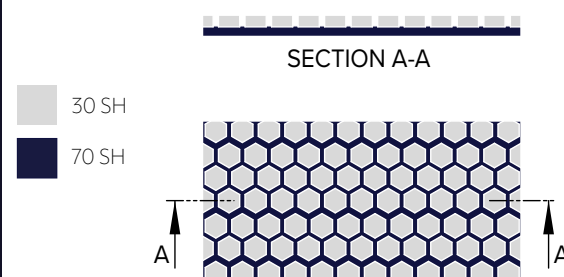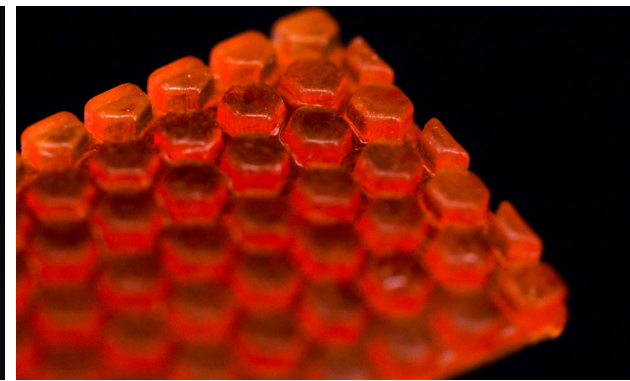
Aim: To replicate the success of frogs' toepads for surface adhesion.

SECTION A-A

30 SH
70 SH

A | | A

Results:

Sandpaper
MDF
Felt

Failure angle

Not weighted: 79° / 59° / 57°
Weighted: 60° / 52° / 49°
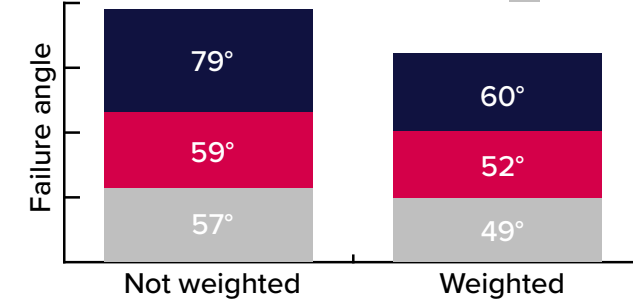
Figure 7a - 7d. Frog toepad images and results.

Snake scales (mechanical interlocking)
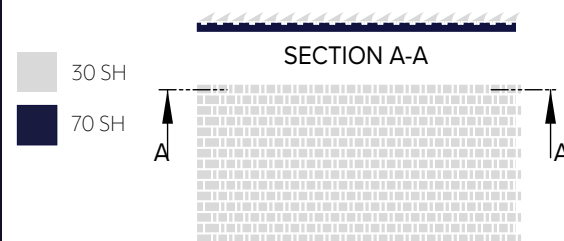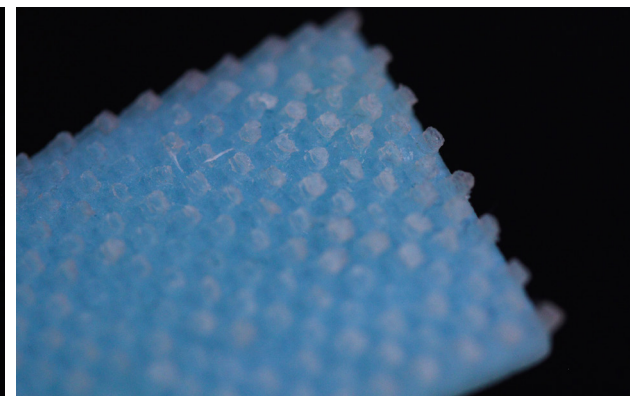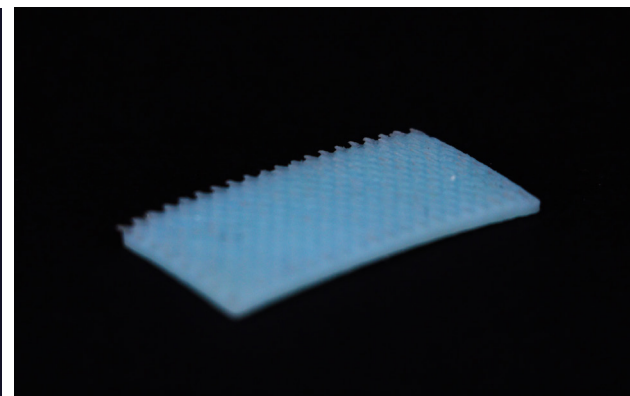
Aim: To replicate the success of snakes' scales for surface adhesion.

SECTION A-A

30 SH
70 SH

A | | A

Results:

Sandpaper
MDF
Felt

Failure angle

Not weighted: 79° / 55° / 180°
Weighted: 58° / 52° / 60°
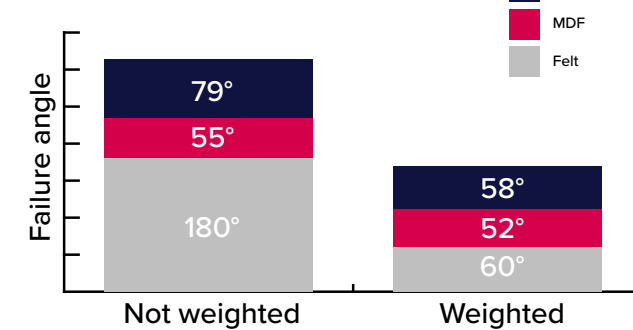
Figure 8a - 8d. Snakes scales images and results.

Adhesive hairs (mechanical interlocking)
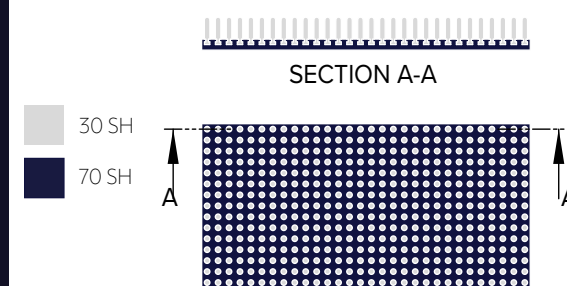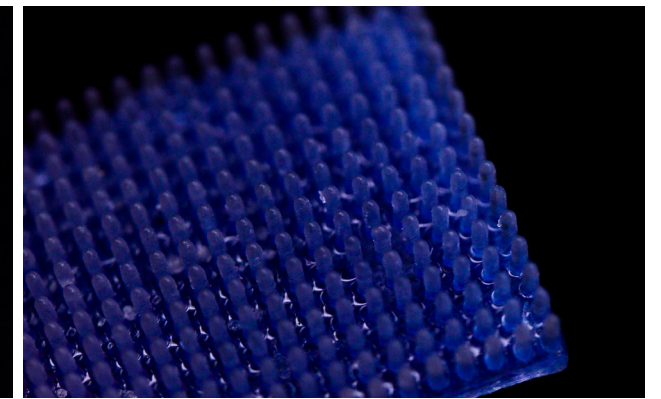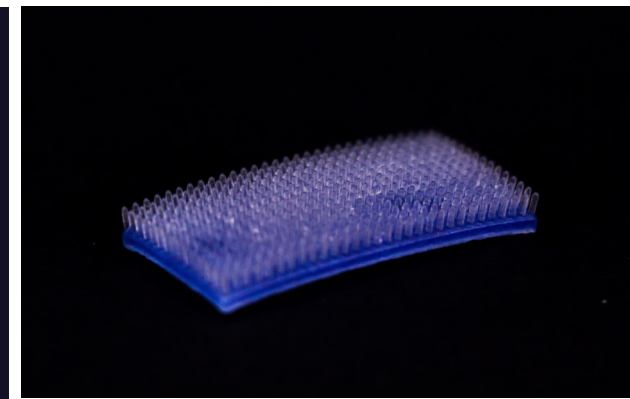
Aim: To create adhesive hairs for surface adhesion.

SECTION A-A

30 SH
70 SH

A | | A

Results:

Sandpaper
MDF
Felt

Failure angle

Not weighted: 79° / 55° / 180°
Weighted: 53° / 44° / 54°
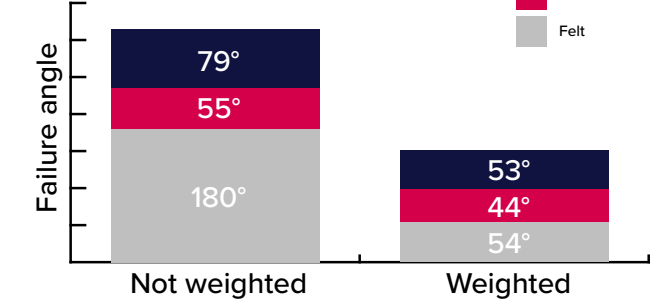
Figure 9a - 9d. Adhesive hairs images and results.

Gecko toepad (dry adhesion)
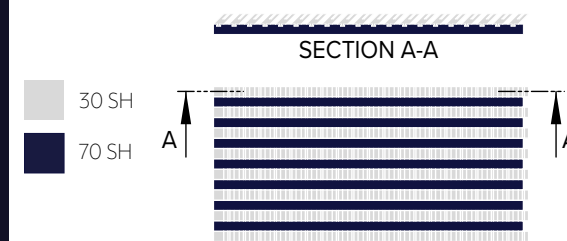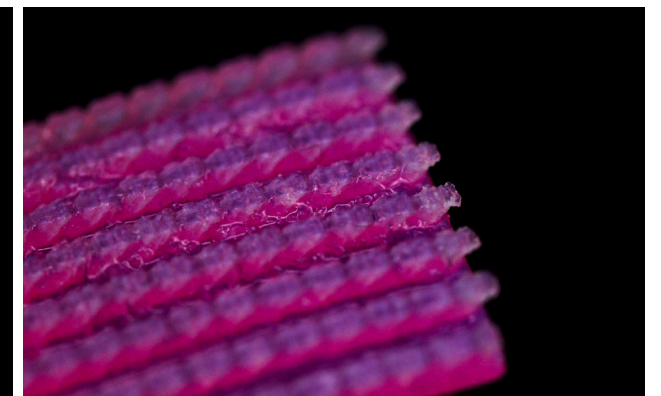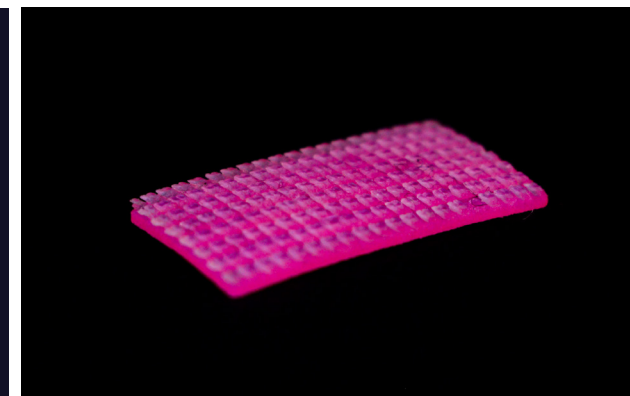
Aim: To replicate the success of geckos' toepads for surface adhesion.

SECTION A-A

30 SH
70 SH

A | | A

Results:

Sandpaper
MDF
Felt

Failure angle

Not weighted: 74° / 55° / 180°
Weighted: 55° / 52° / 68°
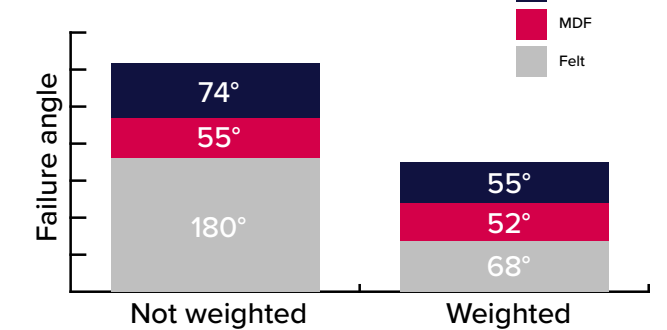
Figure 10a - 10d. Gecko toepad images and results.

Suction cups *(suction forces)*

SECTION A-A

30 SH

70 SH

A   A

Figure 11a – 11c. Suction cups images.
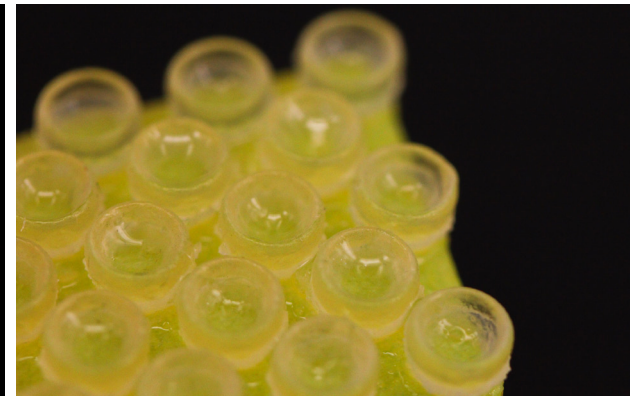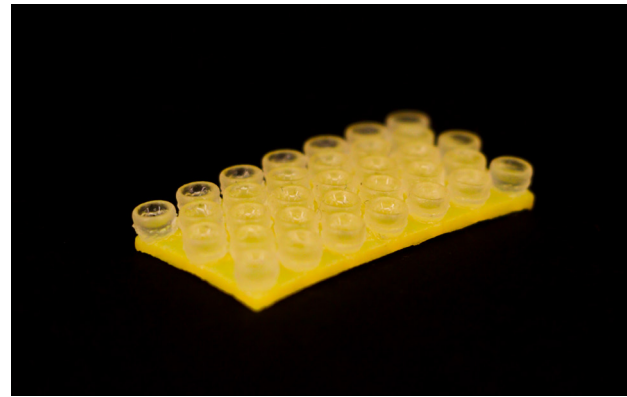
Aim: To replicate the success of octopuses' suction cups for surface adhesion.

Results: The suction cup was not tested using the same setup as the other prints as its adhesion was reliant on a localised pressure being applied to press it against a surface. The cups successfully allowed for the pad to be connected to surfaces, however, the surfaces needed to be very smooth for this to work.

Analysis

The maximum adhesion was observed on the felt material - the snake, gecko, and adhesive hair textures all remained attached to the felt when upside down. However, once weight was added, the failure angle reduced significantly for all tests. The control Agilus pad consistently performed the worst in all scenarios, validating the added performance of adhesive geometry. All of the adhesion geometries were printed as small as physically possible within the printable resolution of the Stratasys J750. Although the gecko toepad geometry could not be replicated at a scale where Van der Waal forces would act as the primary adhesive mechanism, the mechanical interlocking properties still provided an increase in adhesive performance.

Adhesion decreased significantly on the sandpaper and MDF. This is likely due to the successful adhesive pads relying on mechanical interlocking; if the surface texture was too smooth for interlocking, the adhesion mechanism functionality was diminished.

As mechanical interlocking was the method of adhesion that was most successful, this was replicated and reintroduced to assist with locomotion in subsequent soft robot concepts.

Biological inspiration

Muscular hydrostats were used as inspiration to inform the initial designs. Examples of extension, bending, and twisting were examined at a muscular level, and these were then adapted for pneumatic soft robots (*Figure 12*). These three motions were chosen as clear examples could be found throughout nature, and they were each distinctly different and would each require different geometries to successfully mimic the motion.
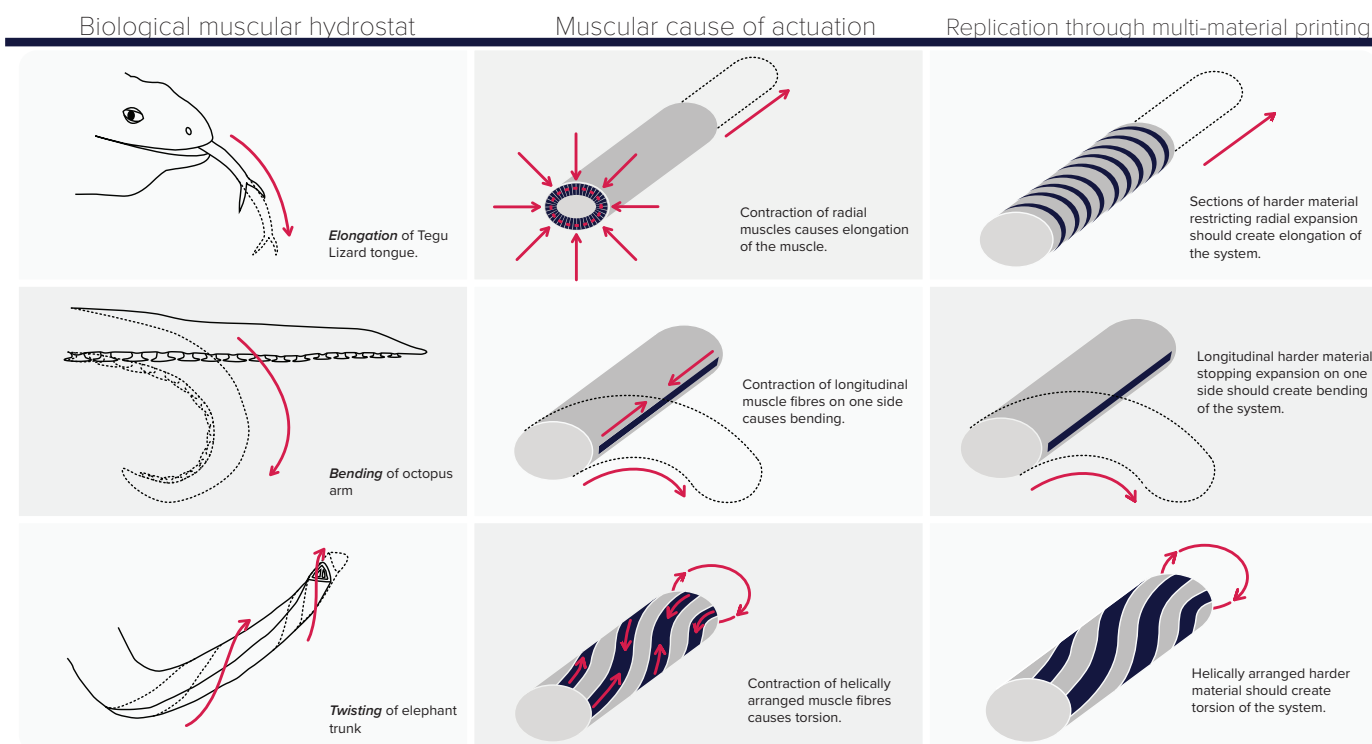
Biological muscular hydrostat	Muscular cause of actuation	Replication through multi-material printing

Elongation of Tegu Lizard tongue.

Contraction of radial muscles causes elongation of the muscle.

Sections of harder material restricting radial expansion should create elongation of the system.

Bending of octopus arm

Contraction of longitudinal muscle fibres on one side causes bending.

Longitudinal harder material stopping expansion on one side should create bending of the system.

Twisting of elephant trunk

Contraction of helically arranged muscle fibres causes torsion.

Helically arranged harder material should create torsion of the system.

Figure 12. Muscular hydrostats and method for printed replication.
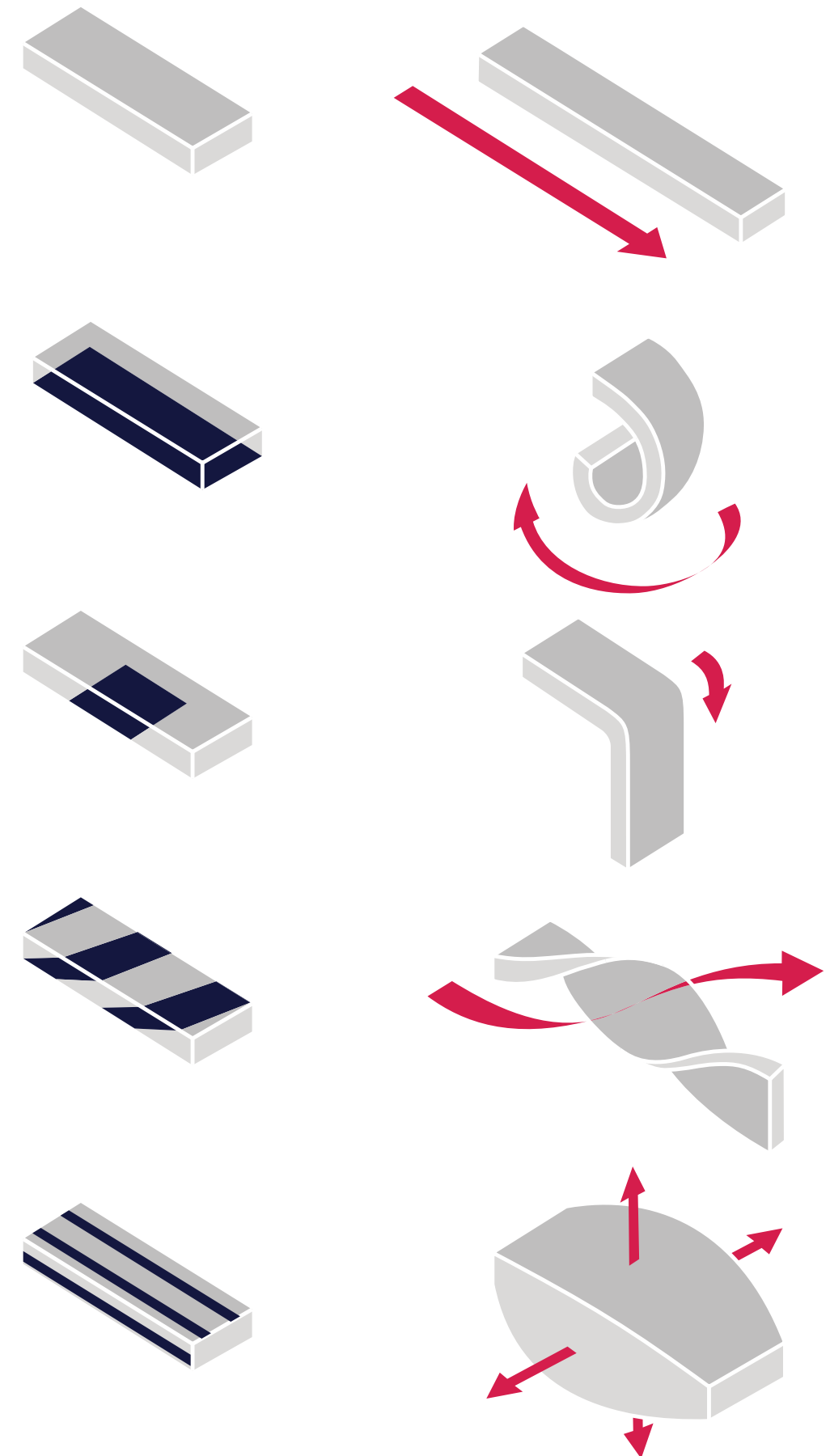
Figure 13. Effect of the configuration of strain restricting regions on soft actuators upon inflation.

Software

To achieve a blueprint for a robust soft robot that can be applied to a wide variety of scenarios, it was vital to create a system where the actuators can be easily altered to perform specific tasks. This has been tackled by using equation driven models in Solidworks that allow the model geometry to adapt when a parameter is changed. Global variables were assigned to the driving parameters, which other dimensions were referred to, which allowed these dimensions to vary in accordance with changes made to the global variables. This system was used to not only create model flexibility when designing for scenarios, but also to streamline the testing and iteration processes. As the experimentation in this research looked to find optimal performance in geometry and materiality, the equation driven models allowed for quick and easy iterations. For example, the helix angle of the twisting actuator was be given multiple values, and separate models were created for each value of helix angle which were 3D printed. The prints were then tested, compared, and the optimal helix angle was determined.

Every actuator was derived from a singular base geometry. A set of curves was defined to build the bellows off. These curves were then repeated in a pattern and rotated around a central axis to create the geometry. To achieve different motions from the actuator, alterations were made from this point to modify the output motion from the actuator. The extending motion geometry operates solely off the base geometry; however, modifications were made to the twisting and bending geometries to achieve the desired motion.

To create a bending motion, a radial asymmetry needed to be incorporated as informed by a

number of precedents across the literature (Ilievski et al., 2011; Martinez et al., 2013; Peele et al., 2015; Hong Kai Yap et al., 2016). This asymmetry could be achieved through geometry or materiality, both of which were tested. To incorporate a degree of twist into the bending motion, the chamber angle was changed so, although the chambers were still patterned along the same axis, they did not remain perpendicular to the axis.

To achieve a twisting motion, a helical element needed to be incorporated (Schaffner et al., 2018), once again, either through geometry or materiality. To explore a twisting motion through geometry, the base geometry was patterned radially rather than axially, and that profile was extruded with a twist angle implemented. As an extension of this model, when the twist angle was set to 0^0, an expansion motion could be achieved through actuation.

Equation driven models

To increase the control over the CAD models, a series of equations were derived. These rely on a set of global variables to drive them. For example:

In the twisting actuator, the twist was defined using the "sweep" feature in Solidworks. The "sweep" feature allows you to enter a value for the profile twist or "sweep angle" which is the total angle of twist over the predetermined length. To build this model, it was important that, if the length of the twisting actuator was changed, the pitch would remain the same. An equation needed to be used to drive the "sweep angle" such that this was always the case. The model's twist was driven by the global variable "helix angle" which describes

the angle of a helix as a straight line that runs tangentially to the helix from the central axis. Equations for the "pitch" and the "sweep angle" were used to allow the model to be driven by a change in value for the "helix angle".

$$\text{"pitch"} = \frac{2\pi r}{\tan(\text{"helix angle"})}$$

$$\text{"sweep angle"} = \frac{360 \times \text{"length"}}{\text{"pitch"}}$$

These equations allow for the length of the twist ("length") to be changed while the angle of the twist ("sweep angle" as defined in the Solidworks "sweep" feature control) remains the same. The "sweep angle" can also be altered through the "helix angle" global variable.

Equations were used to achieve similar results in the other actuators where dimensions and the number of bellows that were patterned had global variables assigned that could easily be changed for iterative and applications purposes.

Base geometry design and parameter control

The base geometry is derived from a series of bellows patterned along a central axis.
The driving parameters can be found in *Figure 14*.

It was important to avoid right angles or sharp corners in the internal geometry of the bellows, as this can create areas of weakness which are prone to tearing.
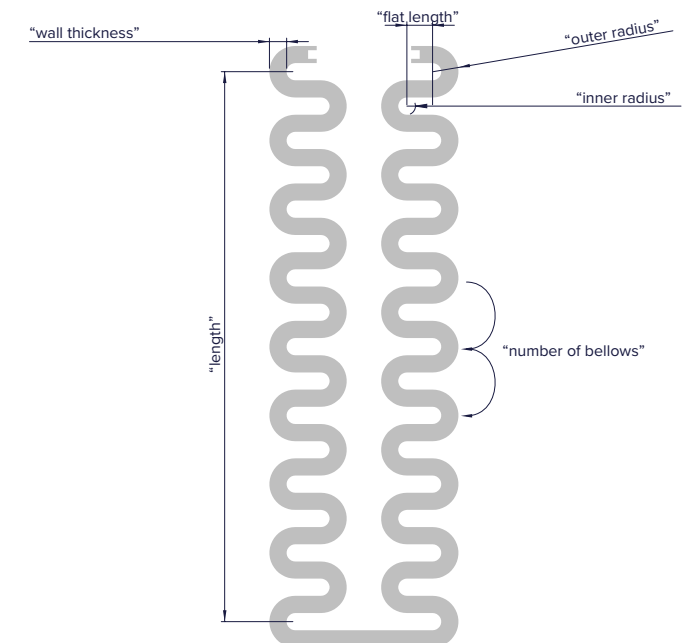

Figure 14. Base geometry design and parameters.

Modularity

The equation driven model design allowed for modularity of complex actuators. When multiple movements were combined into the same Solidworks assembly, they could be simply connected in any configuration using a connection piece. This allowed for an efficient design workflow – after the original Solidworks models had been created, virtually no more time needed to be spent on modelling as the models could be configured individually with an input piece or configured with other sections in an assembly. Once the pieces are mated in an assembly, the individual parts can still be edited and the changes updated in the assembly. For example, if a previous model exhibited a higher bend angle than was wanted in an experiment, the number of bellows could be decreased at a part level and the assembly would automatically change to accommodate this as shown in *Figure 15*.
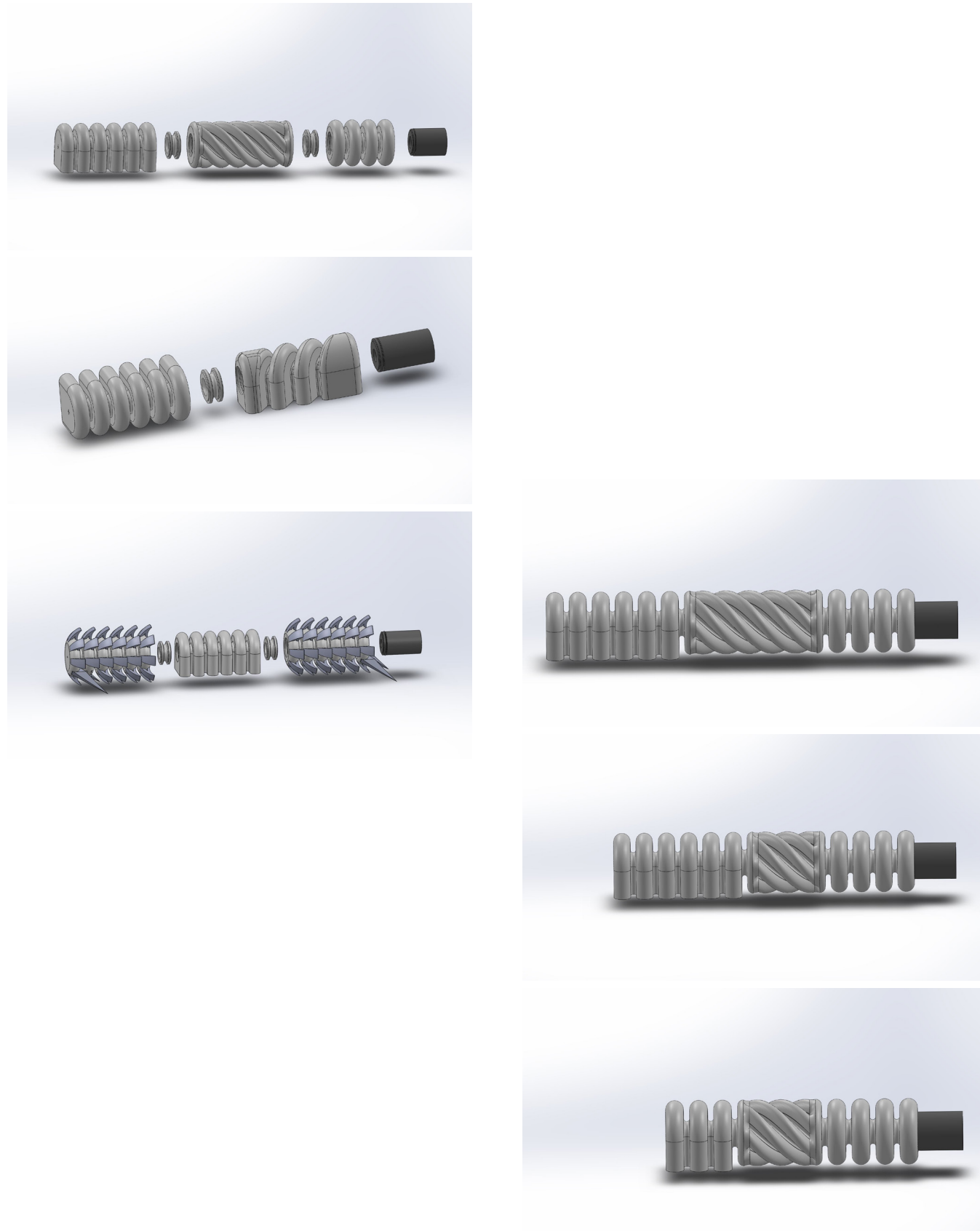
Figure 15. Various configurations of a single Solidworks assembly.

Measurement

In order to accurately quantify the performance of different actuators, individualised recording and testing methods were created (*Figure 16*). The actuators that had their performance quantified were:

- Bending
- Twisting
- Extension
- Expansion

They were each recorded on video with the actuator positioned in the best orientation to demonstrate its deformation. After actuation, the footage was reviewed in Adobe Premiere Pro, and video frames that showed the initial position of the actuator and the actuator in its deformed state were exported. Adobe Illustrator was used to measure the deformation, through the "Info" window which gives information on a lines' angle and length.

Figure 16. Method for measuring each primary inflation motion.

Balloon testing

To test the basic concepts of actuation for soft robots, testing was carried out through the use of balloons and tape (*Figure 17*). Using this method, principles of strain restricting regions to control motion as found in biology and synthetic replications could easily be tested and inflated without the need for designing or assembling of a testing rig. Electrical tape acted as the strain restrictor as the balloon was inflated. These principles could be heavily inspired by the muscular systems found in muscular hydrostats. A key distinction with muscular hydrostats is that they maintain a constant volume at all times and thus, the system for actuation must be adapted to suit a change in volume during actuation. Instead of a muscular contraction occurring to dictate motion like in muscular hydrostats, inflating actuators have a region which maintains its dimensions while others expand around it. By placing the electrical tape in differing configurations on the balloon prior to its inflation, it was found that the balloon would follow a different path during inflation. Both bending and twisting were tested with tape, however, extension occurred once the balloon was inflated without any tape needed so this wasn't tested.

In muscular hydrostats, a contraction of longitudinal muscles on one side of the hydrostats causes a bending motion to occur. To replicate this with a balloon and tape, a strip of tape was placed longitudinally along the balloon to restrict expansion along one side. This worked as anticipated, and a bend was created in the balloon during inflation. This method allowed for precise control over where the bending occurred along the length of the balloon, as is demonstrated by localising the bending in the orange balloon.

In muscular hydrostats, a contraction of helically arranged muscle fibres creates torsion along the system. To replicate this with a balloon and tape, the tape was wrapped around the balloon helically prior to inflation. This also proved to be successful in proving the concept, however, it was found that the helix angle of the tape had to be very specific in order to fully inflate, otherwise the balloon would not inflate past the beginning of the length of tape.

The main drawbacks with taking this system any further was the expansion of the balloons' dimensions after inflation. The surface area of the balloon expanded so significantly that it proved to be challenging to place the tape in certain orientations without the balloon bursting. As the tape expanded very little during inflation, a large stress was created from the axial asymmetry of expansion.

These tests not only worked to prove the driving principles informing future design decisions, but they also informed the system for parametric control. When the balloons were deflated, tape could be placed in any location along their length to inform the motion during inflation.

Bending

Localised bending
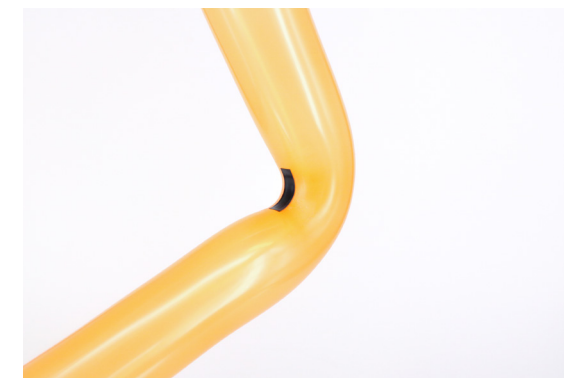
Twisting

Figure 17. Balloon testing experiments.

Print set 1

Goals



Figure 21. Material tears.

The goal for this print set was to explore a singular base geometry which could be modified to achieve three different motions. These motions were:

- Extension
- Bending
- Twisting

This print set worked as a first test to analyse the strength of the material, assess the wall thickness and shore hardness, and begin to establish a technique and process for cleaning the support material from the models and preparation for inflation.

Actuator 1.01 (geometry)
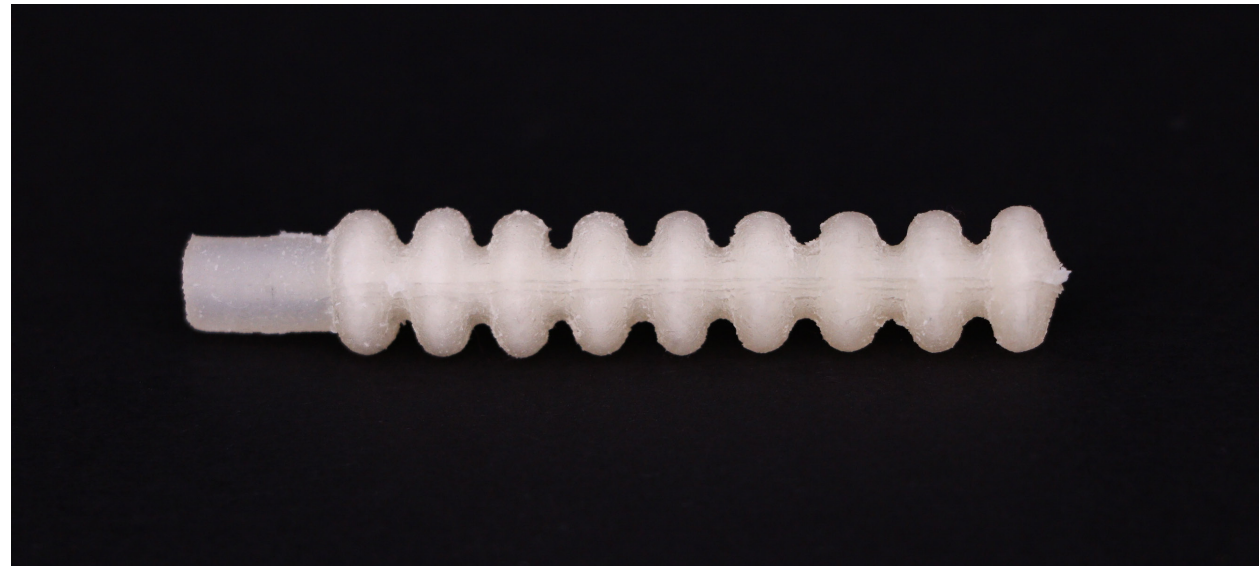
Aim: Create a soft actuator capable of extending when inflated.

Results: Tears occurred during the cleaning of support material from the print.

30 SH
50 SH

Figure 18a - 18b. Actuator 1.01 images.

Actuator 2.01 (geometry & materiality)
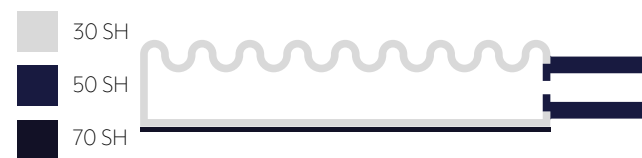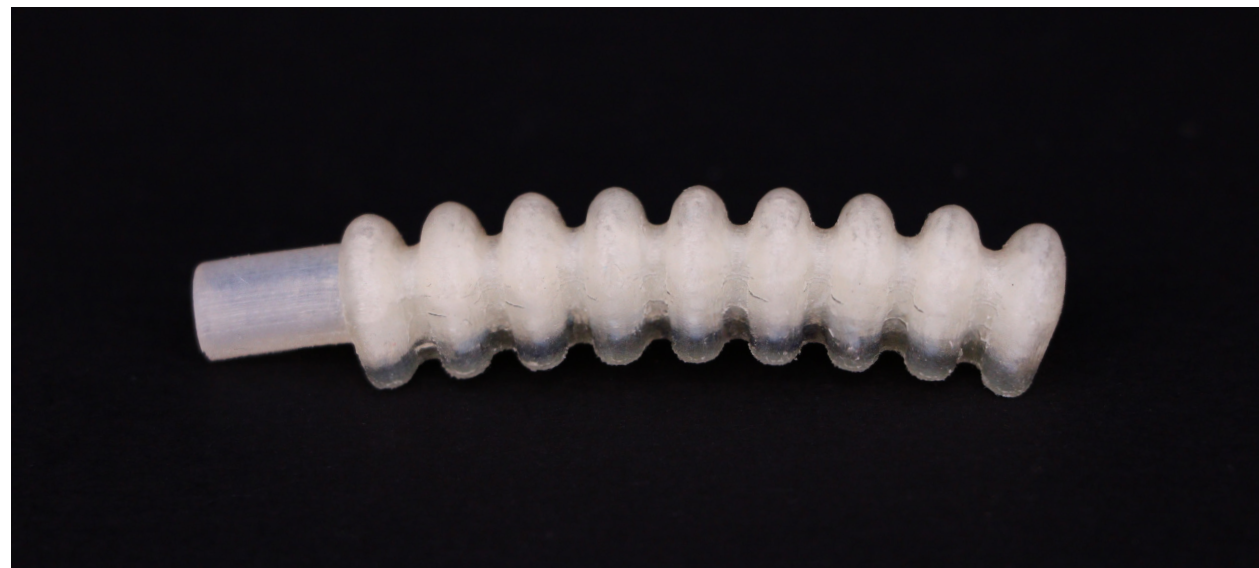
Aim: Create a soft actuator capable of bending when inflated.

Results: Tears occurred during the cleaning of support material from the print. Delamination occurred between the 70SH material on the base and the main soft body.

30 SH
50 SH
70 SH

Figure 19a - 19b. Actuator 2.01 images.

Actuator 3.01 (geometry & materiality)
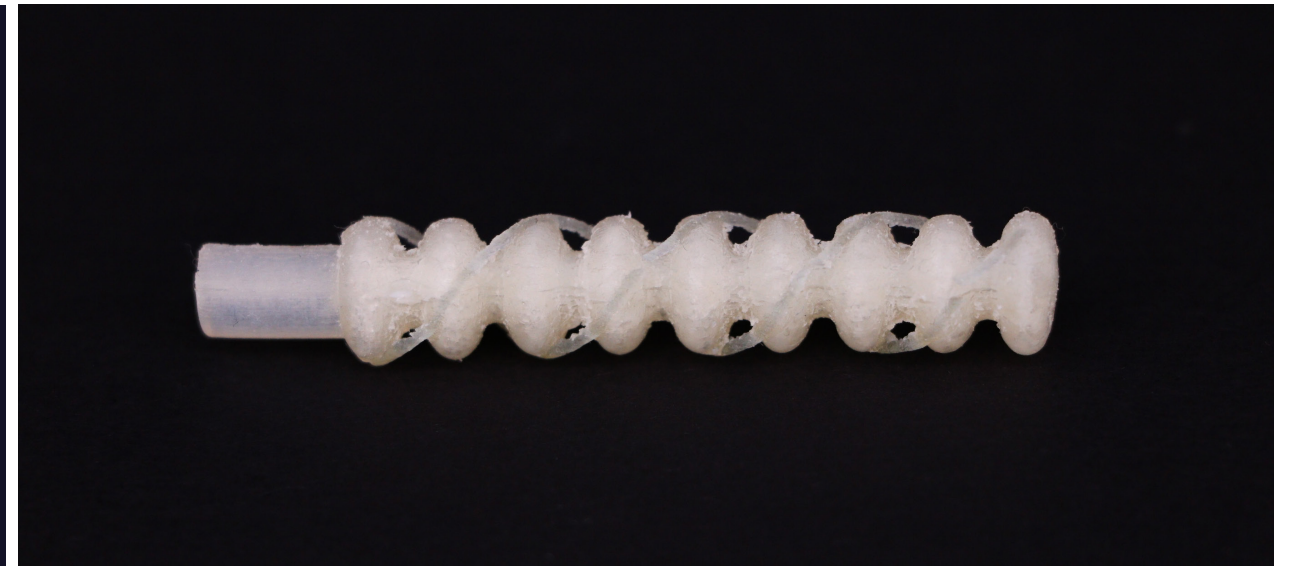
Aim: Create a soft actuator capable of twisting when inflated.

Results: Tears occurred during the cleaning of support material from the print. The helically arranged 60SH material was too thin and broke easily.

30 SH
50 SH
60 SH

Figure 20a - 20b. Actuator 3.01 images.

Analysis

As shown in *Figure 21*, the prints in this set all failed due to tearing before they could be inflated and the motion could be tested. As the models were so prone to tearing, subsequent designs needed to be much stronger to survive cleaning and especially to perform well once inflated. A cleaning process was also be established to minimise the damage done to the prints, and to standardise the procedure across print sets.

Print set 2

Figure 22. Support material cleaning setup.

Goals

This print set aimed to explore the success of the performance of actuators by utilising different properties of the 3D printer. These included actuators designed around:

• Materiality and geometry
• Materiality
• Internal geometry

Extension, *twisting*, and *bending* were evaluated for each of these routes. All of the actuators were printed with a glossy finish on them.

To improve on the previous models the following changes were made:

• Increased chamber wall thickness (0.8mm -> 1.0mm).
• Interlocking geometry at the connection between the main soft body and the input geometry to reduce the chance of tearing.
• Increased main soft body shore hardness (SH30 -> SH35).
• Hard material areas in the bending and twisting actuators were embedded within the main soft body to reduce the chance of separation between bodies.
• A relief valve was added to the end of the chambers. This was to help with the removal of support material from internal chambers and to reduce the chances of bursting at high actuation pressure. This also altered the actuation pressure needed as the new system needed a constant input of air.

To improve the cleaning process of the models, the following workflow was implemented:

1. CAD modelling
2. Printing
3. Soak prints in water
4. Rough removal of support material while in a water bath (*Figure 22*)
5. Solution bath
6. Finer detail support material removal and solution rinsing while in the water bath
7. Washing/drying
8. Glueing relief valves closed
9. Pressurisation

Pressurisation is used as the final step in the post-processing of the actuators as the flow of air helps to loosen the remainder of the support material from the internal chambers of the actuators. The loosened support material is then pushed out the valve at the end of the actuator furthest from the air input. The valves were then closed off with super glue to make the system airtight to decrease the volume of air needed for actuation. Actuation results were taken before and after the valves were sealed to test this hypothesis.

Actuator 1.02 *(geometry)*
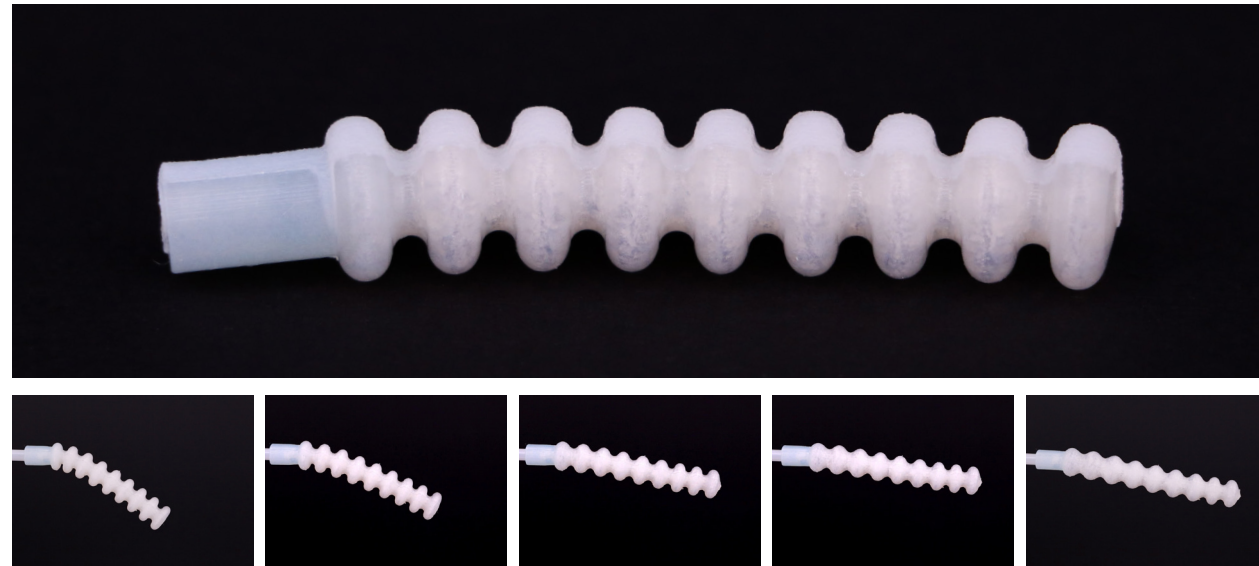
Aim: Determine the success of the extension actuation.

Results: The print successfully extended, however, it burst axially which detracted from the maximum extension of the actuator.

35 SH
50 SH

Figure 23a - 23g. Actuator 1.02 geometry and inflation sequence.
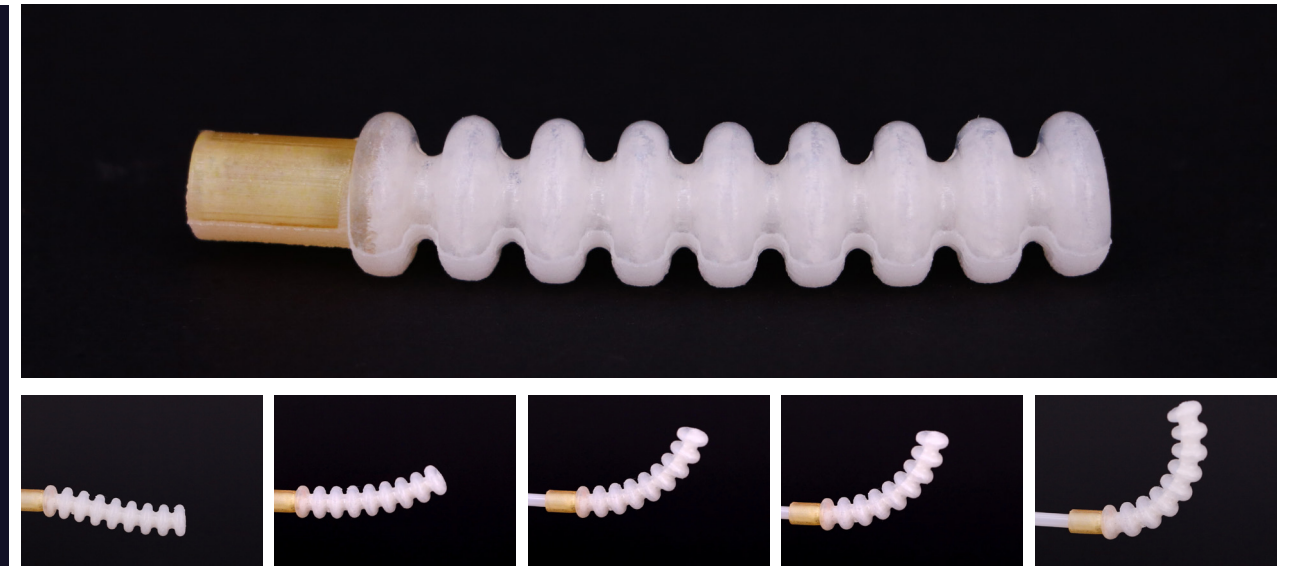
Actuator 2.02 *(geometry & materiality)*
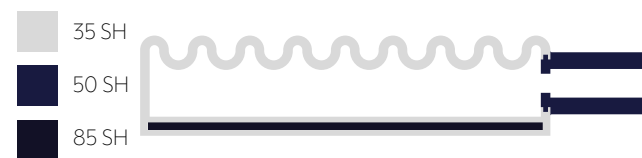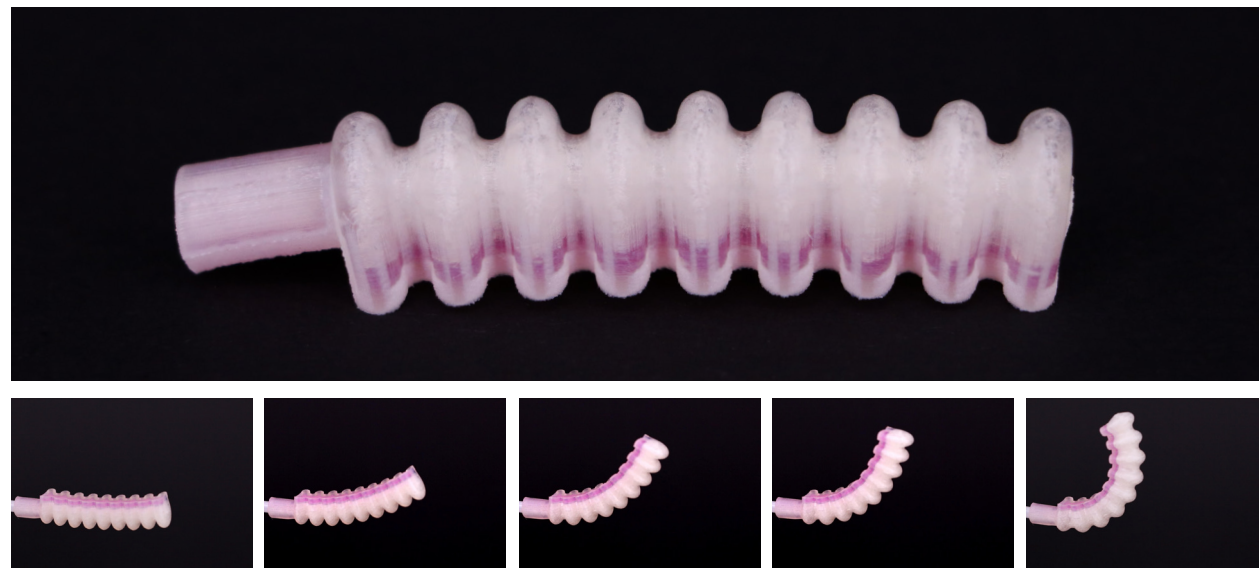
Aim: Determine the success of the bending actuation using geometry and variable materiality.

Results: The print was not able to maintain this deformation angle as the model burst between the 35SH and 50SH geometries.

35 SH
50 SH
85 SH

Figure 24a - 24g. Actuator 2.02 geometry and inflation sequence.

Actuator 2.03 *(geometry)*

Aim: Determine the success of the bending actuation using internal geometry.

Results: The print demonstrated significant bending, however, it burst axially which detracted from the maximum bend of the actuator.

35 SH
50 SH

Figure 25a - 25g. Actuator 2.03 geometry and inflation sequence.

Actuator 2.04 *(bending + twisting)*
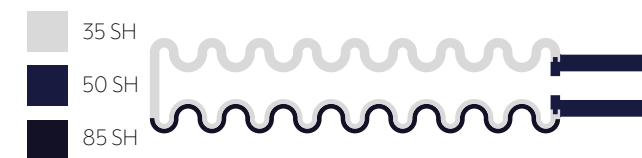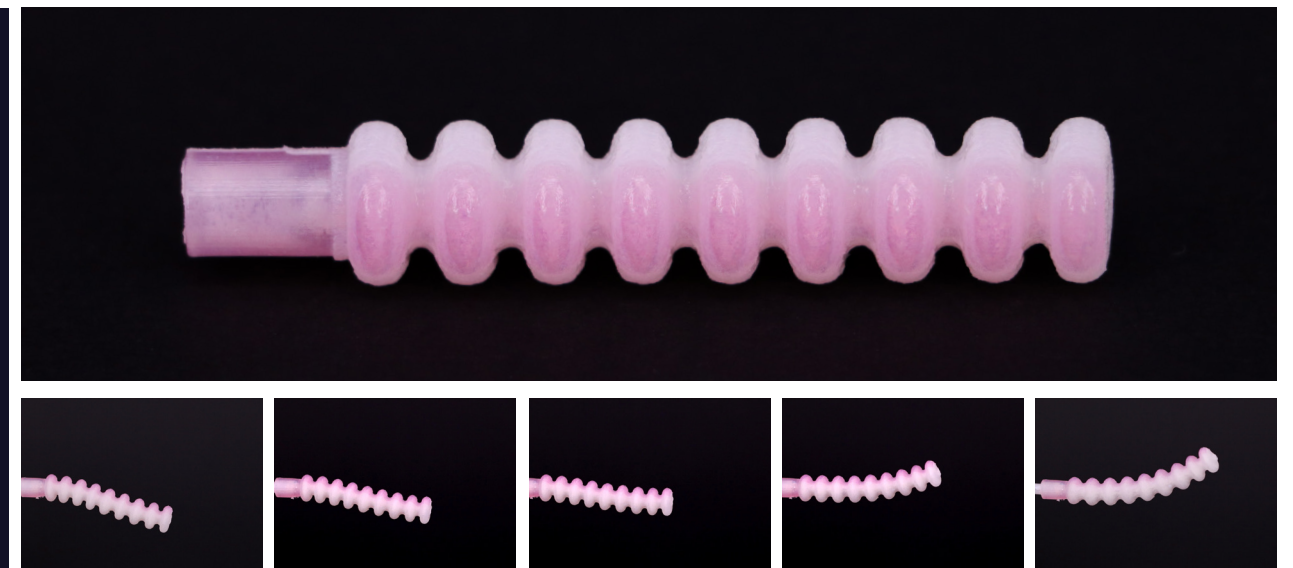
Aim: Determine the success of the bending actuation using variable materiality.

Results: The print demonstrated slight bending, however it was nowhere near as significant as the other two bending actuators.

35 SH
50 SH
85 SH

Figure 26a - 26g. Actuator 2.04 geometry and inflation sequence.

Actuator 3.02 (geometry & materiality)

35 SH
50 SH
70 SH

Aim: Determine the success of the twisting actuation using geometry and variable materiality.

Results: The print was able to reach a maximum twist angle of 2.2°/mm (77° total) and did not have any significant material tears occur.

Figure 27a - 27g. Actuator 3.02 geometry and inflation sequence.

Actuator 3.03 (geometry)
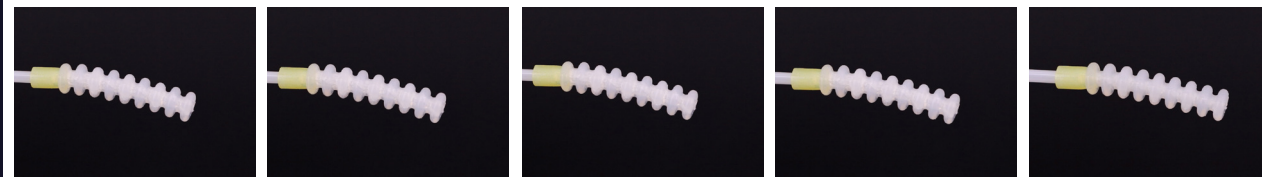
35 SH
50 SH

Aim: Determine the success of the twisting actuation using internal geometry.

Results: The print did not demonstrate any significant motion during actuation, likely due to the large material bulks in geometry restricting its motion.

Figure 28a - 28g. Actuator3.03 geometry and inflation sequence.

Actuator 3.04 (materiality)
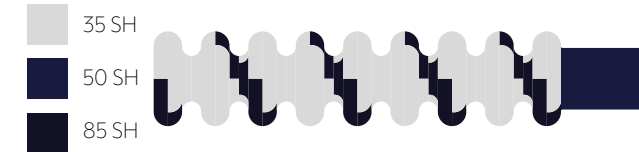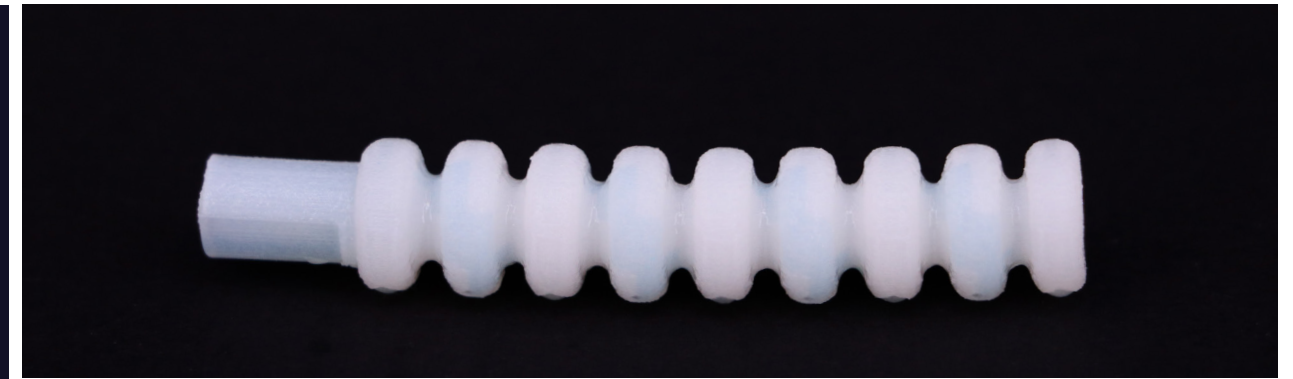
35 SH
50 SH
85 SH

Aim: Determine the success of the twisting actuation using variable materiality.

Results: The print was able to reach a maximum twist angle of 0.8°/mm (27° total) and did not have any significant material tears occur.

Figure 29a - 29g. Actuator 3.04 geometry and inflation sequence.

Analysis

Extension actuator:

The proportions of the extension actuator (1.02) were changed in an attempt to increase the extension achieved while maintaining the design's strength against bursting during inflation.

Bending actuators:

From a visual inspection, the geometry + materiality (2.02) and internal geometry (2.03) prints achieved a much larger bending deformation than the materiality print (2.04). The main problem with the bending actuators was the air leaks that limited the deformation angle. This was likely happening because of the radial asymmetrical nature of the bending deformation which caused the print layers to separate along the horizontal axis where air is escaping. This is addressed in subsequent prints by altering the geometry by strengthening it in the regions most susceptible to bursting.

Twisting actuators:

The geometry + materiality twisting print (3.02) was the most successful, and it reached a twist angle of 77° along its length of 35mm. Although this print was successful, a new geometrical solution was explored to further explore the possible twist angles that are possible.

The valve that was used to remove internal support material was successful, as it allowed more thorough removal of support material and it was easily closed off with superglue once this was accomplished.

Print set 3
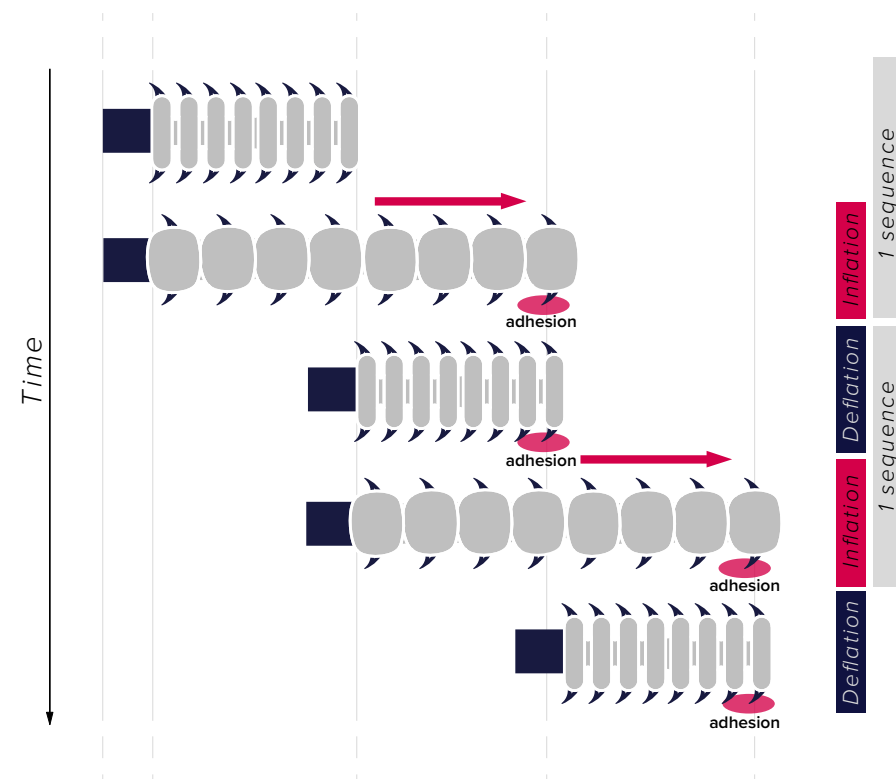
Figure 30. Actuator 1.06 intended actuation sequence.

Goals

The largest problem with the previous print sets was material tearing. This was addressed in this print set through a set of shore hardness tests which aimed to find the optimal shore hardness in regards to performance and material strength. The other prints in the set were also printed at a larger wall thickness (from 0.8mm to 1mm) to address this.

In an attempt to increase performance, the bellows on the prints in this set were condensed, meaning that the inner radii were decreased.

The motion that was least satisfactory in its performance for previous prints was the twisting actuator. This was addressed in this print set with a departure from the previous twisting concepts to introduce a completely new geometry. This was tested with different helix angles to see how it would impact performance. After this twisting geometry was designed and tested, a precedent in the literature was found which presents a similar geometry for twisting actuation. Development of Multi-chamber Pneumatic Twist Actuator for Soft robot (Darekar et al., 2019) details a method for casting a silicon actuator using a sacrificial

3D printed mould at a much larger scale than the actuators presented in this portfolio. Although the research done by Darekar et al. (2019) is intended for high force applications, the complexity of the fabrication process in comparison to the method presented in this portfolio is notable.

A few other new concepts were tested which were derived from existing concepts:

• **Extension/adhesion actuator (1.06):** This print was derived from the extension geometry with the addition of adhesion geometry to attempt to achieve linear locomotion (*Figure 30*).

• **Expansion actuator (4.01):** Derived from the new twisting geometry with the helix angle set to 0°. The concept was designed to achieve a radial expansion upon inflation.

• **Bending/twisting actuator (2.06):** Derived from the bending geometry+materiality model with the bellows offset on an angle from the central axis. This print was designed to follow a helical path upon inflation.
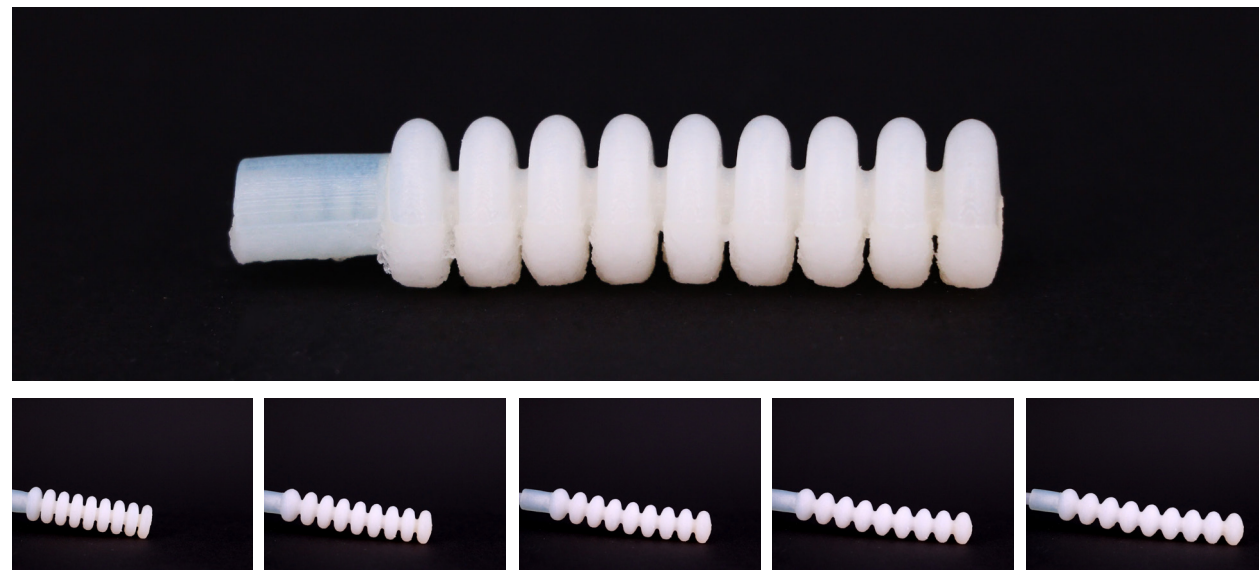
Actuator 1.03 *(shore hardness 40)*
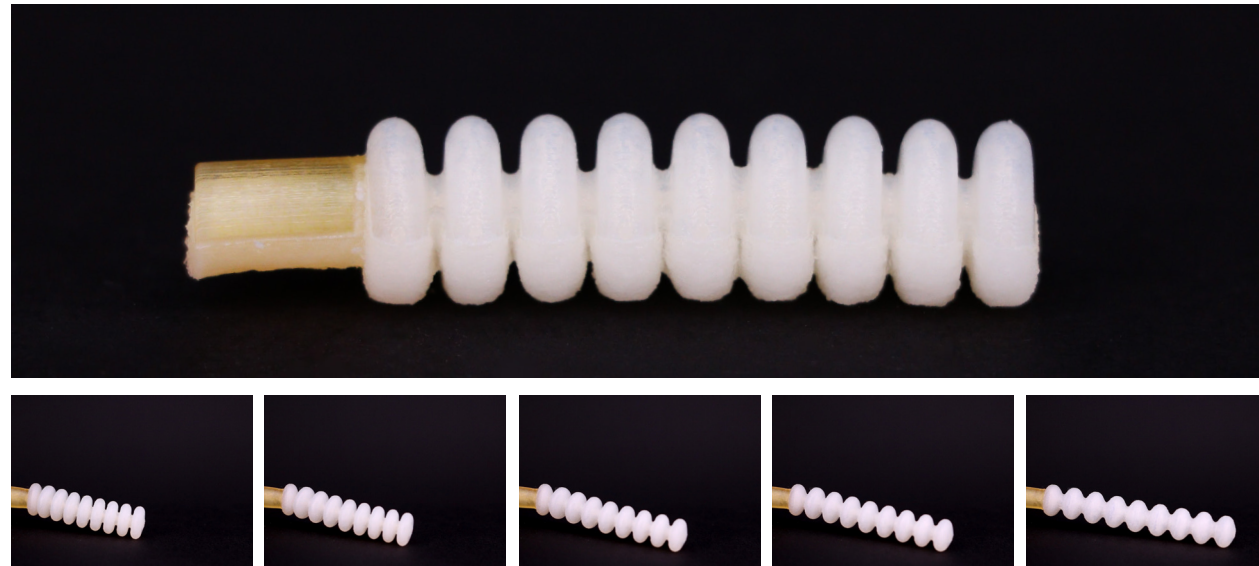
Aim: Determine the best shore hardness for the prints in terms of performance and material strength.

40 SH
50 SH

Results: No material tearing occurred, and the print achieved an extension percentage of 162%.

Figure 31a - 31g. Actuator 1.03 geometry and inflation sequence.
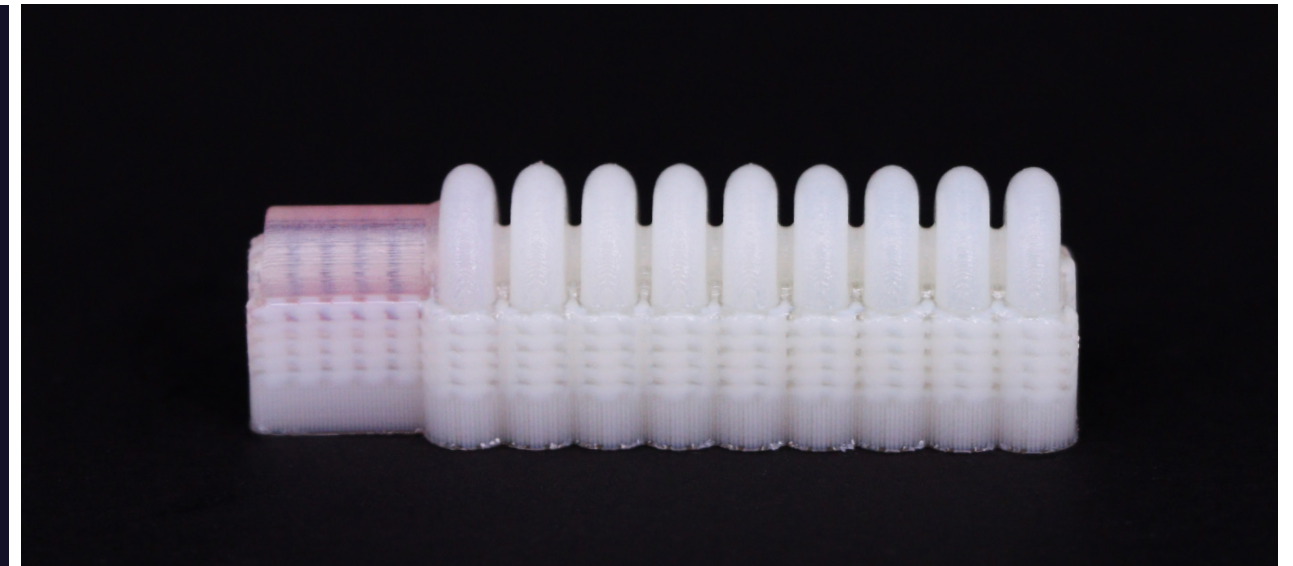
Actuator 1.04 *(shore hardness 50)*

Aim: Determine the best shore hardness for the prints in terms of performance and material strength.

50 SH

Results: No material tearing occurred, the print achieved an extension percentage of 153%.

Figure 32a - 32g. Actuator 1.04 geometry and inflation sequence.

Actuator 1.05 *(shore hardness 60)*

Aim: Determine the best shore hardness for the prints in terms of performance and material strength.

50 SH
60 SH

Results: Significant material tearing occurred during the cleaning of this print which ruled the print out before inflation testing could occur.

Figure 33a - 33g. Actuator 1.05 geometry and inflation sequence.

Actuator 1.06 *(adhesion geometry)*
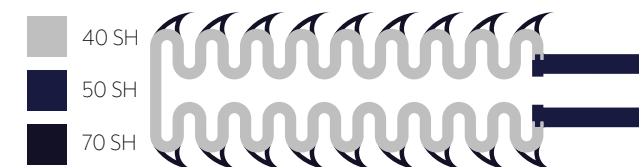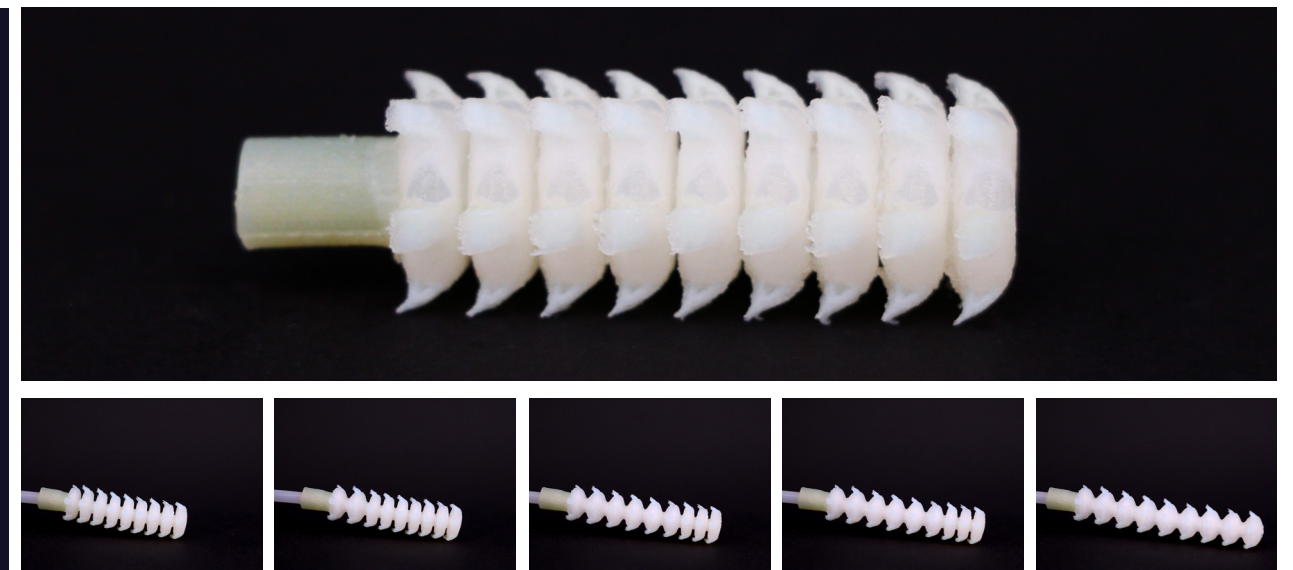
Aim: Create a soft robot capable of linear locomotion by utilising knowledge of adhesion.

40 SH
50 SH
70 SH

Results: The extension percentage 157% was comparable to the other extension geometries, however, the adhesive geometry didn't allow for locomotion to occur.

Figure 34a - 34g. Actuator 1.06 geometry and inflation sequence.

Actuator 2.04
(geometry & materiality)
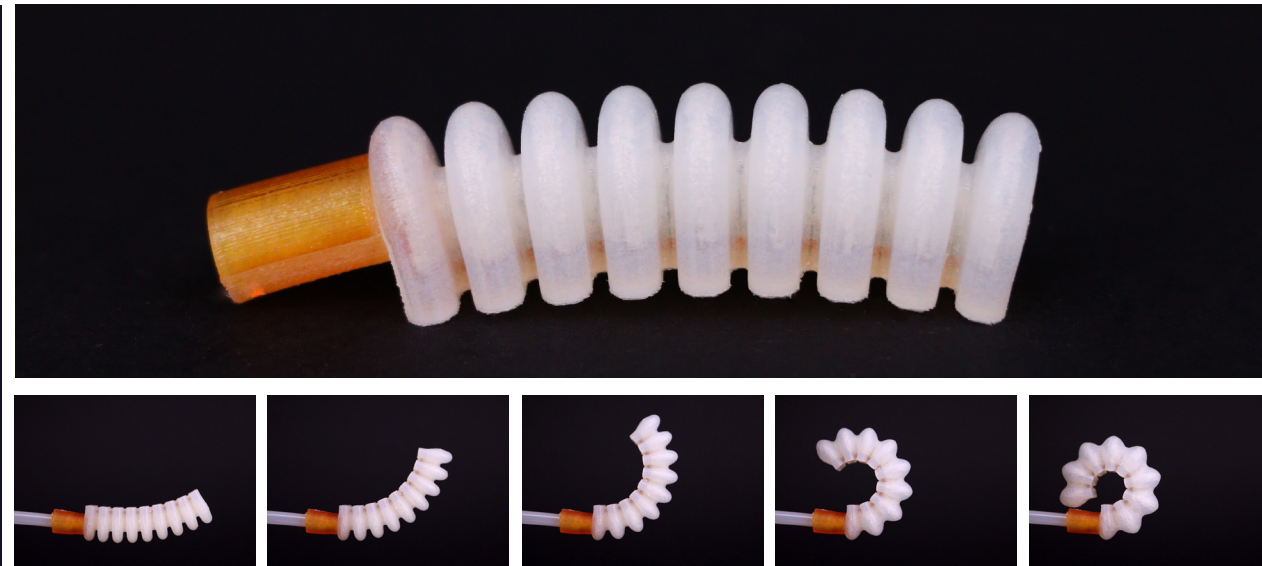
Aim: Determine the success of the bending actuation using geometry and variable materiality.

Results: No material tearing occurred, and at its actuated state the print achieved a change in angle of 7.2°/mm (253° total).

40 SH
50 SH
85 SH

Figure 35a - 35g. Actuator 2.04 geometry and inflation sequence.

Actuator 2.05
(geometry)
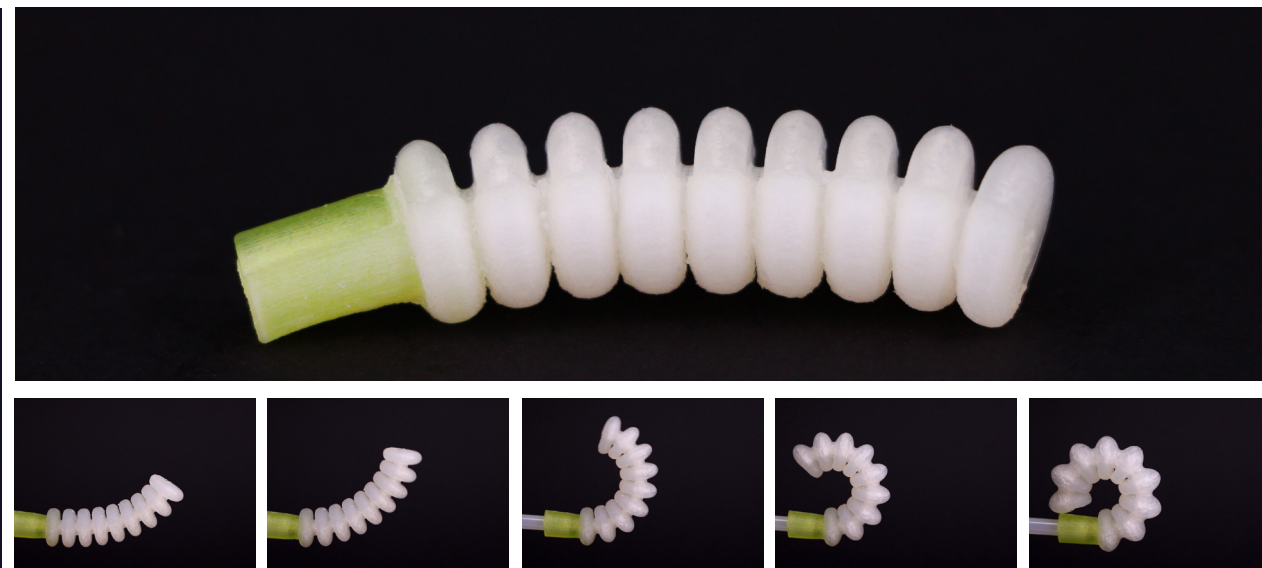
Aim: Determine the success of the bending actuation using internal geometry.

Results: No material tearing occurred, and at its actuated state the print achieved a change in angle of 6.4°/mm (224° total). The print held a moderate bend even when deflated, which inhibited the change in angle.

40 SH
50 SH

Figure 36a - 36g. Actuator 2.05 geometry and inflation sequence.

Actuator 2.06
(bending + twisting)
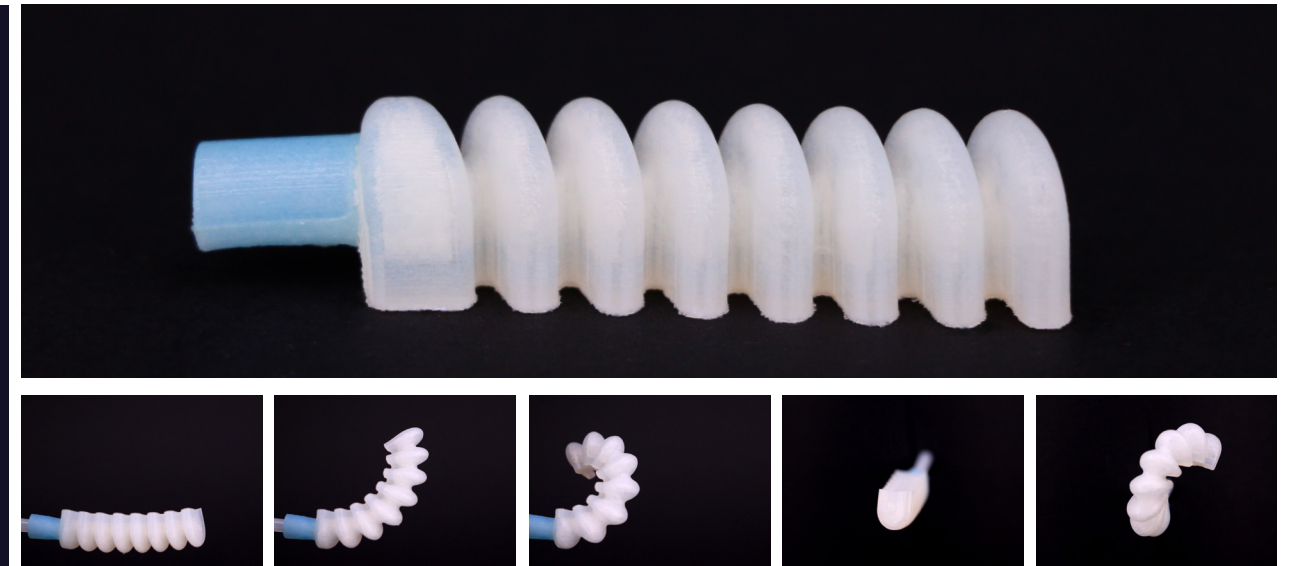
Aim: Create a geometry with the ability to follow a helical path upon inflation.

Results: The print successfully followed a helical path.

25°
40 SH
50 SH

Figure 37a - 37g. Actuator 2.06 geometry and inflation sequence.

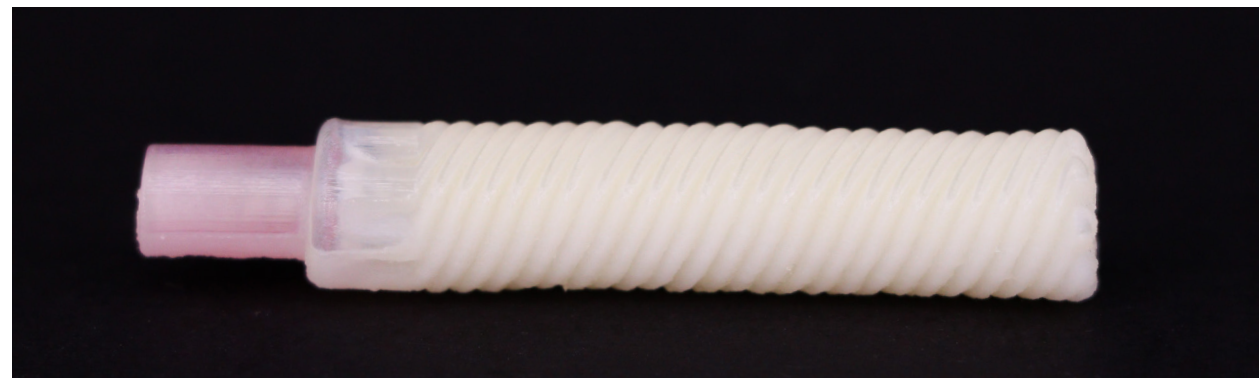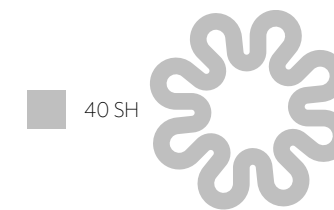## Actuator 3.05
(helix angle 30°)
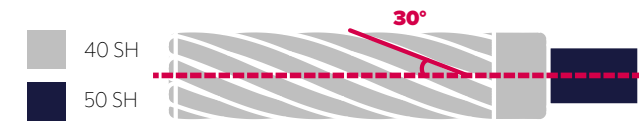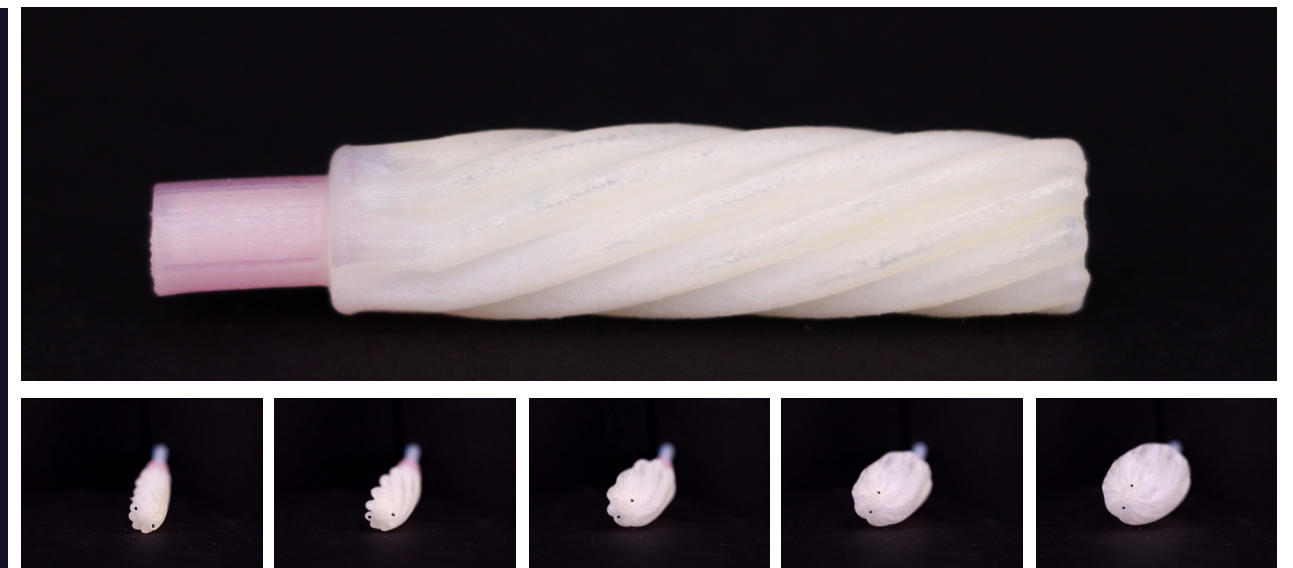
Aim: Create a new twisting geometry with increased performance and find the optimal helix angle.

Results: No material tearing occurred, and at its actuated state the print achieved a twist angle of 3.3°/mm (114° total).

30°
40 SH
50 SH

Figure 38a - 38g. Actuator 3.05 geometry and inflation sequence.

Actuator 3.06
(helix angle 50°)
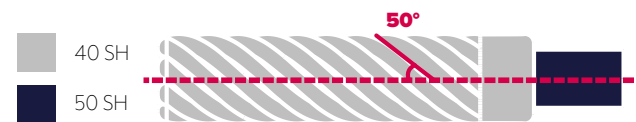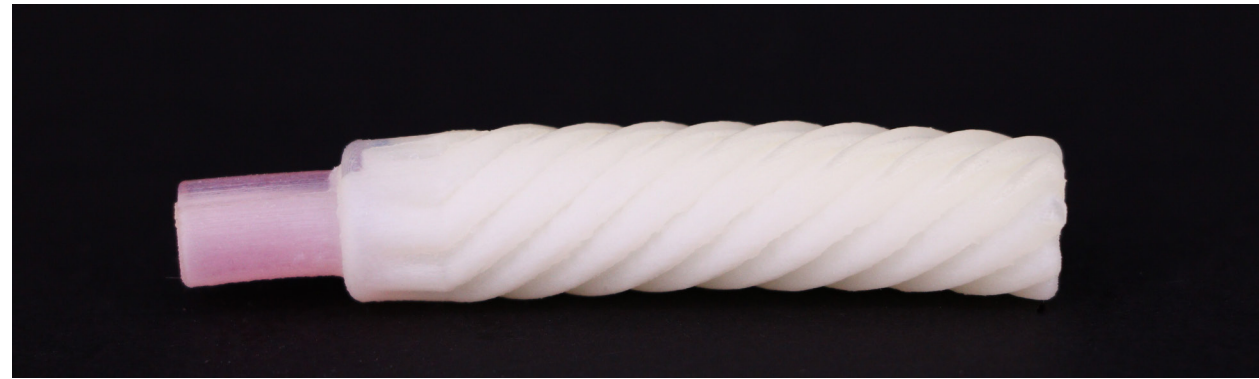
40 SH
50 SH
50°

Figure 39a - 39g. Actuator 3.06 geometry and inflation sequence.

Aim: Create a new twisting geometry with increased performance and find the optimal helix angle.

Results: No material tearing occurred, and at its actuated state the print achieved a twist angle of 7.9°/mm (277° total).

Actuator 3.07
(helix angle 70°)

40 SH
50 SH
70°

Figure 40a - 40g. Actuator 3.07 geometry and inflation sequence.

Aim: Create a new twisting geometry with increased performance and find the optimal helix angle.

Results: Significant material tearing occurred, however a twist angle of 12.4°/mm (435° total) was still achieved.

Actuator 4.01
(20mm length)

40 SH

Figure 41a - 41g. Actuator 4.01 geometry and inflation sequence.

Aim: Create a geometry capable of radially expanding upon inflation.

Results: The print successfully expanded, and reached an expansion percentage of 182%. The print burst, and was unable to perform as well afterwards.

Analysis

Shore hardness testing:

Shore hardness 40, 50, and 60 were tested as 35 shore hardness was not exhibiting the necessary strength. The 60 SH print (1.05) tore during cleaning, deeming it unsuccessful. The 40 SH model (1.03) appeared to give the best result as, although the 50SH model (1.04) didn't tear, it exhibited a 9% drop in performance which was most likely because of the material being stiffer.

Extension-adhesion actuator (1.06):

The extension-adhesion geometry successfully exhibited extension but not adhesion. The adhesion geometry proved to be very delicate, and many broke off during cleaning and handling. The extension percentage of 157% was comparable to the other extension geometries, meaning the adhesion geometry did not have a significant impact on the extension of the actuator. The adhesion geometry did not grip on any surface the actuator was placed on during inflation. This could be because the force pulling the actuator back to its neutral state is larger than the force securing it to the surface.

Bending actuators:

The primary bending tests were a geometry + materiality focused model (2.04), and an internal geometry modelled with a material bulk on one side of the central axis (2.05). Both tests were successful, each exhibiting over 220° of total bend. The main difference between the two models was that the internal geometry model did not return to a straight position, and when deflated it always had a significant bend in it (~60°). This could be detrimental to the performance if an application required the actuator to return to a straight state. The bending + twisting model (2.06) exhibited the desired actuated state of following a helix, however, this was later iterated on further to attempt to create a tighter helix.

Twisting actuators:

Helix angles of 30°, 50°, and 70° were printed and tested with the same length (35mm) and base geometry sketch. The 70° model (3.07) twisted the most along its length at 435° (12.4°/mm) however it also had issues inflating fully. Since the geometry was the most tightly wound, some of the geometry fused together during printing which restricted its motion. The geometry was also compared to the material twist model and the materiality + geometry twist model from print set 2 (3.02), which showed that the new geometry significantly outperformed it.

Expansion actuator (4.01):

The expansion geometry worked as anticipated, and reached an expansion percentage of 182%. It was designed using the same base geometry as the twisting actuators.
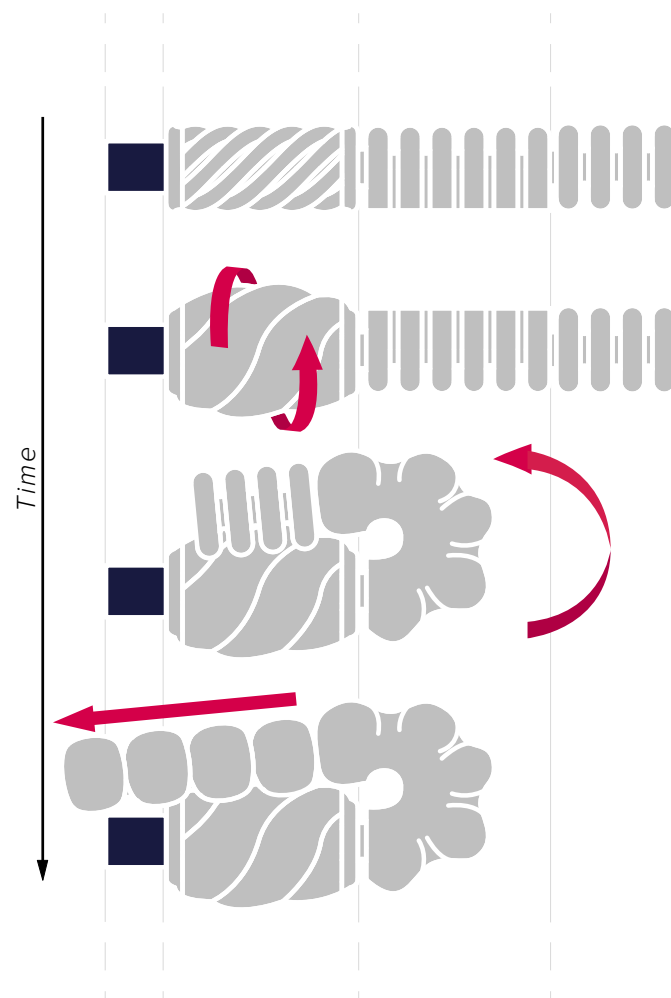
Print set 4

Goals

*Figure 42. Actuator 5.01 intended actuation sequence.*

To optimise the optimal helix angle for the twisting geometry which maximises both twist angle and performance, three further iterations of the same base geometry were tested. These included helix angles of 55°, 60°, and 65°, because the 70° helix angle print from print set 3 had significant tears due to the steepness of the helix angle. Therefore, it was hypothesised that the optimal helix angle would be between 50° and 70°.

To test how the expansion percentage scales, the expansion print geometry was altered to have a length of 35mm rather than 20mm in the first expansion print. This also made it the same length as the other actuators being tested.

A series of internal valves were tested, which, if successful, would stop the inflation of the second half of the actuator until it reaches a certain pressure. The internal valves were placed halfway along the bellows of the extension geometry, and geometric tolerances of 0.05mm, 0.1mm, 0.15mm, and 0.2mm were printed.

The first model with multiple sections of different motion geometries was also printed in this set. The goal was to see how successful the actuation would be when multiple geometries were being inflated in unison (*Figure 42*).

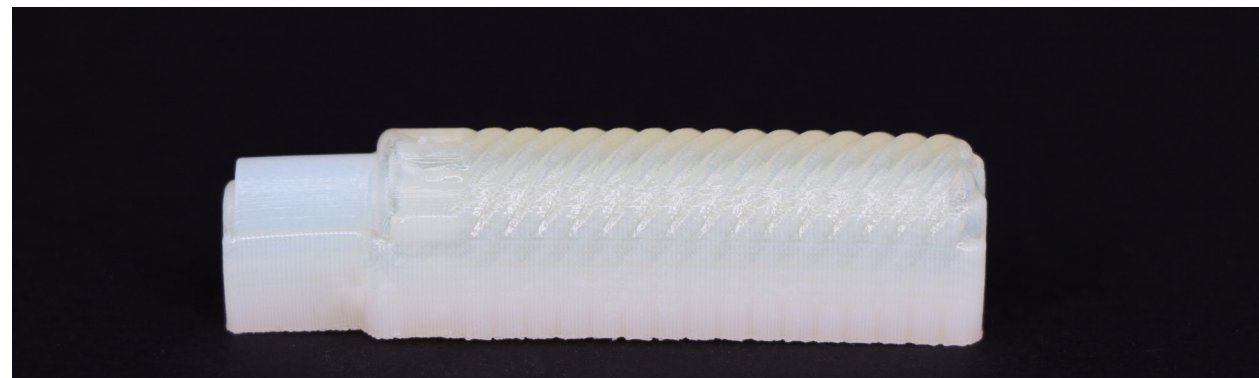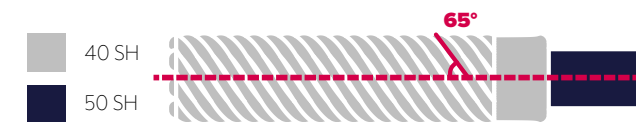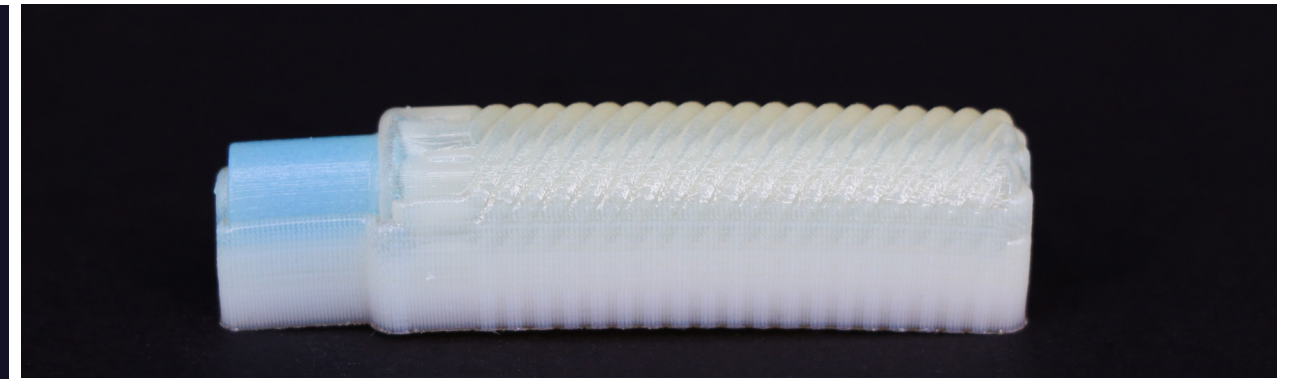**Actuator 3.08** *(helix angle 55°)*
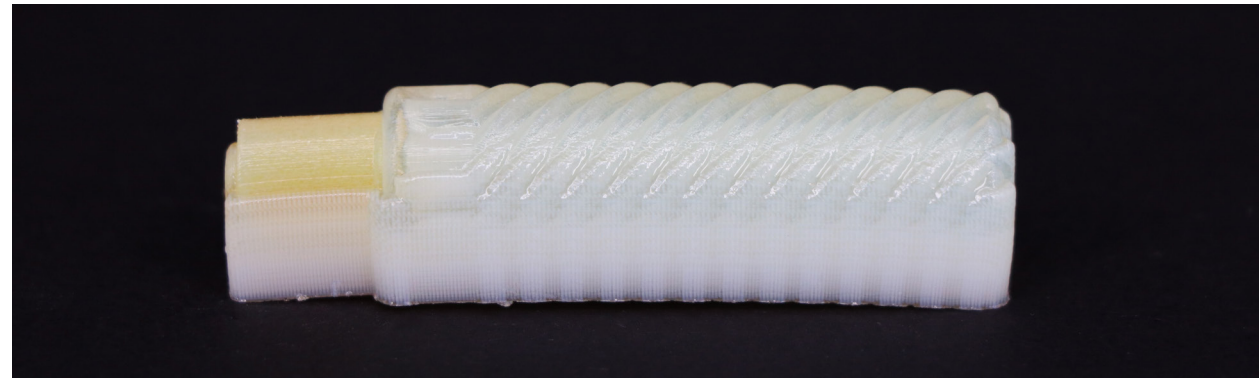
**Aim:** Determine the optimal helix angle to maximise twist angle whilst maintaining performance.

Results: No material tearing occurred, and at its actuated state the print achieved a twist angle of 9.7°/mm (339° total).

55°

☐ 40 SH
■ 50 SH

Figure 43a - 43g. Actuator 3.08 geometry and inflation sequence.

Actuator 3.09 *(helix angle 60°)*

Aim: Determine the optimal helix angle to maximise twist angle whilst maintaining performance.

Results: No material tearing occurred, and at its actuated state the print achieved a twist angle of 11.3°/mm (394° total).

60°

☐ 40 SH
■ 50 SH

Figure 44a - 44g. Actuator 3.09 geometry and inflation sequence.

Actuator 3.10 *(helix angle 65°)*

Aim: Determine the optimal helix angle to maximise twist angle whilst maintaining performance.

Results: Significant material tearing occurred, resulting in a comparatively low twist angle of 6.4°/mm (255° total) being achieved.

65°

☐ 40 SH
■ 50 SH

Figure 45a - 45g. Actuator 3.10 geometry and inflation sequence.

Actuator 4.02 *(35mm length)*
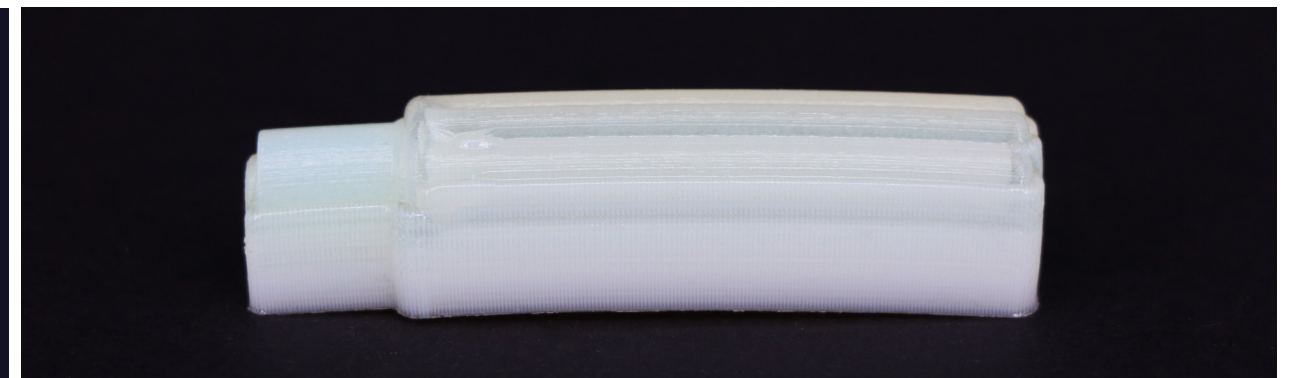
Aim: Determine how the length of the expansion geometry impacts the expansion percentage.

Results: The print successfully expanded, and reached an expansion percentage of 211% before bursting.

☐ 40 SH

Figure 46a - 46g. Actuator 4.02 geometry and inflation sequence.

Actuator 5.01 (twisting, bending, extension)
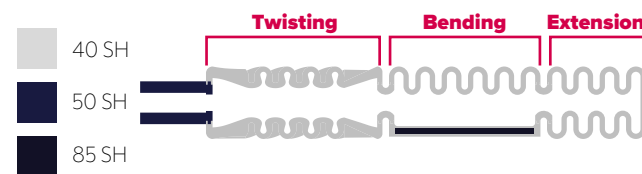

Figure 47a - 47b. Actuator 5.01 geometry.

Aim: Create a soft robot capable of achieving multiple motions through one input.

Results: Large tears occurred in the connections between sections. Rough actuation testing showed that the twisting section actuated before the other sections could reach actuation pressure.
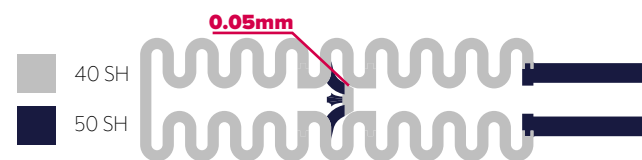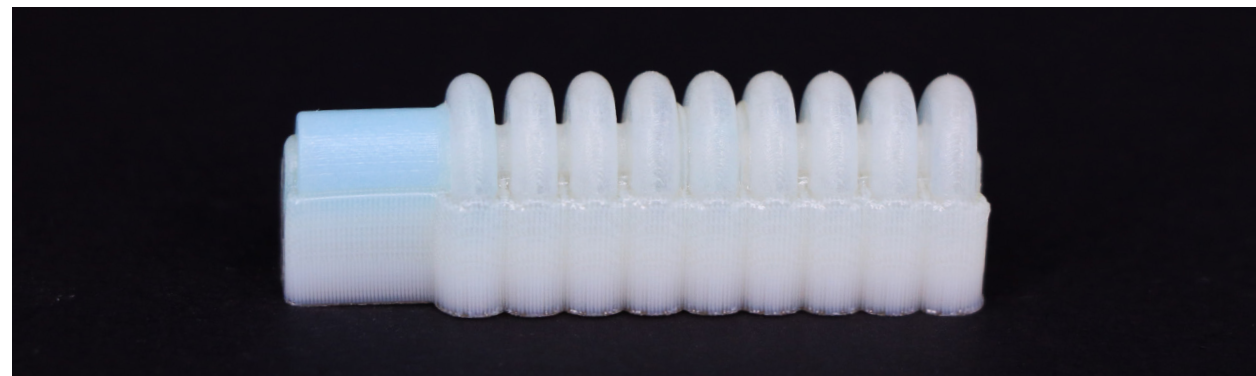
Actuator 1.07-1.09 (internal valve 0.1mm to 0.2mm tolerance)

Figure 49a - 49b. Actuator 1.07-1.09 geometry.

Aim: Create a valve capable of controlling the sequence of actuation.

Results: As the 0.05mm tolerance valve failed, the larger gaps were assumed to also not restrict the airflow.

Actuator 1.07 (internal valve 0.05mm tolerance)

Figure 48a - 48g. Actuator 1.07 geometry and inflation sequence.

Aim: Create a valve capable of controlling the sequence of actuation.

Results: The 0.05mm valve did not restrict the airflow through to the second section of the actuator, deeming it unsuccessful.

Analysis

Twisting actuators:

Helix angles of 55°, 60°, and 65° were tested in this print set. The 65° helix angle burst before it could fully inflate, likely due to the steepness of the helix angle. The 55° and 60° prints worked well, although the 60° print was irregular in its performance - sometimes only parts of the geometry would inflate. As the performance of the 55° helix angle was the most predictable while still reaching a larger twist angle than the 50° print, it was determined to be the most successful of the twisting prints.

Expansion actuator (4.02):

The expansion geometry actuated in the same way as the first expansion print did, however, the longer length (35mm as opposed to 20mm) allowed for a 29% increase in expansion percentage. This print also appeared to burst more quickly than the shorter version, which could be due to the larger expansion percentage.

Complex actuator (5.01):

This print, although it tore before proper actuation testing could be carried out, highlighted a key issue for complex actuation. The actuator was tested through rough inflation testing with a ball pump, where the twisting section inflated and burst before the bending and extension sections reached a large enough pressure to inflate. As the twisting section has a different base geometry to the other two sections, the pressure required for inflation was significantly different.

Internal valves:

The internal valve design tested in this print set was unsuccessful as it did not cause the first section to inflate before allowing air into the second section. This could be due to certain intricacies in the geometry or due to allowing for too large a geometric tolerance. However, it was also very likely that the geometry of the valve was too small and delicate, and was either broken during cleaning or was completely ineffective during inflation.

Print set 5

Goals

This print set included 3 prints, all exploring different variations of complex actuation containing multiple geometric sections. The primary goal for this print set was to explore the possibilities of complex actuation. By using different geometric variations, an understanding of the main challenges could be determined.
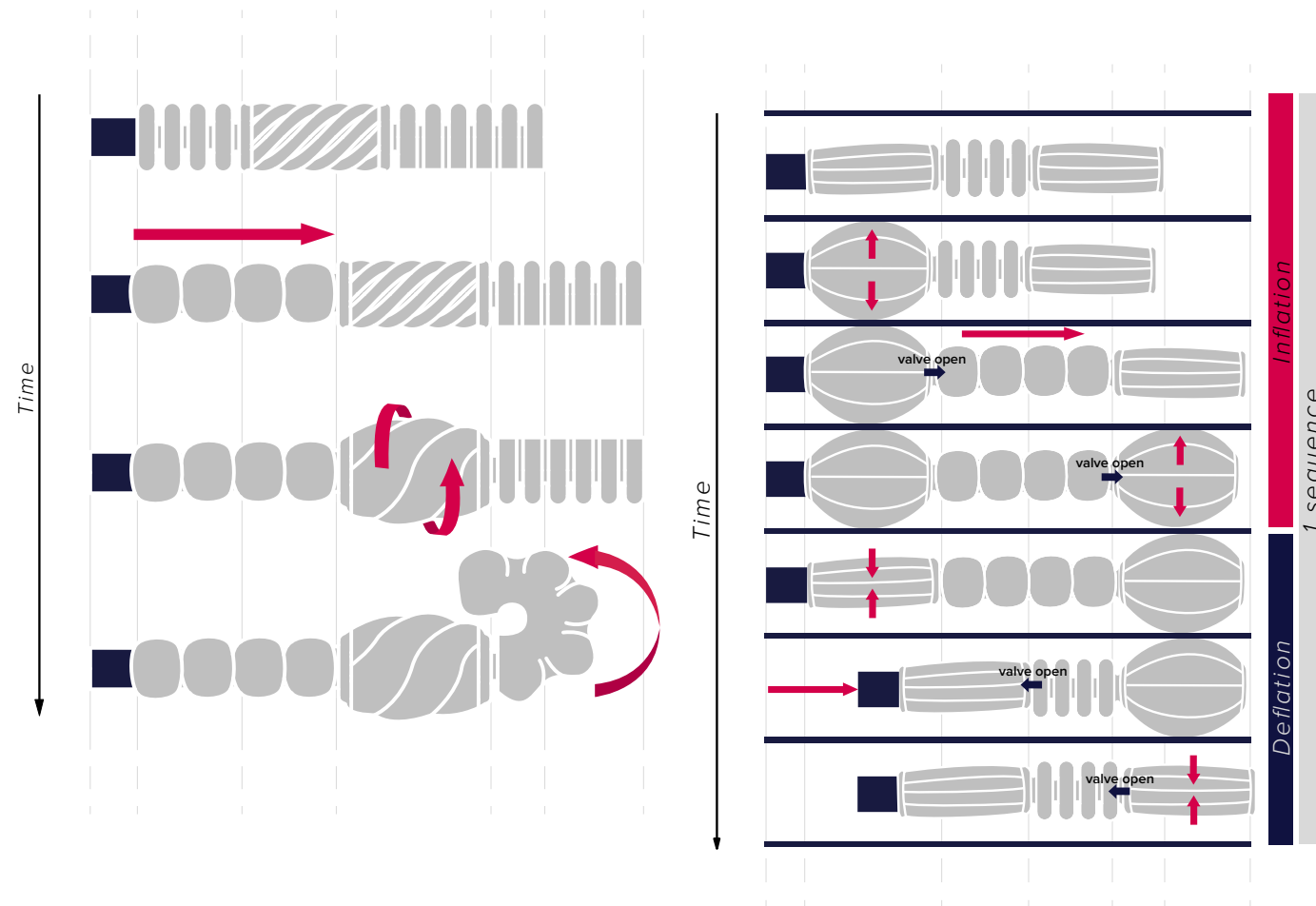

Figure 50. Actuator 5.02 intended actuation sequence.
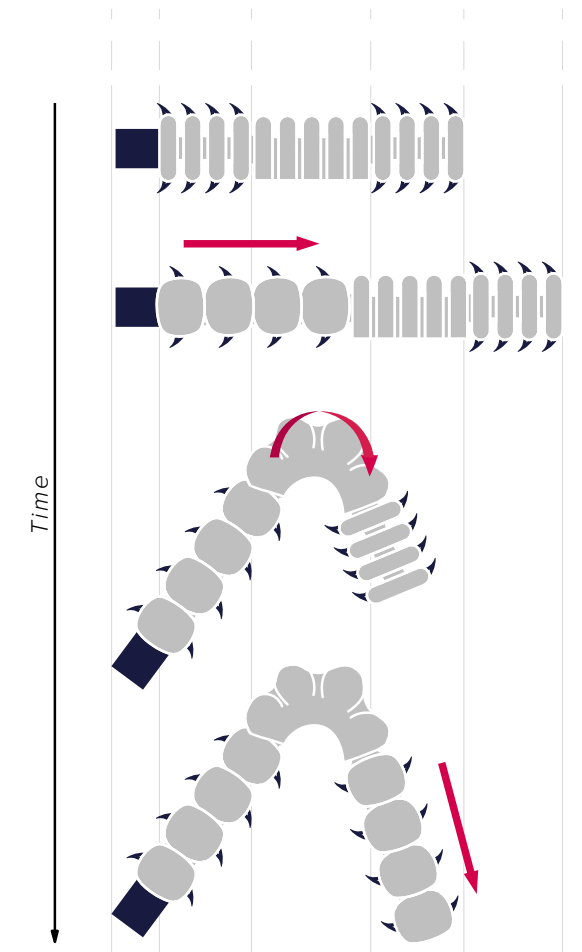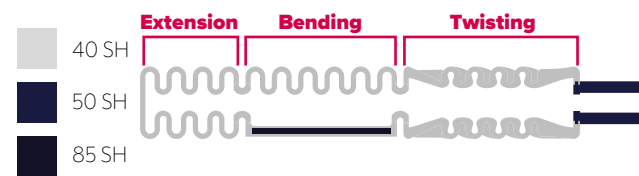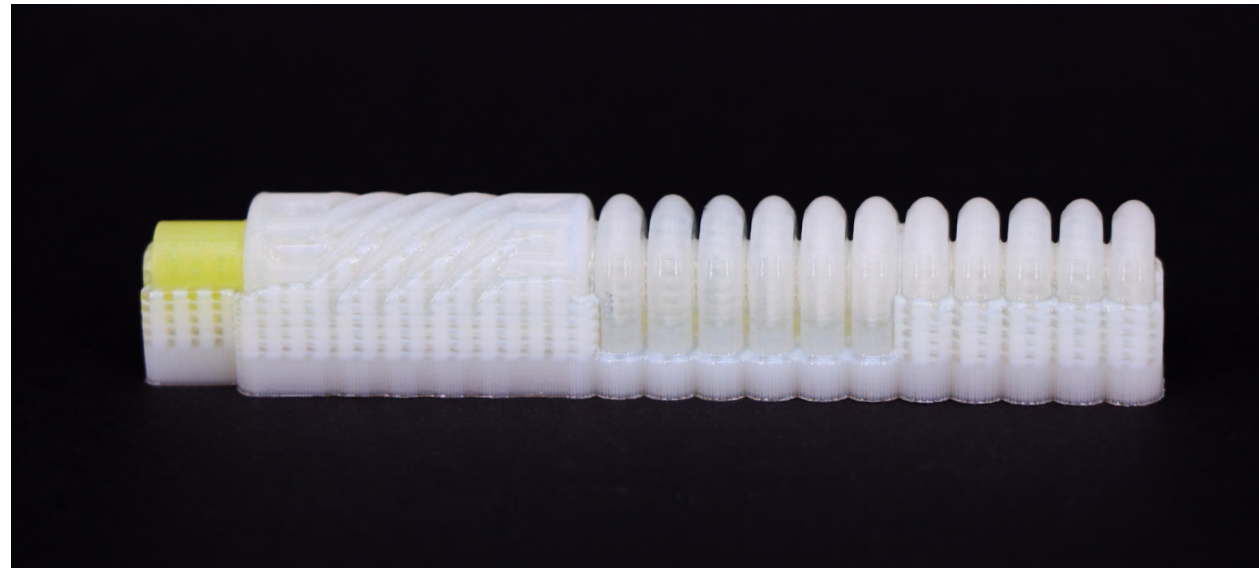
Figure 51. Actuator 5.03 intended actuation sequence.

Figure 52. Actuator 5.04 intended actuation sequence.

Actuator 5.02 *(twisting, bending, extension)*

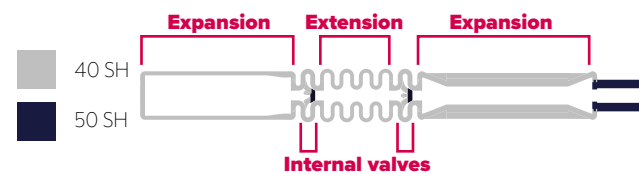**Extension**   **Bending**   **Twisting**

40 SH
50 SH
85 SH

Aim: Create a soft robot capable of achieving multiple motions through one input.

Results: This test confirmed that the twisting section actuates and bursts before the other sections are able to inflate.

Figure 53a - 53b. Actuator 5.02 geometry.

Actuator 5.03 *(expansion, extension)*

Expansion   **Extension**   **Expansion**

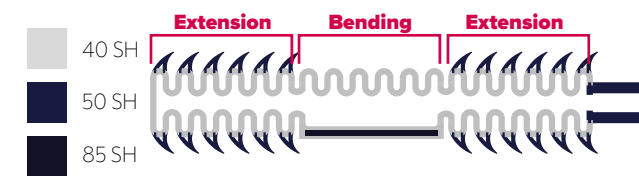40 SH
50 SH

Internal valves

Aim: Create a soft robot with sequenced actuation through one input.

Results: The internal valves were unsuccessful in sequencing the inflation as they were in testing. The expansion sections burst before the extension section could inflate.

Figure 54a - 54b. Actuator 5.03 geometry.

Actuator 5.04 *(bending, adhesion/extension)*

Extension   **Bending**   **Extension**

40 SH
50 SH
85 SH

Aim: Create a soft robot capable of locomotion by utilising surface adhesion.

Results: All sections successfully inflated, however, the adhesive hooks did not provide enough grip to pull the actuator along.

Figure 55a - 55b. Actuator 5.04 geometry.

Analysis

The main problem that was identified from this print set is that the expansion/twisting geometry bursts before a pressure can be reached which inflates the other sections. Actuator 5.04 successfully actuated, as the print did not contain the expansion/twisting geometry. To equalise the pressure needed to actuate a soft robot with both expansion/twisting and extension/bending sections, parameters such as shore hardness and material wall thickness should be changed to compensate for the difference in inflation pressure. The bend section in actuator 5.04 seemed to be detrimental to the performance of the actuator as it pushed the actuator onto its side rather than bending vertically as was intended.

Print set 6

Time

Figure 56. Actuator 5.05 intended actuation sequence.

Time

Inflation

Deflation

1 sequence

Figure 57. Actuator 5.06 intended actuation sequence.

Goals

The primary goal for this print set was to successfully actuate three different models that demonstrate complex actuation.

This print set iterated on the previous concepts addressing their issues. In an attempt to equalise the pressure needed to actuate the twisting/expansion geometry and the bending/extension geometry, a couple of changes were made:

1. The shore hardness of the twisting/expansion sections were increased from 40 to 50.
2. The wall thickness of the bending/extension sections was reduced from 1mm to 0.8mm.

Time

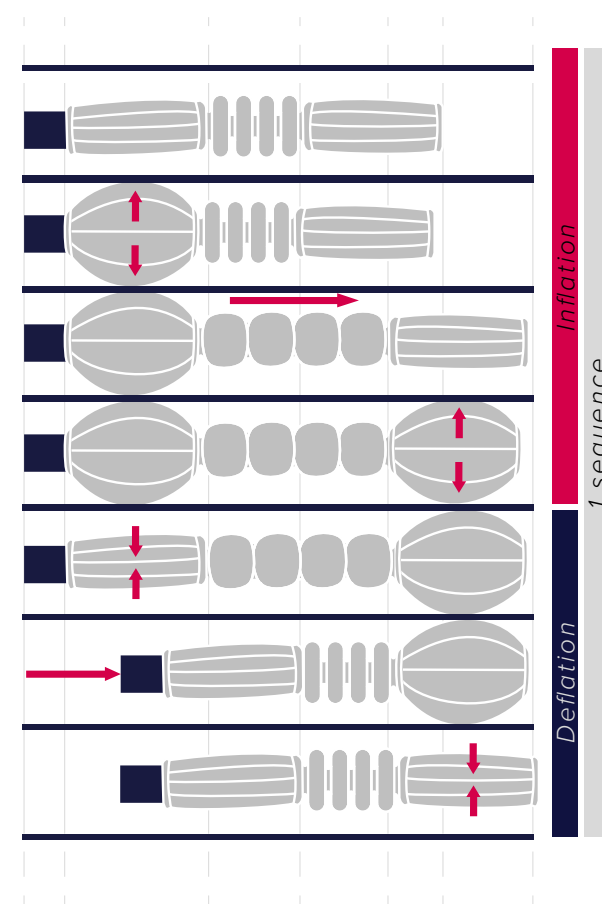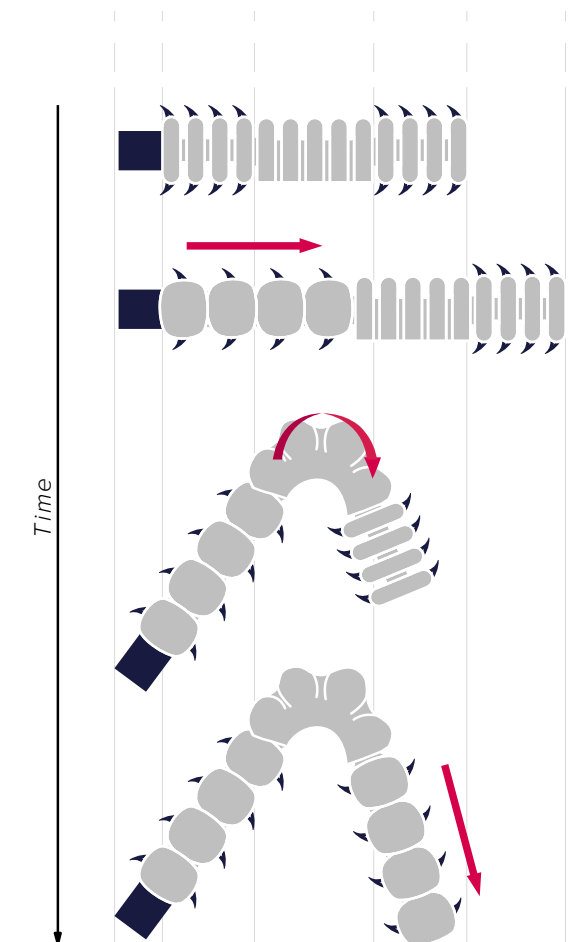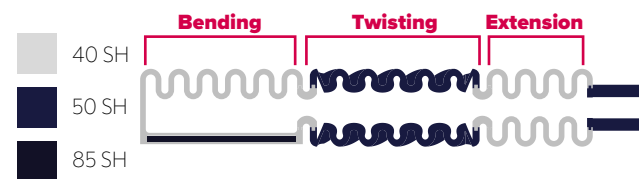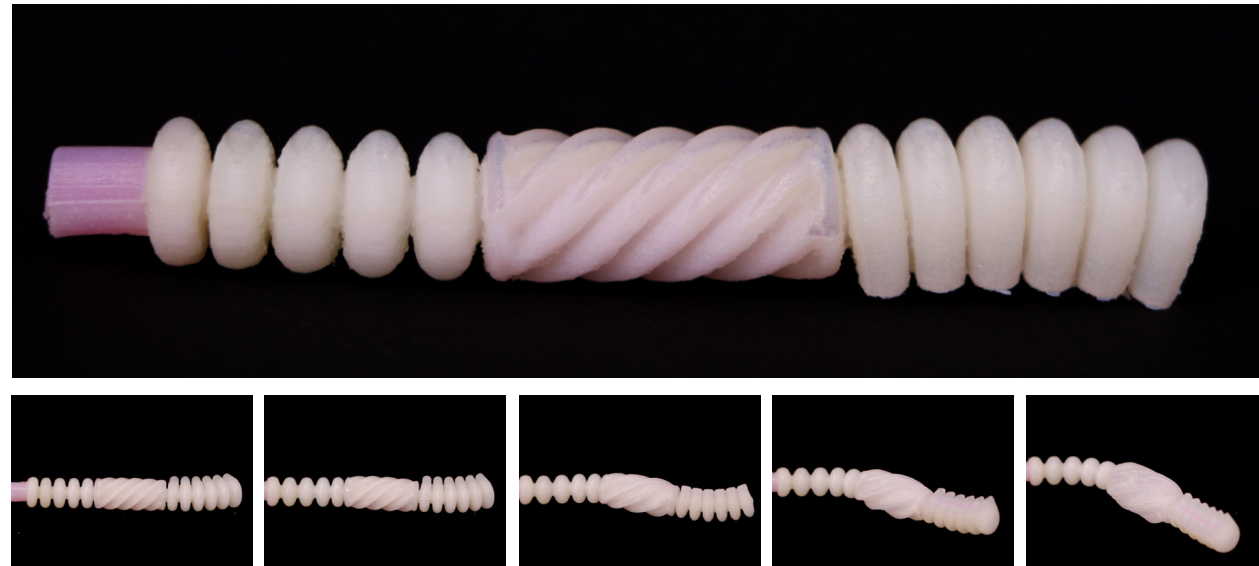*Figure 58. Actuator 5.07 intended actuation sequence.*

Actuator 5.05
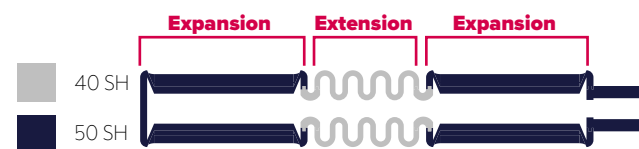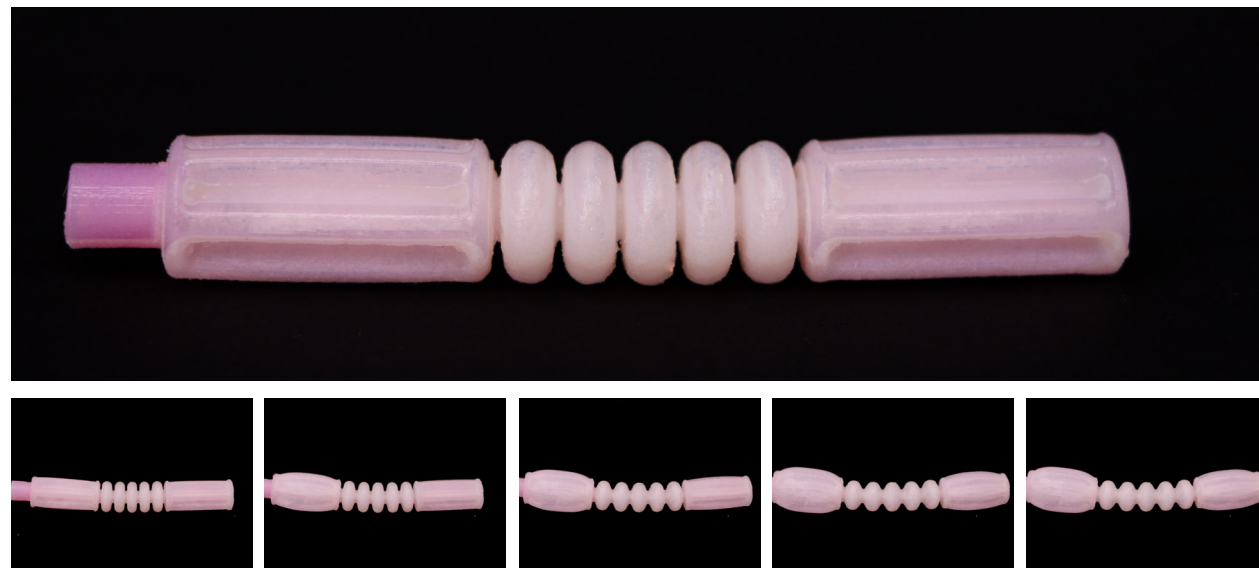### (twisting, bending, extension)

Aim: Create a soft robot capable of achieving multiple motions through one input.

Results: The extension and twisting sections successfully actuated. The bending section did not fully inflate due to the twisting section bursting.

Figure 59a - 59g. Actuator 5.05 geometry and inflation sequence.

Bending   Twisting   Extension

40 SH
50 SH
85 SH

Actuator 5.06
### (expansion, extension)

Aim: Create a soft robot capable of achieving multiple motions through one input.

Results: The print successfully actuated in all three sections, however, the expansion in the second expansion was much smaller than in the first. Bursts in the expansion sections limited the success in repeated tests.

Figure 60a - 60g. Actuator 5.06 geometry and inflation sequence.

Expansion   Extension   Expansion

40 SH
50 SH

Actuator 5.07
(bending, adhesion/extension)
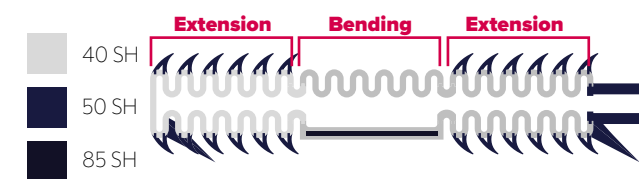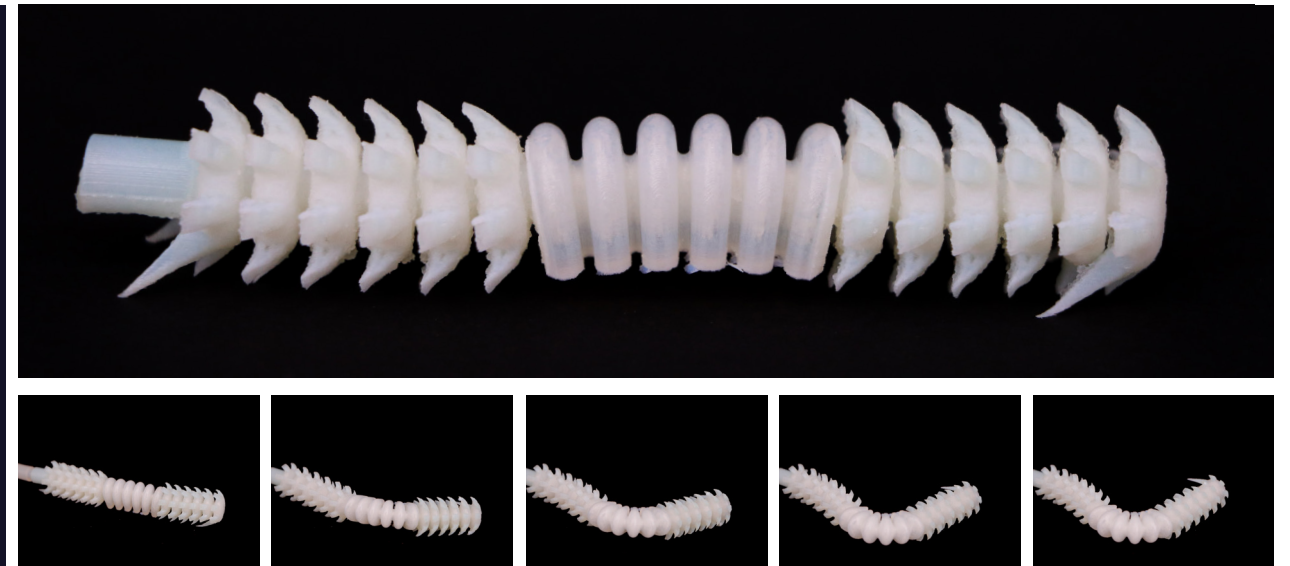
Aim: Create a soft robot capable of locomotion by utilising surface adhesion.

Results: All sections successfully inflated. The addition of longer hooks did not help to orient the print in the intended direction and it still fell onto its side from the bending section inflating.

Figure 61a - 61g. Actuator 5.07 geometry and inflation sequence.

Extension   Bending   Extension

40 SH
50 SH
85 SH

Analysis

The two prints that had a combination of the bending/extension and twisting/expansion geometry once again burst during inflation and did not fully actuate. Even the changes made in shore hardness and to wall thickness to equalise the pressure across all sections did not have any noticeable impact and the prints still burst quickly. The order that the sections were patterned appeared to have an effect. In actuator 5.05, the extension section fully actuated, but the bending section did not. This is likely because the extension section was before the twisting section relative to the input, so it could reach its actuation pressure before the twisting section inflated and burst. This could mean that prints with the expansion/twisting sections after the bending/extension sections would achieve greater success, however, this would severely limit the number of possibilities of the complex actuation that could be achievable. Actuator 5.07 fully actuated, however, it was unsuccessful in its movement. The longer hooks at the front and back ends of the print designed to keep it upright during inflation did not work as the print still fell on its side.
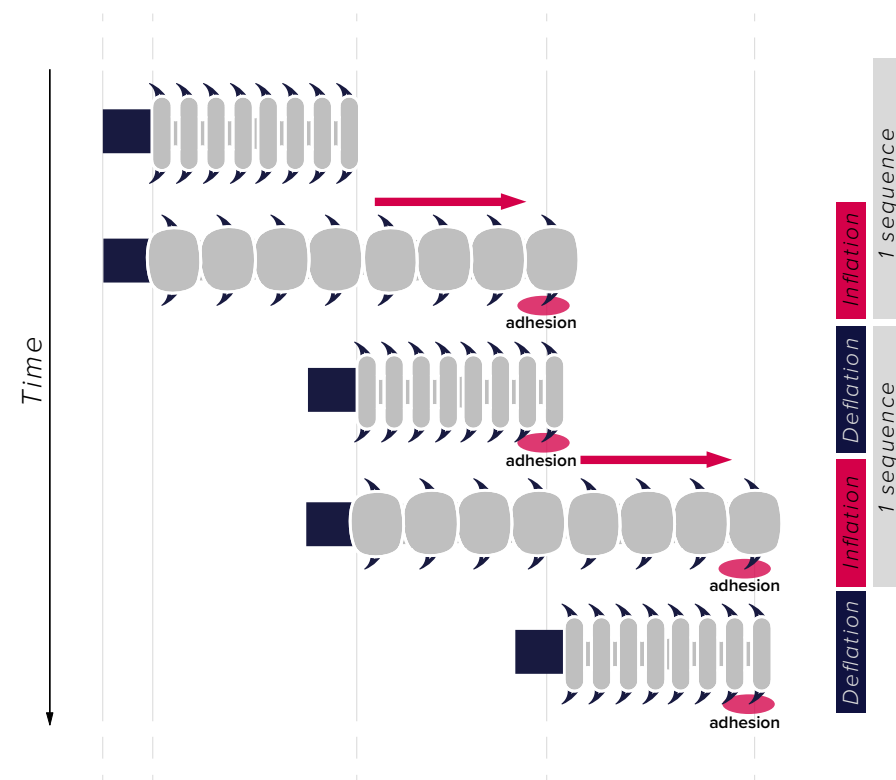
Print set 7

Goals

Figure 62. Actuator 1.11 intended actuation sequence.

- To print a larger scale extension print to compare its durability and performance to other models. This was printed with an increased wall thickness of 1.5mm.
- Print a bending+twisting actuator on a steeper offset angle to compare its performance to the previous bending+twisting print.
- Iterate on the original extension+adhesion print to improve the durability of the adhesive hooks. A surface was also 3D printed to help the extension+adhesion print successfully achieve linear locomotion.
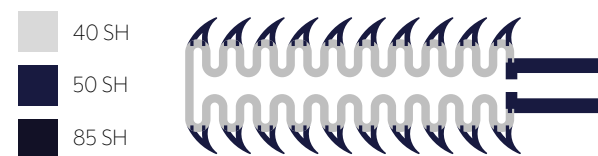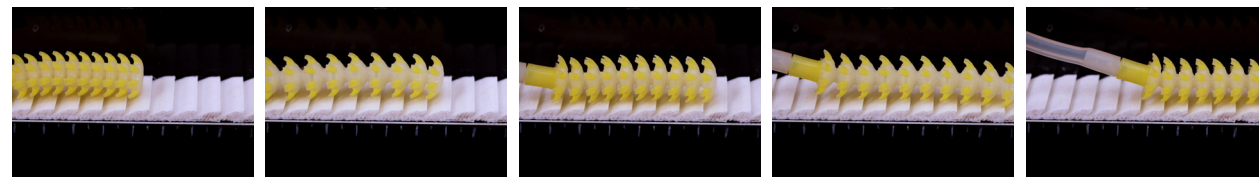
Actuator 1.10 *(large scale)*
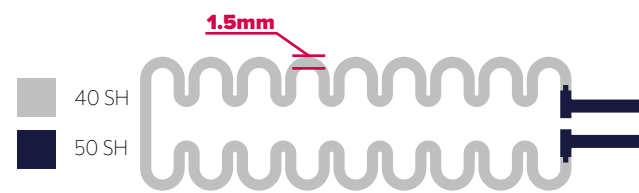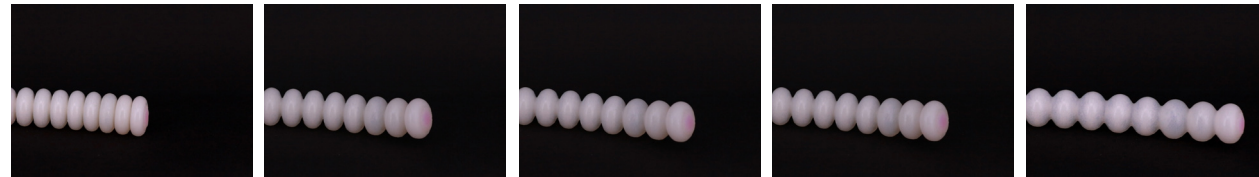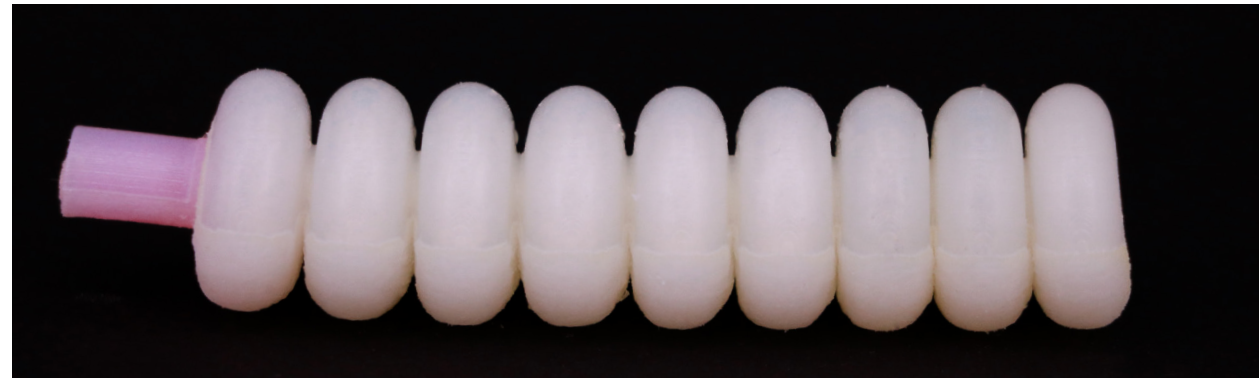
Aim: To assess how scale and wall thickness effect on the actuators strength and performance.

Results: The print fully actuated at 7psi without bursting. An extension percentage of 165% was reached.

1.5mm
40 SH
50 SH

Figure 63a - 63g. Actuator 1.10 geometry and inflation sequence.

Actuator 2.07 *(bending + twisting)*

Aim: Assess the effect of the bellow offset angle on the actuator's ability to follow a helical path upon inflation.

Results: The print successfully followed a helical path, and demonstrated a steeper helix angle to the 25° bellow offset print.

40°
40 SH
50 SH

Figure 65a - 65g. Actuator 2.07 geometry and inflation sequence.

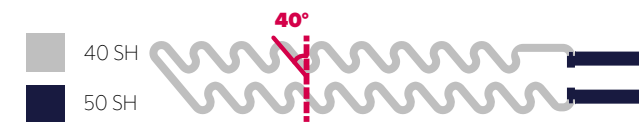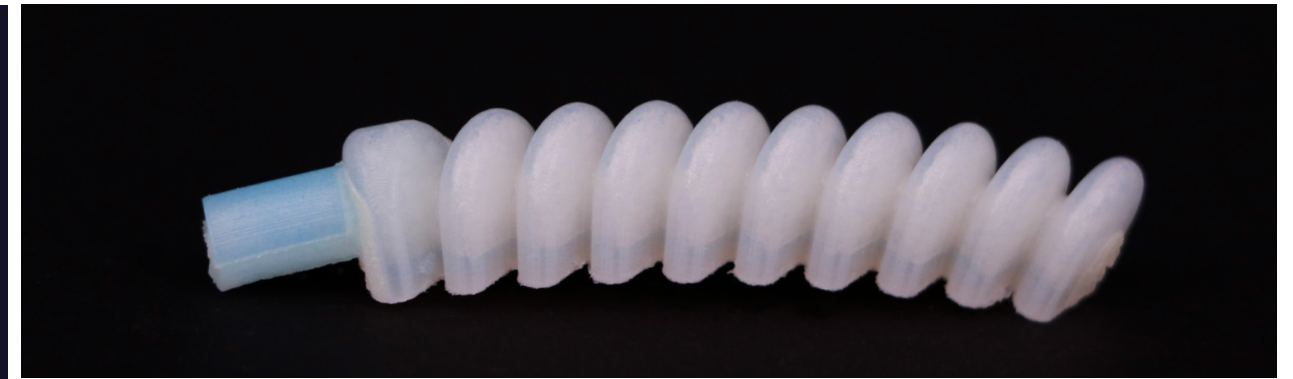## Actuator 1.11 *(adhesion geometry)*

Aim: Create a soft robot capable of locomotion by utilising surface adhesion to a designed surface.

Results: The print successfully adhered to the printed surface, and was able to pull itself along at 2.3mm/s.

40 SH
50 SH
85 SH

Figure 64a - 64g. Actuator 1.11 geometry and actuation sequence.

Analysis

Scaled extension actuator (1.10):

This print demonstrated much better durability to previous extension prints. This was evident from its high actuation pressure and its ability to hold the pressure. When this actuator was deflated, it took much longer for the actuator to depressurise than the other extension actuators, which could indicate that the air is only being let out through the pump, whereas, with the smaller extension prints, faster depressurisation could have occurred due to small tears in the print allowing air to escape.

Extension/adhesion actuator (1.11):

This was the first print to successfully demonstrate linear locomotion. By calibrating the pressure limit of the pump to the maximum inflated state of the actuator, the pump pulsed its airflow, allowing the actuator to inflate and deflate repeatedly. The adhesion geometry on the actuator was able to successfully hook onto the adhesive surface, which pulled the actuator forward when it was deflated and this was repeated to achieve locomotion. The actuator moved at 2.3mm/s, which was increased in later testing to 2.9mm/s by decreasing the space between the hooks in the adhesive surface.

Bending + twisting actuator (2.07):

The increase of the bellows offset from the previous bending + twisting print had a clear impact on the helix angle that the print followed during actuation. When the offset angle of the bellows is increased, so is the offset of the actuation from the primary axis of bend.
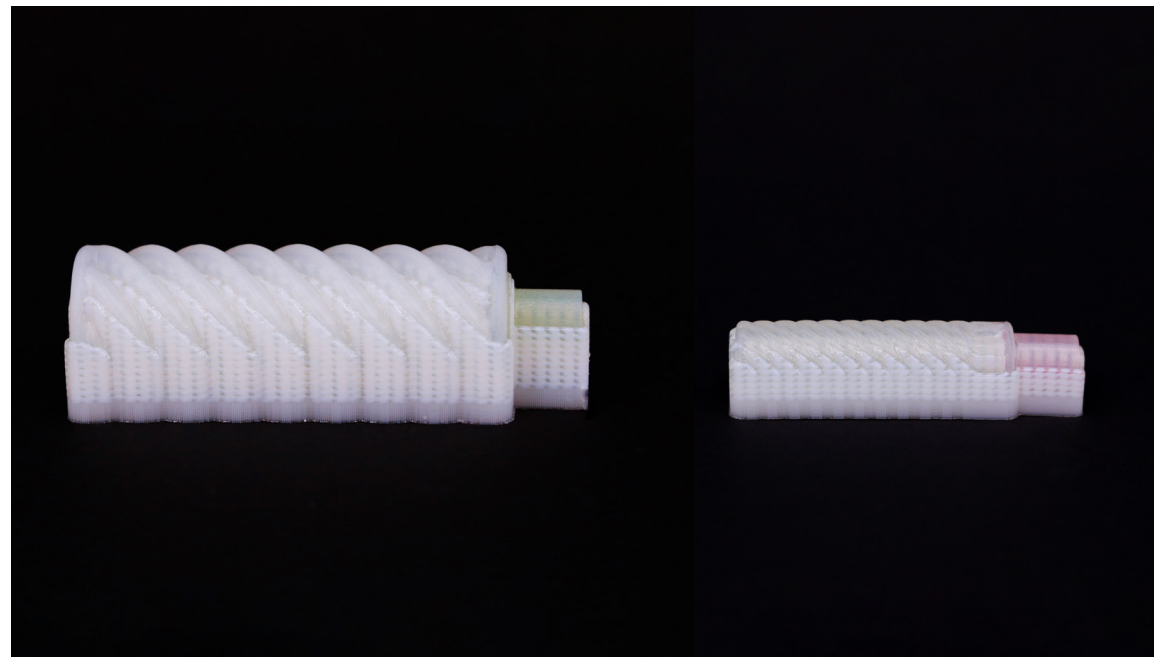
Print set 8

Goals

This print set tested two actuators at a larger scale for twisting and expansion. Like the bending test, the wall thickness was increased to 1.5mm. The goal was to determine whether the increase of wall thickness would allow the print to actuate at a pressure comparable to the scaled bending print.

The second goal of this print set was to re-evaluate the internal valve geometry so that it was more compatible with the print resolution. To do this, the complex geometry was replaced with a simple hole in the middle of two extension sections. The diameter of the hole was given three separate values, to determine the pressure at which the hole would allow air to pass through.
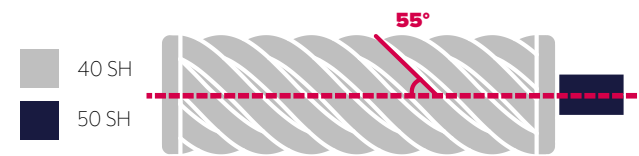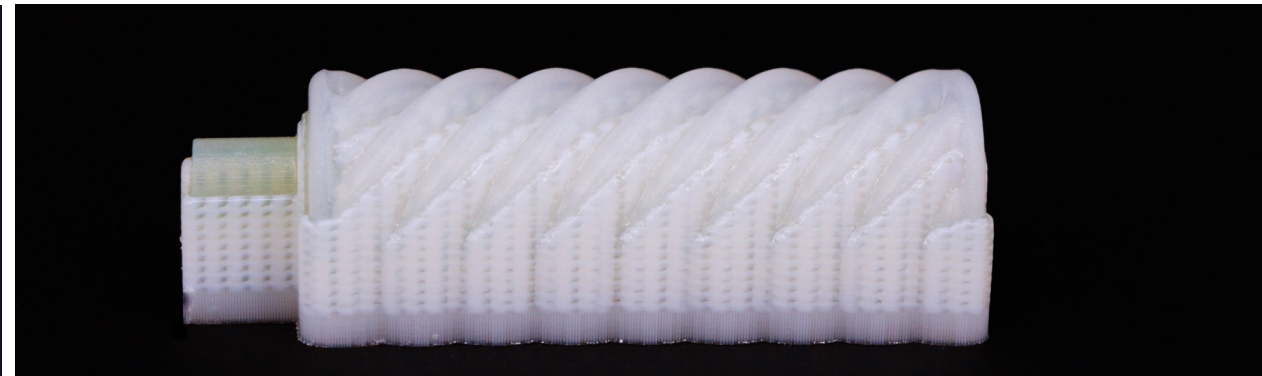
Figure 66. Difference in size of large scale prints.

Actuator 3.11 *(scaled up)*

Aim: To assess how scale and wall thickness effect on the actuators strength and performance.

Results: Small geometric gaps in the lofts at the ends let air out in the first tests. Once these were patched with glue, the print burst along one of the inner radii at 5psi. A twist angle of 5.0°/mm (258° total)was reached.

Figure 67a - 67g. Actuator 3.11 geometry and inflation sequence.

40 SH
50 SH
55°

Actuator 1.11-1.13 *(internal valve 0.1mm to 0.3mm)*

Aim: Create a valve capable of controlling the sequence of actuation.

Results: 0.1mm and 0.2mm valve holes did not let any air through up to 10psi. The 0.3mm valve hole let air through to the second section at 4psi.

Figure 69a - 69g. Actuator 1.11-1.13 geometry and inflation sequence.

40 SH
50 SH
0.05mm

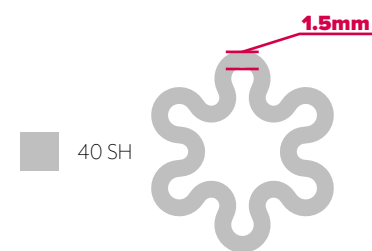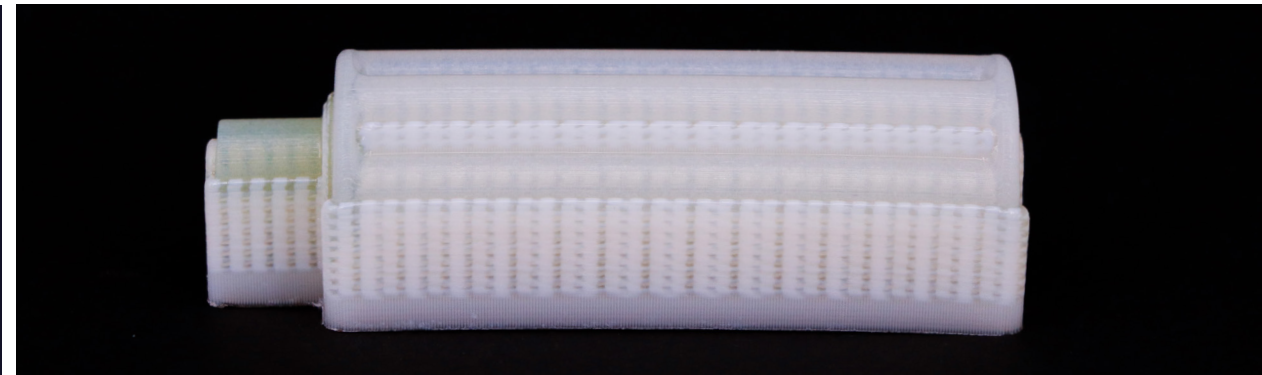## Actuator 4.03 *(scaled up)*

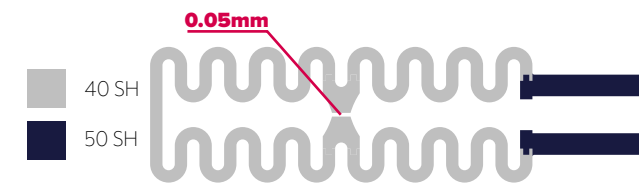**Aim:** To assess how scale and wall thickness effect on the actuators strength and performance.

Results: Small geometric gaps in the lofts at the ends let air out in the first tests. Once these were patched with glue, the print burst along one of the inner radii at 5psi. An expansion percentage of 148% was reached.

40 SH
1.5mm

Figure 68a - 68g. Actuator 4.03 geometry and inflation sequence.

Analysis

The large scale prints in this set did not yield much success. For them to be a success, they needed to actuate at the same pressure as the extension geometry at the same scale. As the extension print required 7psi to fully actuate and the large scale prints in this set burst at 5psi, this was deemed a failure.

The pressure relief valves yielded some success, where the 0.3mm valve managed to hold pressure until reaching 4psi, at which point the air flowed through to the second half of the actuator and it fully inflated. The main issue with this, however, was that when the actuator was retested after the initial test, the valve no longer restricted the airflow and the actuator fully inflated without successful actuation sequencing. This was likely due to the valve being blocked by material until it reached 4psi initially, and after the material had been removed the air flowed freely through the valve.

Print set 9

Goals

This print set aimed to explore how the print orientation of the models on the Stratasys J750 would impact their performance. Both the twisting and the expansion geometry prints were printed laying horizontally and standing vertically on the print bed (*Figure 70*). These models were chosen as they are the models that burst at the lowest pressures across the experimentation. To test the pressure at which they burst, the pump's maximum pressure was increased in 0.5psi increments.

Figure 70. Horizontal and vertical print orientations.

Actuator 3.12 *(horizontal print orientation)*
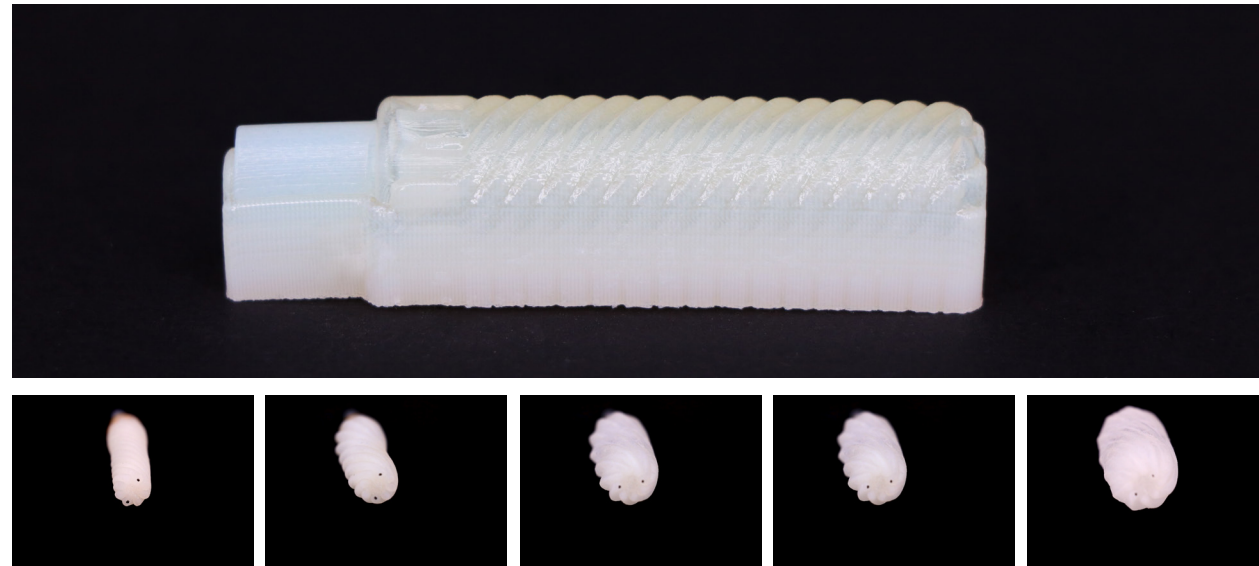
Aim: Assess the effect of the model's print orientation on the performance of the actuator.

Results: The print failed at 1psi ± 0.5 and reached a twist angle of 9.9°/mm before bursting (345° total).

Figure 71a - 71g. Actuator 3.12 geometry and inflation sequence.

Actuator 3.13 *(vertical print orientation)*

Aim: Assess the effect of the model's print orientation on the performance of the actuator.

Results: The print failed at 1.5psi ± 0.5 and reached a twist angle of 9.5°/mm before bursting (331° total).

Figure 72a - 72g. Actuator 3.13 geometry and inflation sequence.

Actuator 3.14 *(angled print orientation)*

Aim: Assess the effect of the printer's UV power levels on the performance of the actuator.

Results: The print failed at 1psi ± 0.5, however, this was due to a large material tear that occurred during cleaning along one of the troughs and it only reached a twist angle of 1.7°/mm before bursting (59° total).

Figure 73a - 73g. Actuator 3.14 geometry and inflation sequence.

Actuator 4.04 *(horizontal print orientation)*
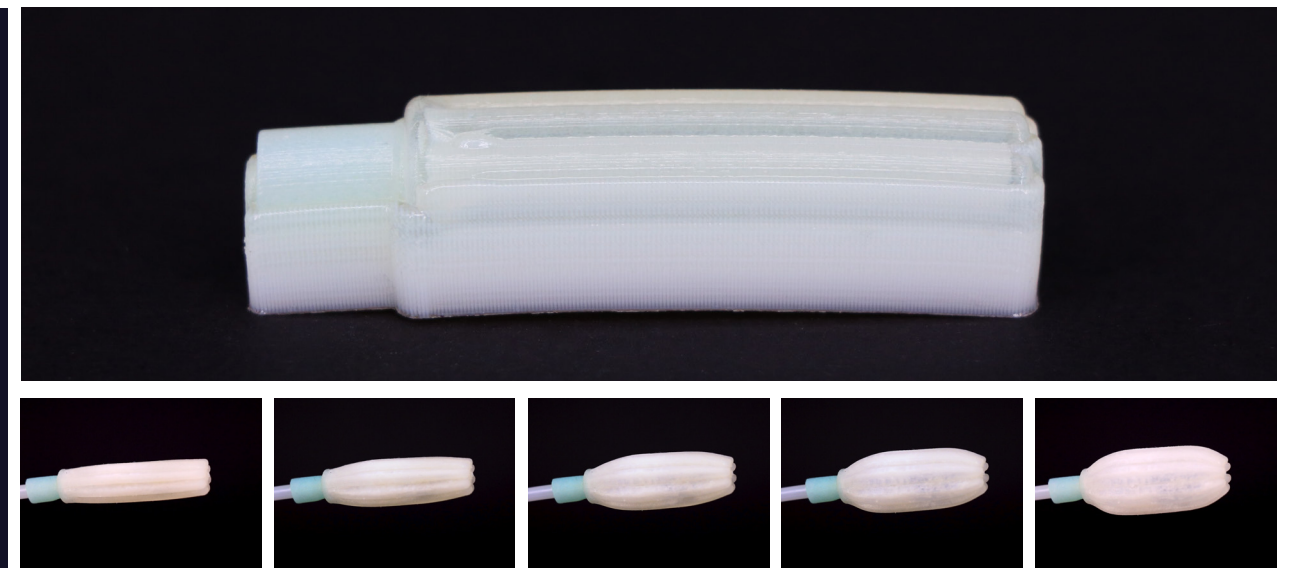
Aim: Assess the effect of the model's print orientation on the performance of the actuator.

Results: The print failed at 1psi ± 0.5 and reached an expansion percentage of 167% before bursting.

Figure 74a - 74g. Actuator 4.04 geometry and inflation sequence.

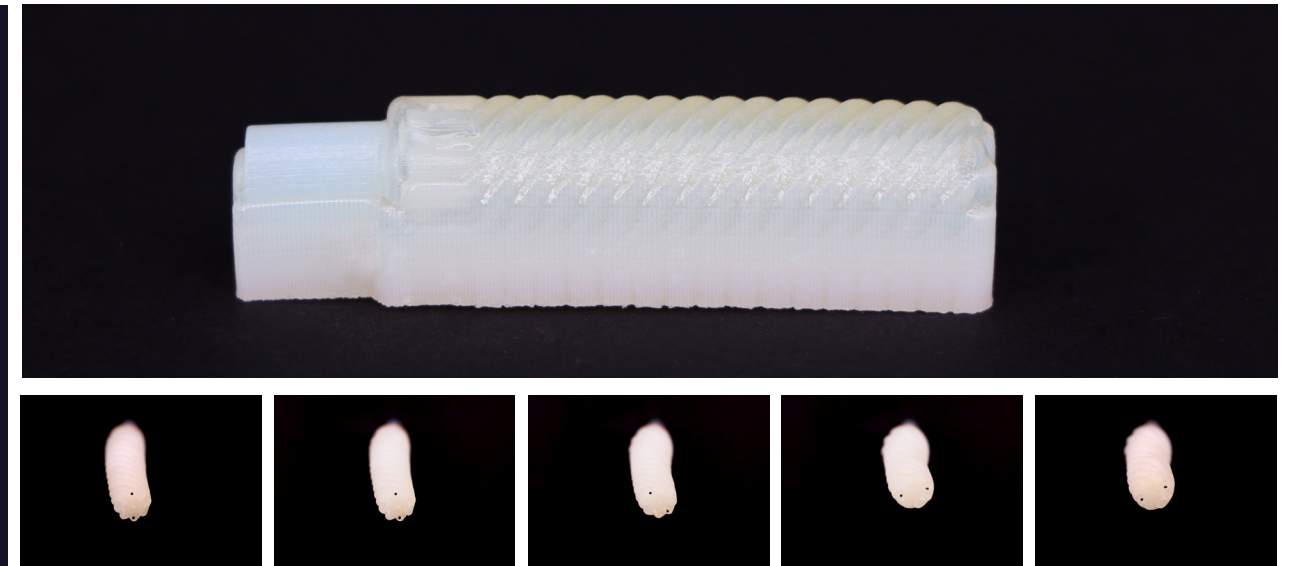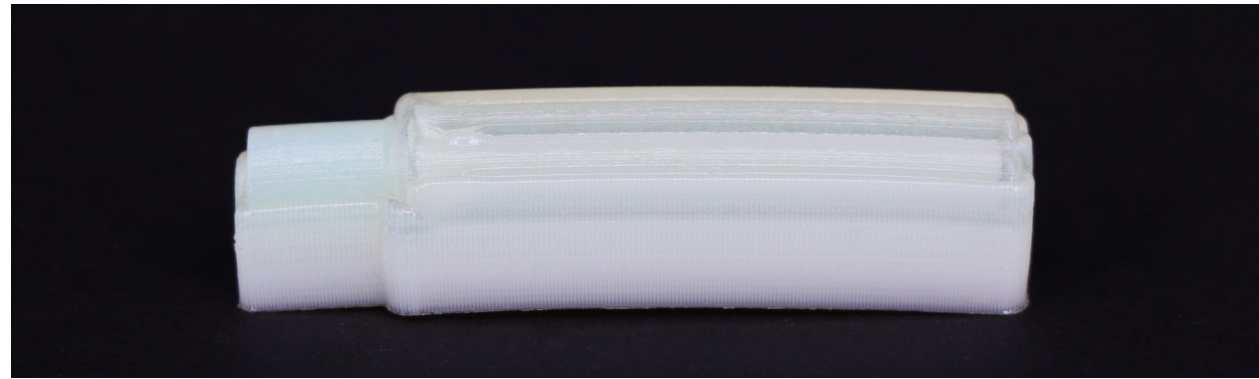*Figure 75a - 75g. Actuator 4.05 geometry and inflation sequence.*

Aim: Assess the effect of the model's print orientation on the performance of the actuator.

Results: The print failed at 1.5psi ± 0.5 and reached an expansion percentage of 212% before bursting.

Analysis

Although the accuracy of the pressure testing isn't high enough to draw conclusions at these pressures, there was a clear difference in the expansion percentage between the vertically and horizontally oriented expansion prints. A similar result appeared to occur in the twisting prints, however, the expansion percentage was not recorded. The angled orientation twisting print (3.14) exhibited a larger weakness during cleaning than either the vertically (3.13) or horizontally (3.12) oriented prints, which suggests that having the troughs align with the print direction does negatively impact the durability of the material. This is also supported by the difference in expansion percentages between the vertically (4.05) and horizontally (4.04) oriented expansion prints. The twist percentage of the vertically and horizontally oriented prints also supports this. The horizontally oriented print showed a slightly larger twisting percentage than the vertically oriented print (14° larger). For the vertical orientation print, the layer print direction is offset by 35° from bellows angle, whereas for the horizontal orientation the layer print direction is offset by 55° from the bellows angle. From these results, it was concluded that the bellows that are at a larger offset angle from the print layers tend to be less prone to tearing and that the optimal print orientation is when they're perpendicular to each other. Therefore, the print orientation of the models does have an impact on performance, even though it may be only slight.

Print set 10

Goals

This print set aimed to explore how the UV light power of the Stratasys J750 affects the performance of the models. The models for this print set were printed with the lowest UV power, with the hope that this would allow the resin to fuse the layers together more than the standard UV light power that has been used for all other prints. Like print set 9, the twisting and expansion actuators were printed in both horizontal and vertical print orientations which allowed for direct comparisons in performance to be made with print set 9, which were all printed with standard UV levels.

Figure 76. Horizontal and vertical print orientations.

Actuator 3.15
(low UV, horizontal print orientation)
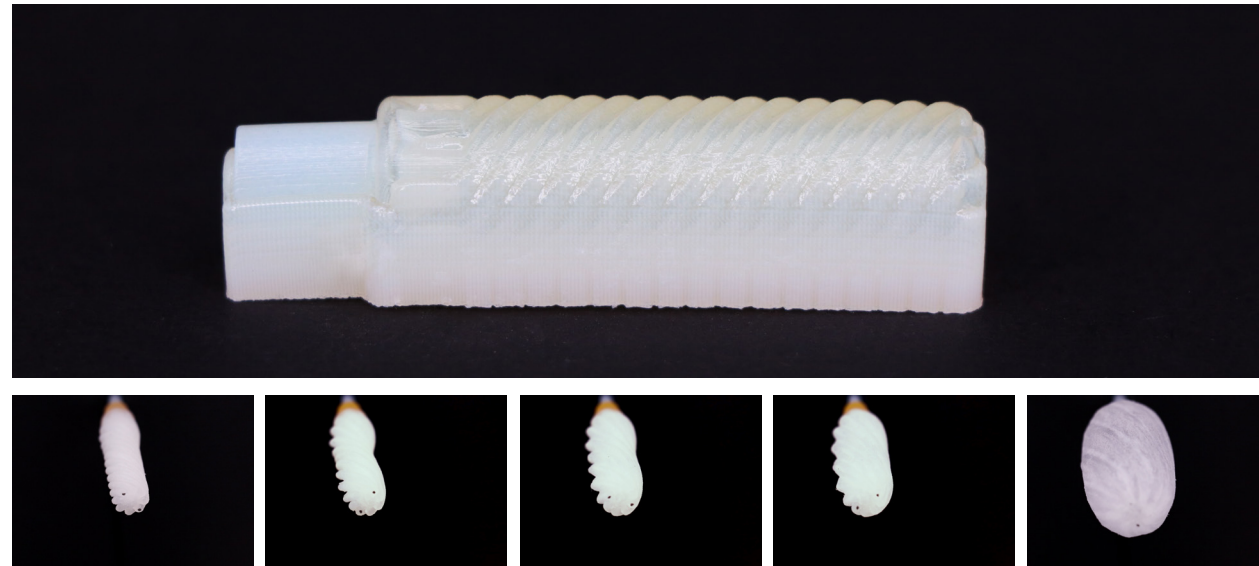
Aim: Assess the effect of the printer's UV power levels on the performance of the actuator.

Results: The print failed at 1.5psi ± 0.5 and reached a twist angle of 9.5°/mm before bursting (303° total).

Figure 77a - 77g. Actuator 3.15 geometry and inflation sequence.

Actuator 3.16
(low UV, vertical print orientation)

Aim: Assess the effect of the printer's UV power levels on the performance of the actuator.

Results: The print failed at 1.5psi ± 0.5 and reached a twist angle of 8.7°/mm before bursting (356° total).

Figure 78a - 78g. Actuator 3.16 geometry and inflation sequence.

Actuator 4.06
(low UV, horizontal print orientation)

Aim: Assess the effect of the printer's UV power levels on the performance of the actuator.

Results: The print failed at 1psi ± 0.5 and reached an expansion percentage of 181% before bursting.

Figure 79a - 79g. Actuator 4.06 geometry and inflation sequence.

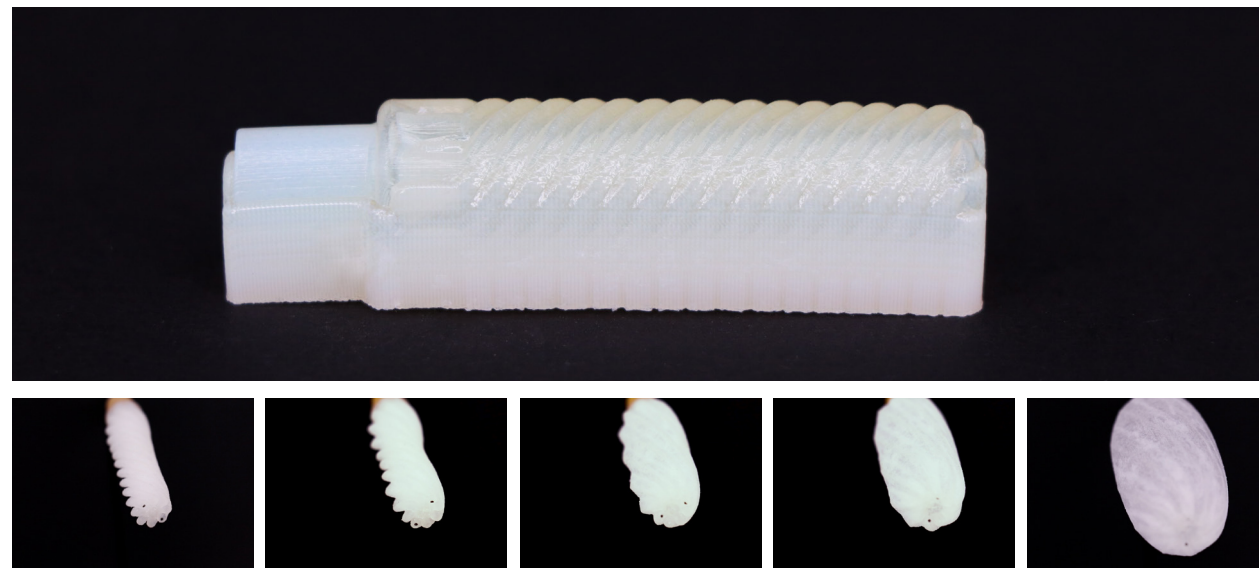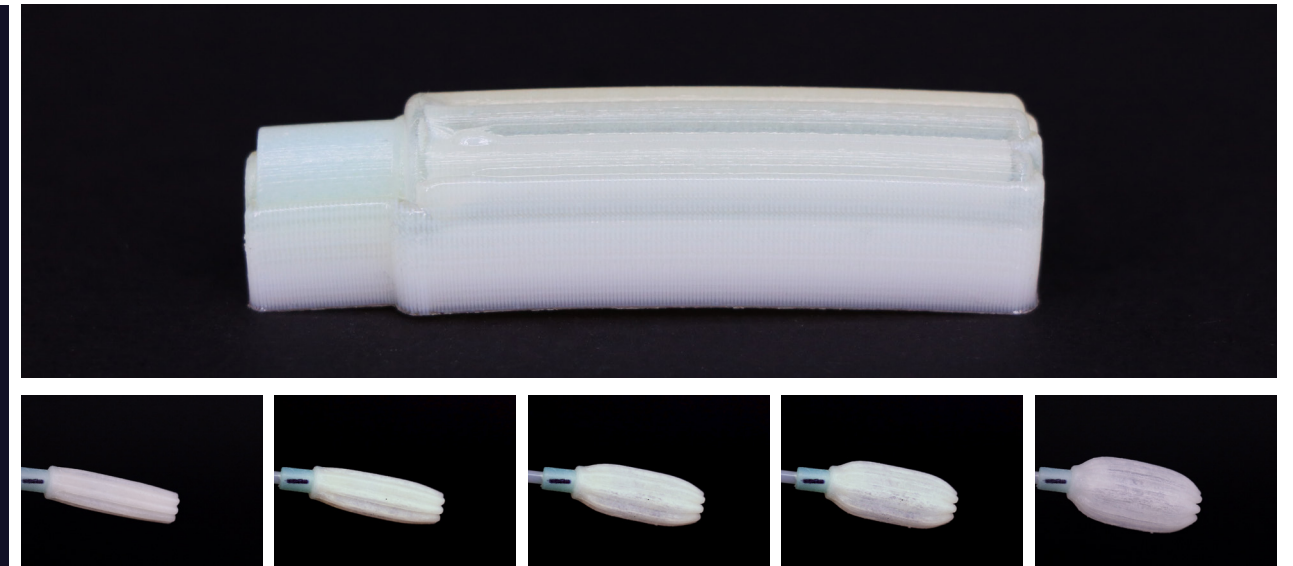## Actuator 4.07
(low UV, vertical print orientation)
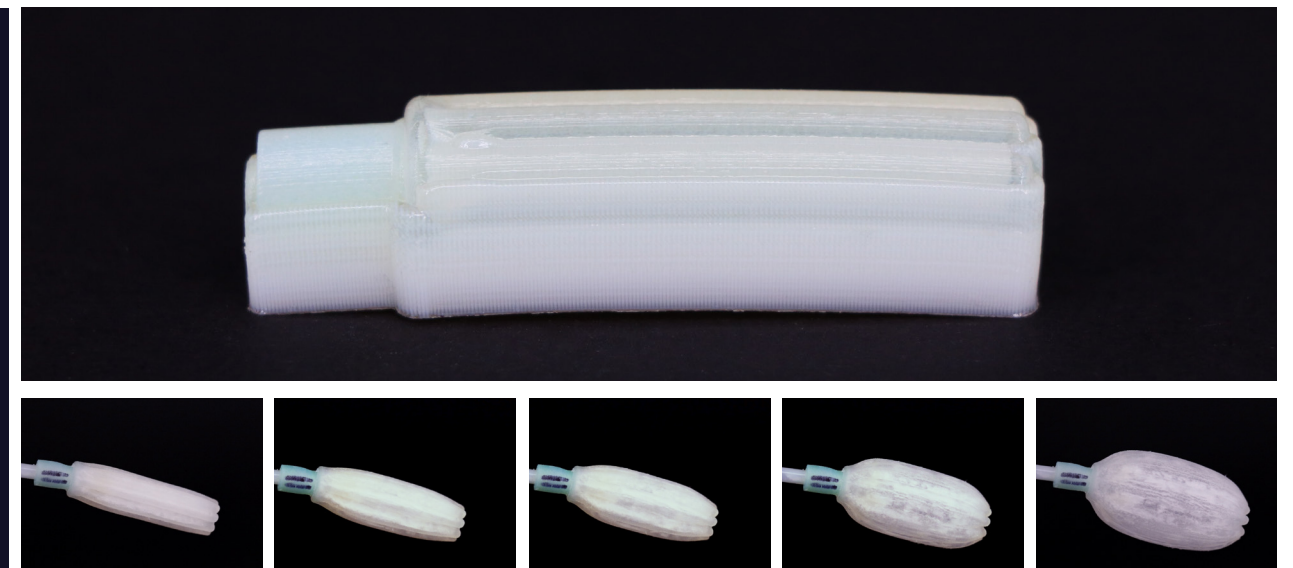
Aim: Assess the effect of the printer's UV power levels on the performance of the actuator.

Results: The print failed at 1.5psi ± 0.5 and reached an expansion percentage of 212% before bursting.

Figure 80a - 80g. Actuator 4.07 geometry and inflation sequence.

Analysis

The difference in performance between the two tests is contradictory, as the low UV horizontal expansion test (4.06) outperformed the normal UV horizontal expansion test (4.04) but both low UV twisting tests (3.15 & 3.16) performed worse than the normal UV (3.12 & 3.13). This suggests that uncontrolled variables such as variations in print quality and manual cleaning are what is changing the performance – not the UV levels. This hypothesis could be tested by printing many of the same model and testing their maximum performances to find averages to determine the variation in the prints that need to be taken into account. This has not been done for this project as it does not help to accomplish the project goals, and is suggested as a useful topic for future study.

Print set 11

Goals

This print set was done on a Connex 350 3D printer rather than the Stratasys J750 so that a different soft material could be trialled. The Connex 350 had Tango, an alternative to Agilus, loaded in its print tray. Tango has slightly different material properties to Agilus, and has a 27SH as opposed to 30SH for Agilus. This material was tested so that its performance could be directly compared with the Agilus material. Each of the main four established primary motions were printed in this material.

Figure 81. Tango and Agilus materials.

Actuator 1.14 *(Tango material)*

27 SH

Aim: Assess the performance of the Tango material in comparison to the Agilus material over a number of different geometries.

Results: The print failed at 10psi and reached an extension percentage of 166% before bursting.
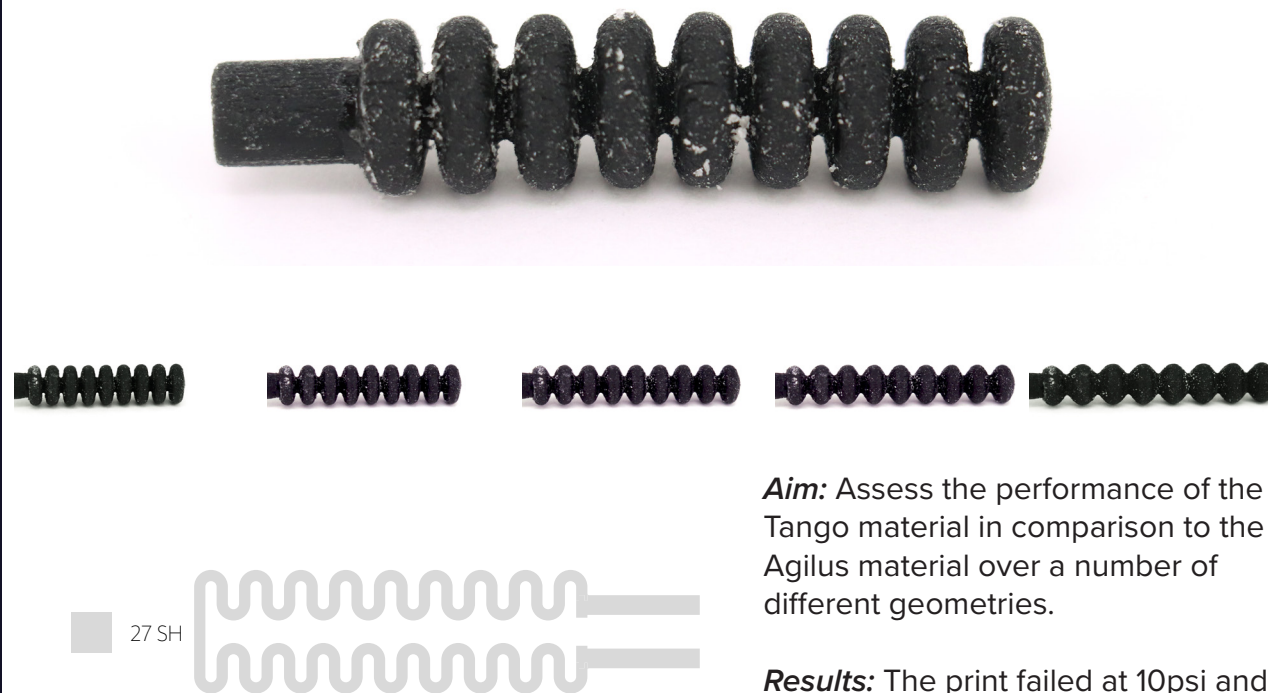
Figure 82a - 82g. Actuator 1.14 geometry and inflation sequence.
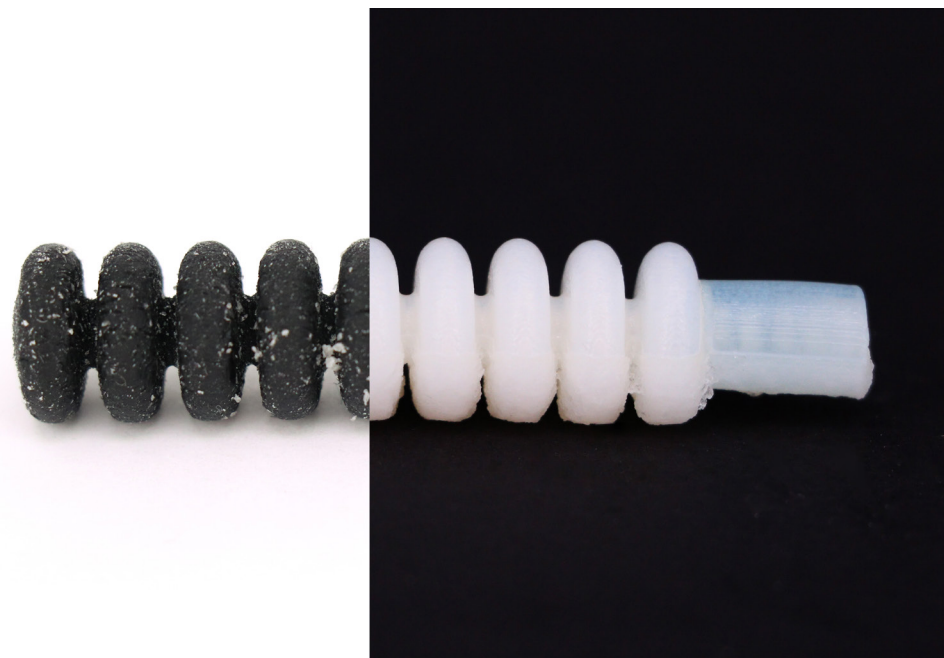
Actuator 3.17 *(Tango material)*

27 SH

Aim: Assess the performance of the Tango material in comparison to the Agilus material over a number of different geometries.

Results: The print failed at 1psi ± 0.5 and reached a twist angle of 10.2°/mm before bursting (356° total).

Figure 84a - 84g. Actuator 3.17 geometry and inflation sequence.

Actuator 2.08 *(Tango material)*

27 SH

Aim: Assess the performance of the Tango material in comparison to the Agilus material over a number of different geometries.

Results: The print failed at 10psi ± 0.5 and reached a maximum bend angle of 7.0°/mm before bursting (246° total).
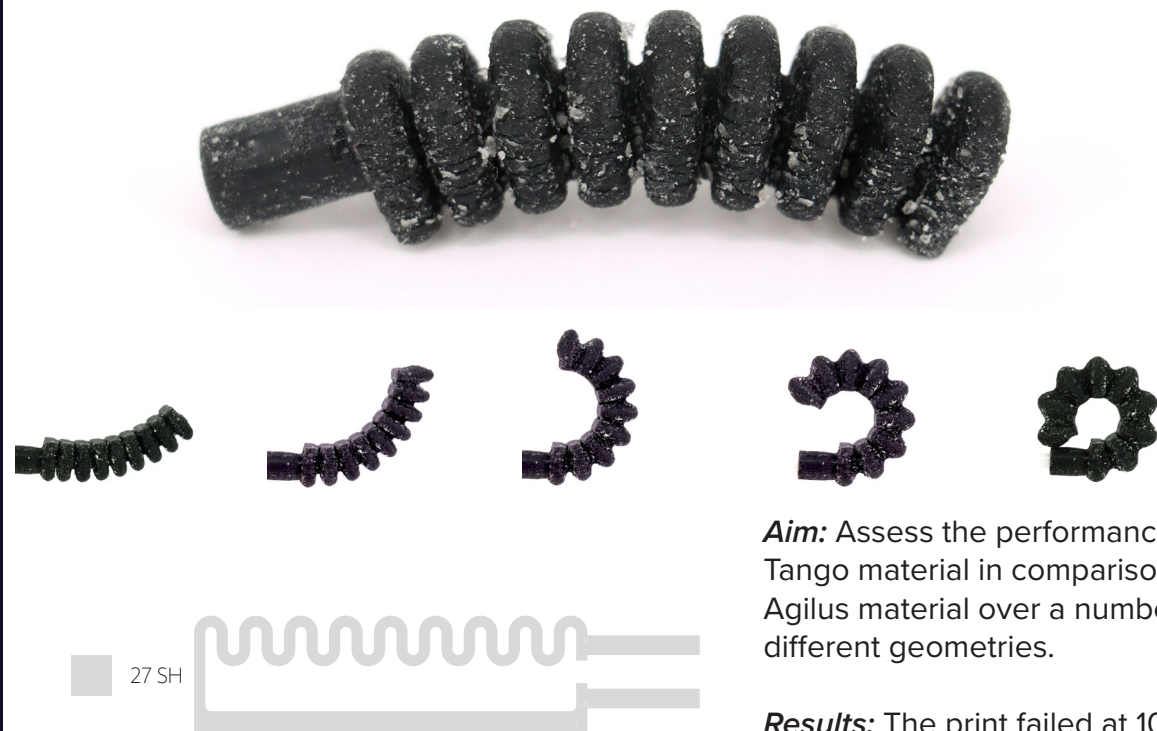
Figure 83a - 83g. Actuator 2.08 geometry and inflation sequence.

Actuator 4.08 *(Tango material)*

27 SH

Aim: Assess the performance of the Tango material in comparison to the Agilus material over a number of different geometries.

Results: The print failed at 1.5psi ± 0.5 and reached an expansion percentage of 194% before bursting.

Figure 85a - 85g. Actuator 4.08 geometry and inflation sequence.

Analysis

The variations in performance to the Tango prints and their Agilus counterparts were minimal. The Tango prints for the twisting and extension geometries achieved larger deformations than their Agilus counterparts, however, the difference in performance was insignificant (10.2°/mm compared to 10.0°/mm for the twisting print, 166% compared to 162% for the extension print). The expansion and bending geometries performed worse than their Agilus counterparts; 194% compared to 211% for the expansion geometry, and 7.2°/mm compared to 7.0°/mm for the bending geometry. Although a direct comparison in the performance of materials cannot be made due to the difference in material shore hardness, the results for all prints did not yield largely different results worth pursuing further to achieve complex motion.

It is important to note that although the failure pressure of actuators 1.14 and 2.08 were 10psi, they deformed to reach their actuated state at a much lower pressure. This large difference in failure pressure was indicative of the issues that arose around the complex actuators throughout the experimentation.

Print set 12

AgilusClear (Shore-A 30)

Shore-A 35

Shore-A 40

Shore-A 50

Shore-A 60

Shore-A 70

Shore-A 80

Shore-A 95

Vero (Shore-A 100)

Figure 86. Stratasys J750 Shore A Hardness used for strain restricting region in print set 12.

Goals

This print set aimed to explore how the shore hardness of the strain restricting layer in the bending actuator would affect the total bend angle (*Figure 86*). This was done to further understand the relationship between materiality and geometry.

Actuator 2.09
(strain restricting shore hardness 40)

Aim: Assess the effect of the shore hardness of the strain restricting region on the total deformation.

Results: The print was able to reach a maximum bend angle of 7.1°/mm (250° total).
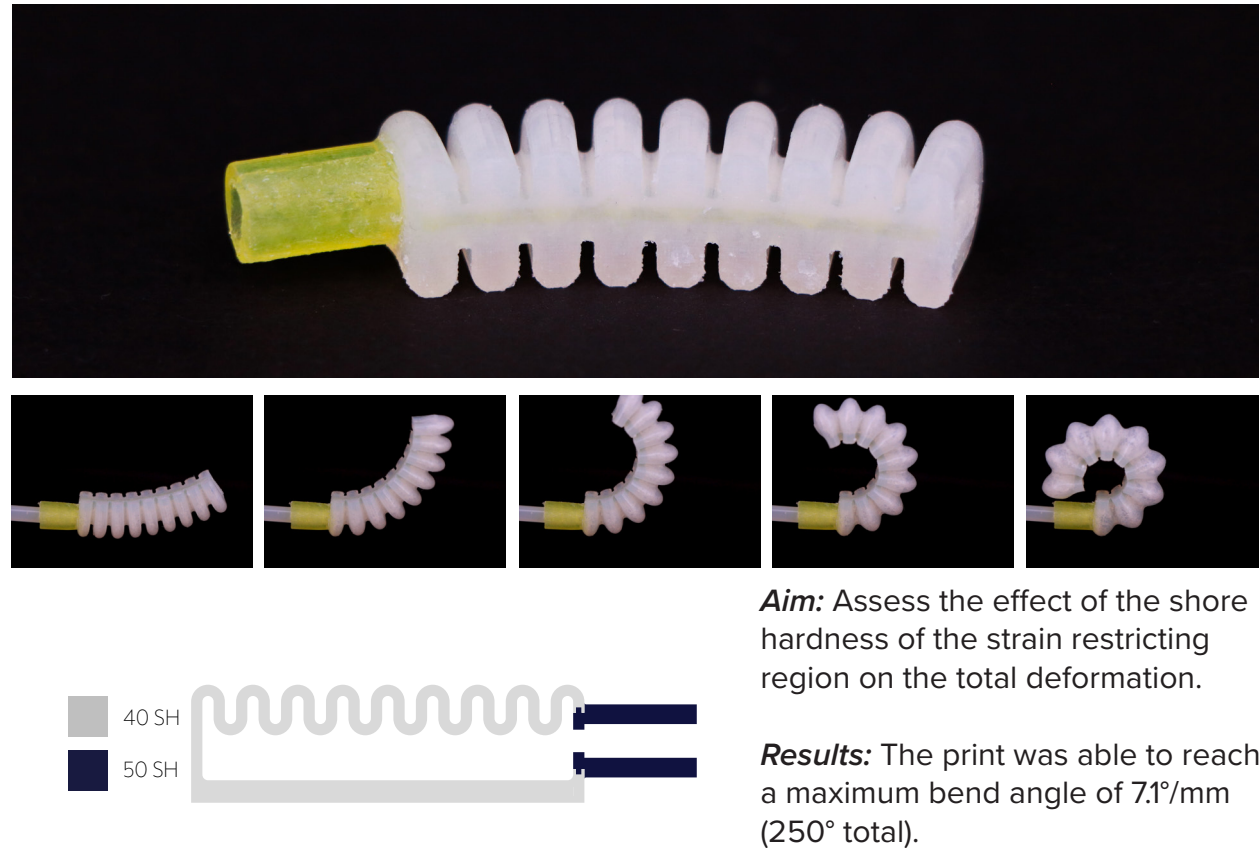
Figure 87a - 87g. Actuator 2.09 geometry and inflation sequence.

- 40 SH
- 50 SH

Actuator 2.10
(strain restricting shore hardness 100)

Aim: Assess the effect of the shore hardness of the strain restricting region on the total deformation.

Results: The print was able to reach a maximum bend angle of 3.3°/mm (116° total).

- 40 SH
- 50 SH
- 100 SH
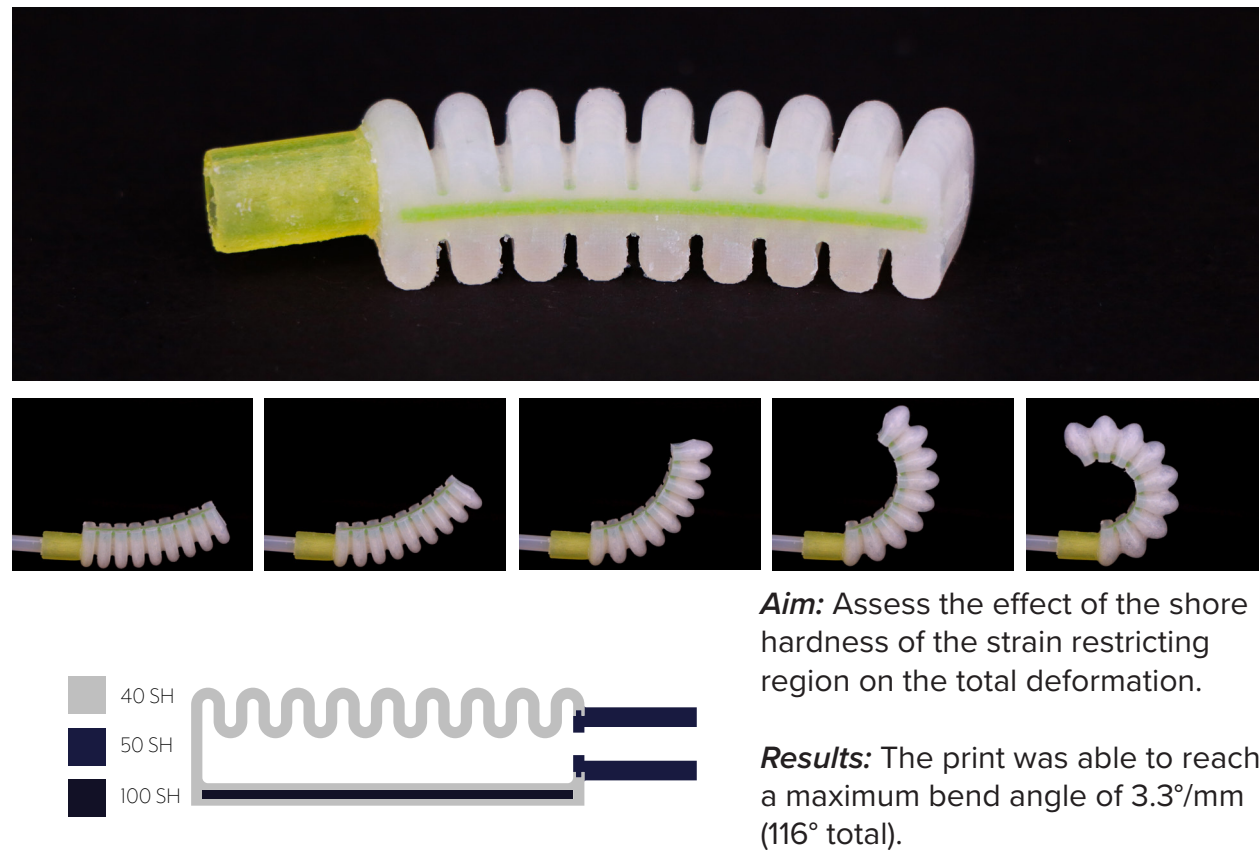
Figure 88a - 88g. Actuator 2.10 geometry and inflation sequence.

Analysis

This print set shows that the shore hardness of the strain restricting region on the bending actuator does have an effect on its performance. The low shore hardness print (2.09) achieved a very similar total bend to actuator 2.04 (7.1°/mm to 7.2°/mm) . From this it can be inferred that, if the shore hardness is too high, this will start to decrease the performance of the actuator, otherwise its effect is negligible.

FINAL PRINTS
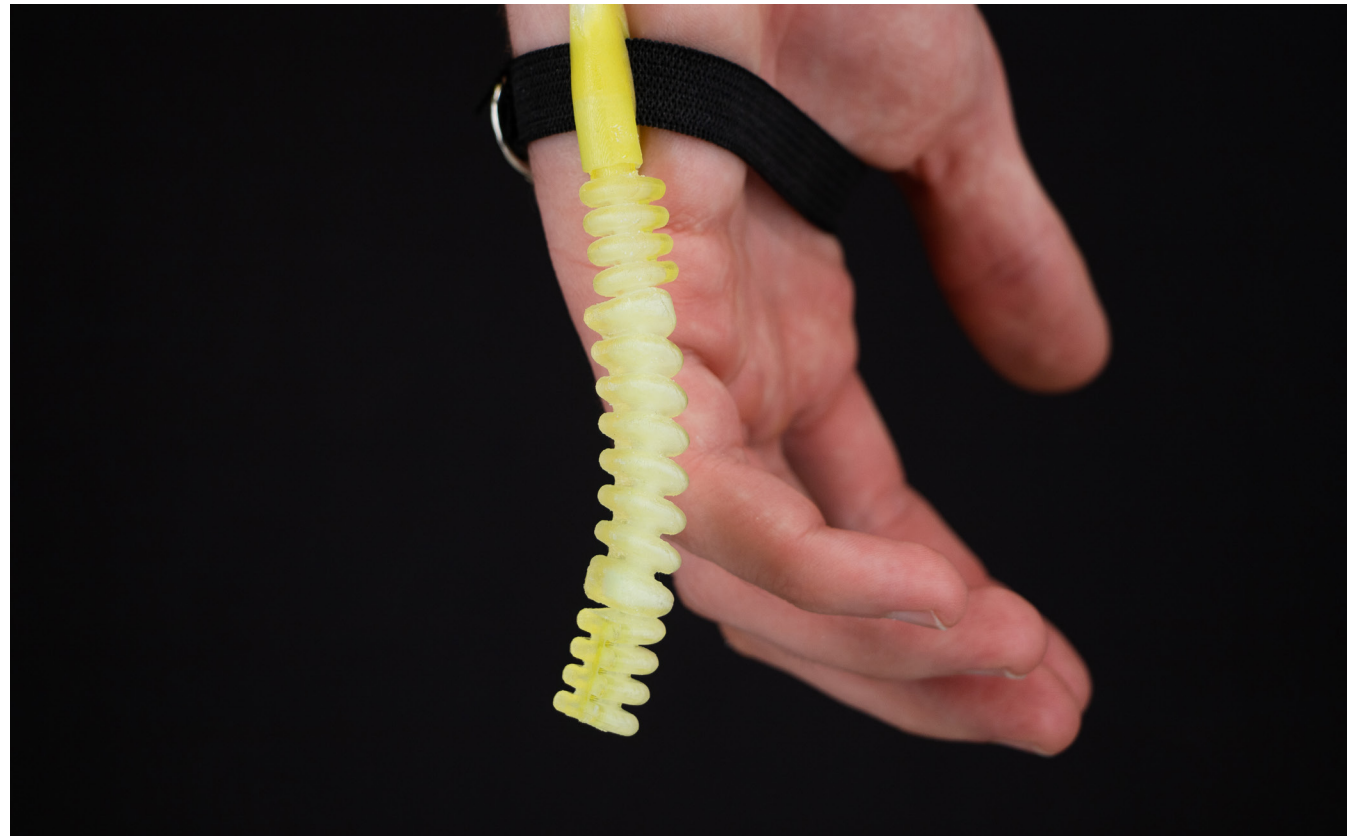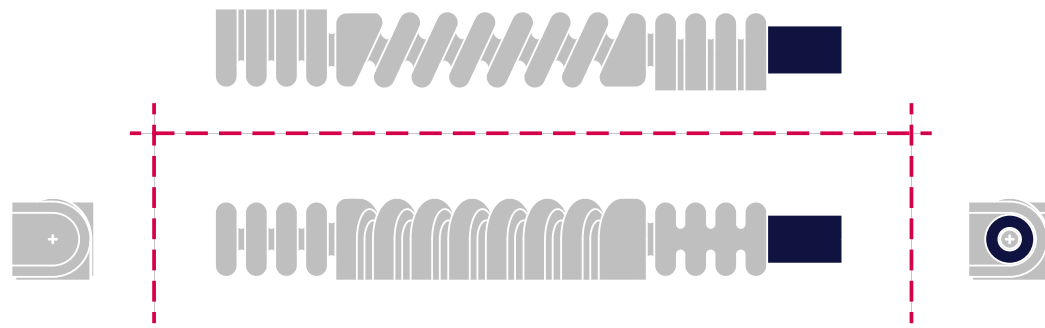
Pneumatic finger

Taking inspiration from prosthetic artist and researcher Dani Clode and her Third Thumb project (2017), this print demonstrates an actuation with multiple segments capable of three-dimensional motion. By combing different orientations of the bending geometry as well as the bending/twisting geometry, the print is able to wrap around the pinkie finger when inflated. Although this print demonstrates no practical purpose in itself, it demonstrates how configuring the motions that have been identified throughout the literature can be utilised to achieve complex actuation capable of human interaction.
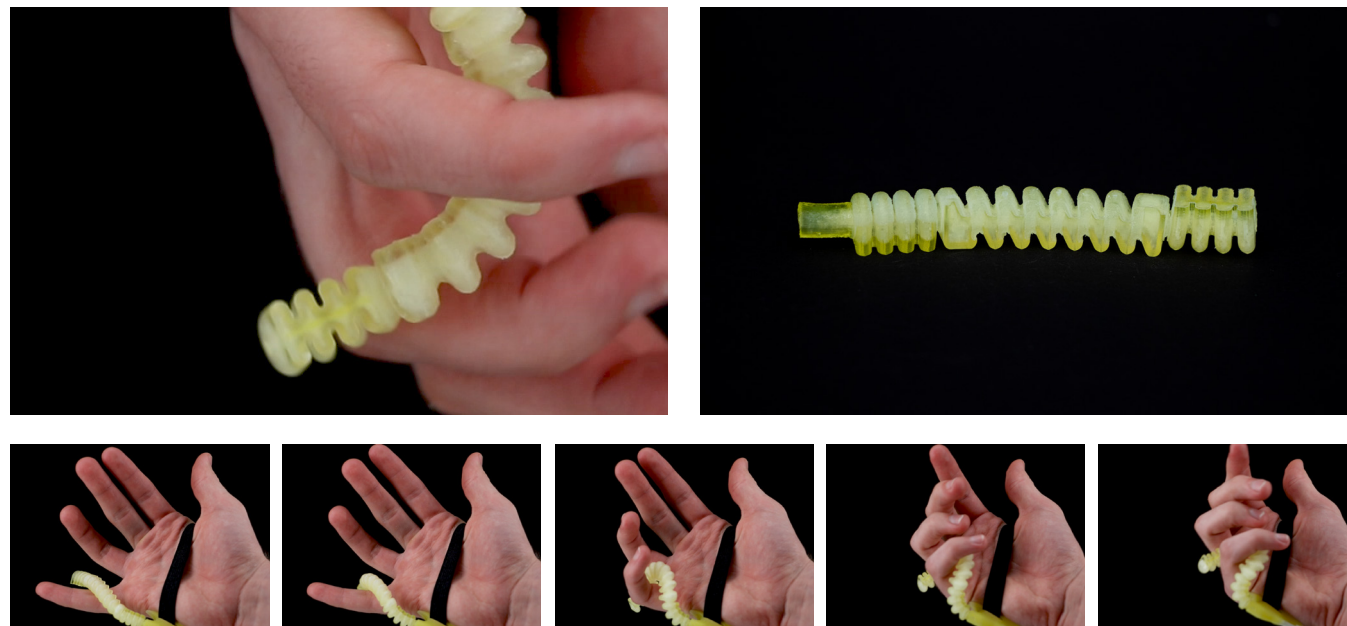
Figure 89a - 89i. Pneumatic finger print geometry and actuation sequence.

SECTION A-A

Gripper

This final gripper modified the bending motion to have a pointed tip and connected three actuators to a printed pneumatic splitter. The geometry was modified so that it could pick up a larger range of objects as the pointed tip allowed it to curl further around objects. This print successfully demonstrates the compliance of soft robots, as the gripper was able to pick up a lemon, half a garlic clove, a cherry tomato, and a marble all without any trouble. The gripper changed its hold depending on the size of the object it was wrapping around, and as a result, was able to pick up objects of varying size and weight.
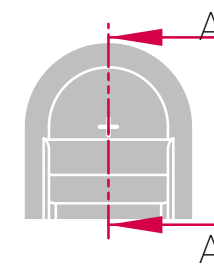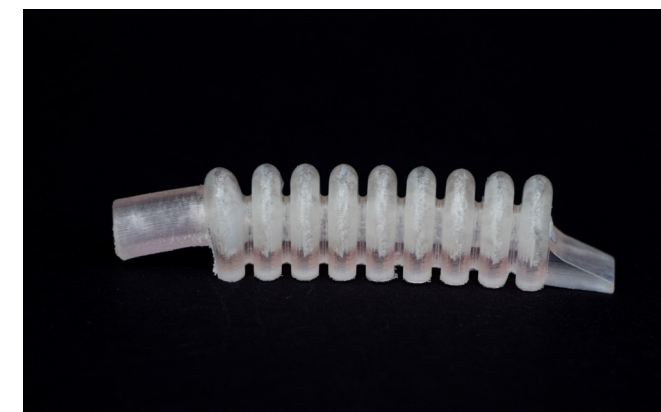
Figure 90a - 90g. Gripper print geometry and demonstration gripping various objects.

SECTION A-A

Locomotive extender

By utilising the previous success of the actuator 1.11, this print utilises the deformation achieved by the extension motion and the added gripping abilities of mechanical interlocking geometry to traverse a short obstacle course. The actuator was able to crawl through a small gap, traverse a length of level terrain, and scale a small incline by switching between inflation and deflation states. This print, although reliant on a special interlocking terrain, demonstrates the locomotive capabilities of a multi-material 3D printed soft robot actuated through only one pneumatic input.

Figure 91a - 91i. Extension/adhesion print geometry and locomotion along a course.

Video of final demonstrators can be found at: https://vimeo.com/manage/videos/501302018

DISCUSSION

Summary

This portfolio has explored the possibilities and complexity of motion achievable in pneumatically actuated soft robots. By taking inspiration from muscular hydrostats found across the animal kingdom, 3 primary motions were identified, explored, optimised, and finally combined to achieve a variety of complex motions.

This research has demonstrated that soft robots printed on the Stratasys J750 can not only actuate with performance that can rival other soft robots using alternative fabrication methods, but it also gives a further insight into the relationship between geometry and materiality during actuation. This is most evident in the bending motion. As the most documented soft robotic motion, this research has demonstrated that bending is also very achievable through multi-material printing. By experimenting with the shore hardness of the strain restricting layer in the actuator, it was found that materiality can have a substantial impact on the performance of the actuator. It was also found that the geometry of the actuator significantly impacts the performance – possibly more so than the materiality as seen in actuators 2.03 and 2.04 (*Figure 92*). Although these actuators are not directly comparable, they are derived from the same geometry and demonstrate that in this research, it was much easier to achieve the desired motion through altering the geometry of the actuator rather than the materiality.

The motion that required the fewest changes to its geometry was the extension actuator. This was the motion that served as a base model for all other motions, and the geometry was based on literary examples (Drotman et al., 2017, p.5533) which allowed for early success. As this motion proved to be successful and reliable, it was used to test new design ideas. The extension geometry was used as a base geometry for the internal valve concepts and the scaled print. The internal valves were ultimately unsuccessful, as they did not reliably restrict airflow to sections of the actuator. The scaled prints proved that when the wall thickness of the actuators was increased, they were less prone to material tears and bursting during inflation. Unfortunately, due to the large cost of the larger scale prints, more widespread large scale testing was not feasible for this portfolio.
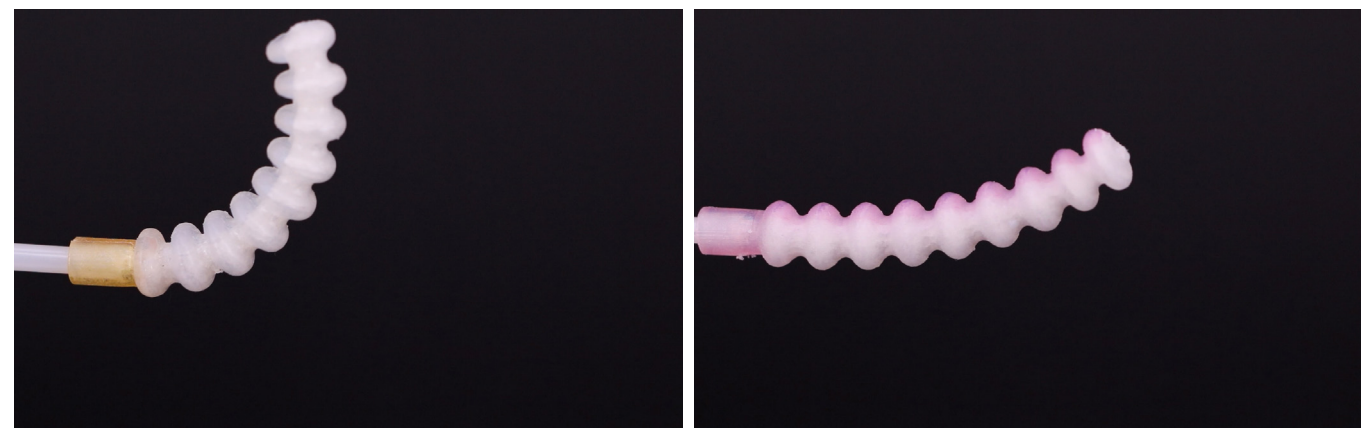
The motion that yielded the most success was the twisting geometry. Once the bellows were patterned axially (first in print set 3) the twisting actuators achieved much larger twist angles than their literary counterparts. The largest twist angle found in an actuator in the literature was 5.6°/mm (Schaffner et al., 2018) which utilised helically arranged strain restricting regions to achieve twist. This research presents a maximum twist angle of 12.4°/mm (actuator 3.07) although the actuation with this geometry was unreliable and material failures occurred after repeated actuation. A twist angle of 9.7°/mm (actuator 3.08) was reached for which the actuator was able to reliably reach across repeated tests (*Figure 93*). This result is significant because it demonstrates a novel geometry for twisting soft robots that can achieve a high twist angle that can't be fabricated with a moulding and casting process. As an extension of the twisting geometry, an expansion motion was also created which yielded some success. This motion was achieved when the helix angle of the twisting Solidworks model was set to 0°. This allows for a complex model with this motion to easily switch between the twisting and expansion geometry without having to switch separate models in and out of the assembly.

The early testing of adhesion geometries demonstrated that mechanical interlocking was the adhesion method most successful at the printable resolution of the Stratasys J750. All of the geometries which allowed for mechanical interlocking significantly outperformed the geometries which did not. This was particularly evident on the felt material, which worked much like Velcro to allow for the mechanical interlocking geometries to stay attached when upside down. This was expanded upon for the final locomotive extender concept, which successfully utilised mechanical interlocking surface adhesion to achieve linear motion at 2.3mm/s.

Figure 92. Actuators 2.03 (left) & 2.04 (right) in their inflated states.

Figure 93. Impact of the helix angle of the twisting geometry on the total twist angle.

Figure 94. Successful combinations of motion for complex actuation.

Bending	40 SH 50 SH 85 SH *Actuator 2.04*		*Bend angle* *7.2°/mm* *(253° total)*
Twisting	40 SH 50 SH 55° *Actuator 3.08*		*Twist angle* *9.7°/mm* *(339° total)*
Expansion	40 SH *Actuator 4.05*		*Expansion percentage* *212%*
Extension	27 SH *Actuator 1.14*		*Extension percentage* *166%*

Figure 95. Largest deformation results for each key motion.

Limitations

The main drawback that was encountered during this research was that the soft Agilus material on the Stratasys J750 was prone to tearing, especially after repeated actuation (*Figure 96*). Experiments were done to assess how the print orientation of these models and UV light print exposure would affect their performance, as well as how the Tango material compares both in terms of tearing and overall performance of motion. The only one of these variables that did have an impact on the performance of the actuators was the print orientation, although for this research it was minimally significant.

The tearing of the material also had a large impact on the possibilities for complex actuation. All prints that included both the extension/bending geometry as well as the twisting/expansion geometry failed to some extent (*Figure 94*). This was because the twisting/expansion geometry actuator burst at a lower pressure (1.5psi) than the actuation pressure of the extension/bending geometry actuator (approx. 4psi). This was particularly evident in Print set 11. This was largely caused by the different base geometries of the models – the extension and the bending actuators were derived from the same base geometry, as were the twisting and expansion actuators. Further changes to parameters such as wall thickness and shore hardness could be made for more successful results, however, this was not tested as it would require drastic alterations to be made to the base geometry of the actuators.

This research aimed to assess the possibilities of soft robotic actuation through one pneumatic input, and limitations were reached as the edge of the range of capabilities using this method was encountered. Sequencing of motion proved to be challenging using one input because the internal valves were unsuccessful. Although they were able to restrict airflow between sections for the initial inflation of the actuator, this was not able to be repeated. This was likely because the initial restriction of airflow was caused b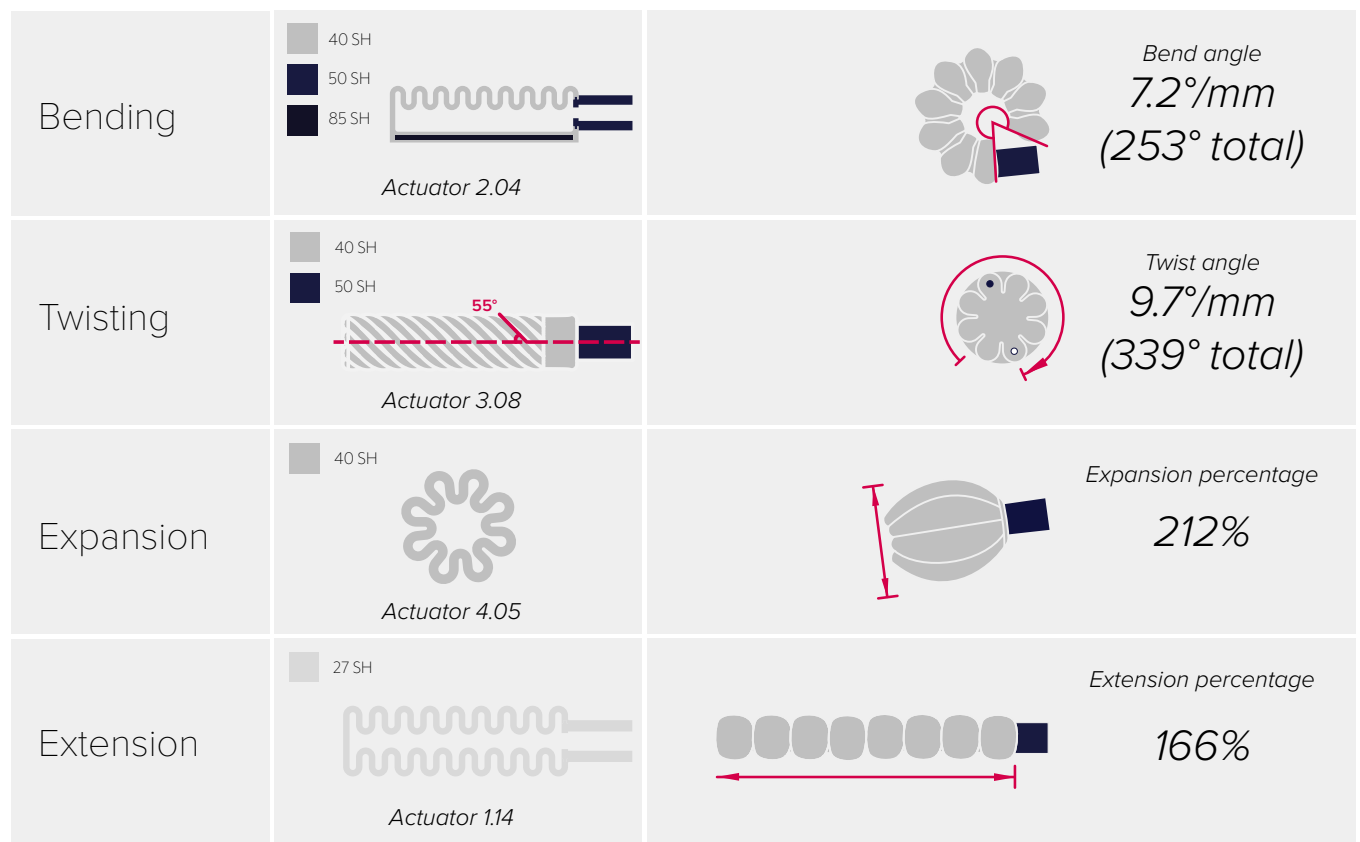y an internal blockage of support material or that the airflow passing through the valve damaged the valve so that it was unable to restrict airflow again. This suggests that sequencing of motion may require the utilisation of multiple pneumatic inputs.

Limited access to the Stratasys J750 printer due to Covid-19 impacted the number of prints that were possible in the experimentation section of this research. Earthquake strengthening of the building also took place during the experimentation phase of this portfolio, which further restricted the access to the Stratasys J750 printer. In response, compromises were made regarding the total number of print sets that could be produced, and the range of goals for the print sets was lowered. As experiments had to be condensed onto fewer print trays, the learning opportunities and iterative changes that could be made between each print set was restricted.

Figure 96. Print set 1 material tear.

Future Research

This portfolio demonstrates an exploration of Polyjet printed soft robots with a singular pneumatic input. As an extension of this, future research could explore Polyjet printing of soft robots with multiple pneumatic channels to expand on the control and capabilities of the actuators. As was found across the literature, soft robots with multiple channels can allow for individual control of certain sections for complex actuators, which can achieve advanced motion. This portfolio has encompassed a wide range of experiments through one pneumatic channel, and in doing so, the limits of control that are possible using this method were found. Future research should take this into account while expanding on the overall possibilities of motion with additional pneumatic channels.

Future research is needed to establish the performance of complex Polyjet printed soft robots at a larger scale. Due to the large cost of large scale prints, these were explored very little in this portfolio, however, they offered promise in their strength and actuation repeatability – shown especially in actuator 1.10 in print set 7. This could allow for further exploration of a combination of motions which are not inhibited by bursting at low actuation pressures.

Simulation software was used for this research to create a digital model to compare to the experimental results. Solidworks, Abaqus, and ANSYS were all tested to try to simulate pneumatic actuation but none achieved results comparable to the experimental data. If good simulation results could be achieved, this could be used as a tool to accurately showcase how a parametric model system will inflate before it was printed, which would mean far fewer experiments would be needed before the intended result was accomplished.
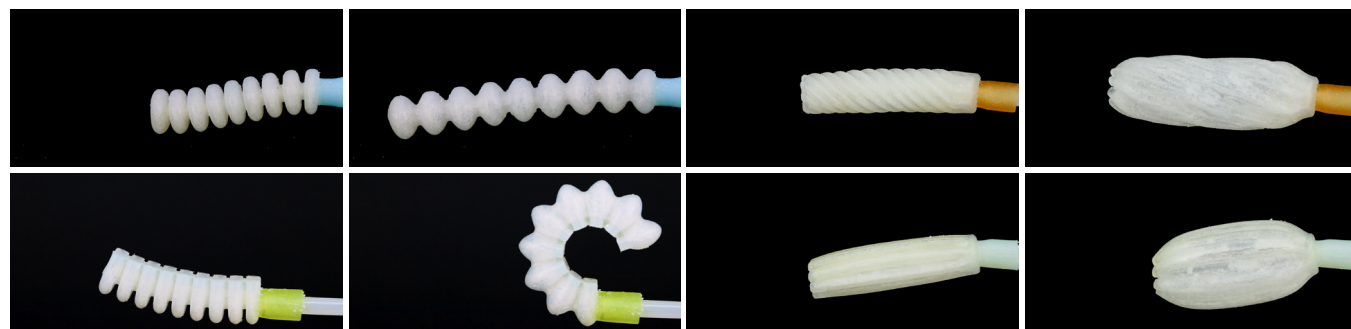

Figure 97. Primary motions in their deflated and actuated states.

Implications

The method used to parametrically build CAD models of the actuators provides new insight into the role of software to inform soft robots. By using equations to drive the key dimensions and parameters of Solidworks models, a streamlined design process has been created which allow for dexterity in the fine control, modification, and combination of the models. This was utilised to efficiently design each print, so that more time could be spent on testing and creation of new prints. As demonstrated in the final pneumatic finger design, the flexibility of motion shown in this research can allow for potential design opportunities which prioritise the aesthetic qualities of motion rather than the functional qualities. By applying this research method to future design projects, unforeseen aesthetic and emotional opportunities could be uncovered.

This research builds on existing research that shows how, by taking inspiration from biology, designs can be enhanced. Biological inspiration has been used not only to inform how certain motions function in natural systems and how this can be synthetically replicated, but also in later stages of the design process to increase performance. The final locomotive extender showcases a method for how mechanical interlocking adhesion can be exploited to allow for locomotion in a simple bellows-type actuator (*Figure 98*).

Very limited research in the field of soft robotics has been done using Polyjet printing. The variety in materiality and geometry in this research vastly expands on the body of knowledge in this field, and because of that, has produced new information regarding the pros and cons on using this technology as a fabrication method for soft robots. The Agilus material created problems concerning tearing and bursting of the actuators, but the geometries for actuators that yielded the most success could possibly be printed with more success using other 3D printing technologies that allow for geometric freedom similar to the Stratasys J750.

Figure 98. Locomotive extender traversing an obstacle course.
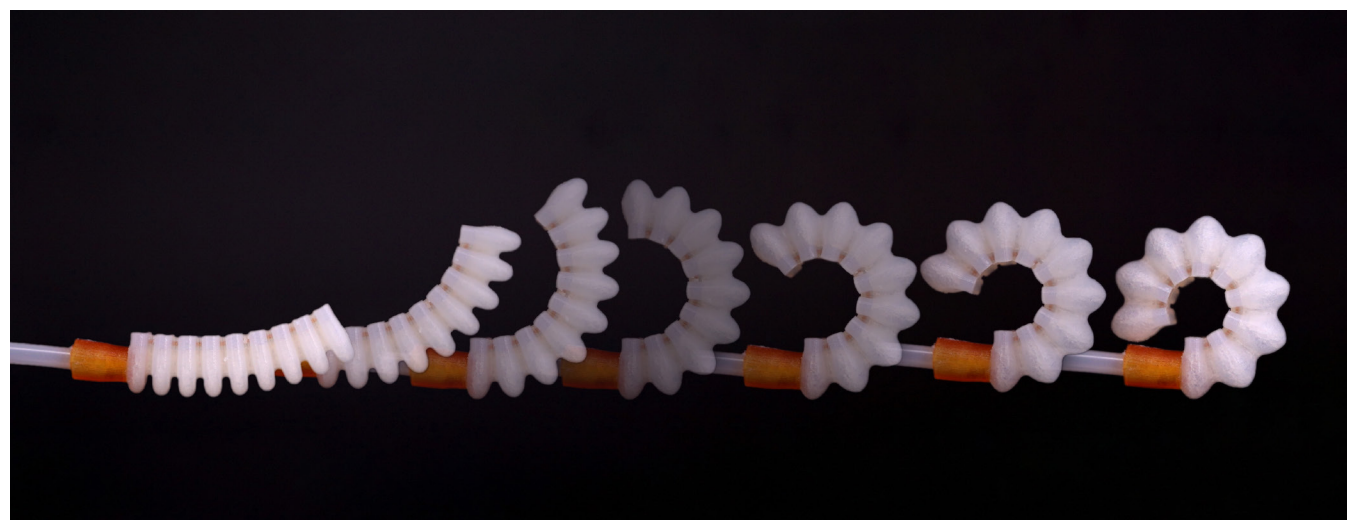
Applications

Figure 99. Bending actuator inflation sequence.

As this research gives a method for combining modular sections of motion, it can be used for a wide range of applications. As shown in the final print set, the parametric models can be modified and configured for vastly different purposes. As identified in the literature review, end effectors for grippers have large commercial potential (MGrip, n.d.). By utilising the fine control of the models, end effectors for a gripper could be configured for different applications, such as produce and baked goods at different scales. These grippers offer a lot of potential as they are able to pick up irregular objects with organic forms. This was shown in this project in the final gripper which was able to pick up objects from marbles to lemons – objects that have a large difference in size and mass.

Locomotion is also an area with large potential for this research. Locomotion has been demonstrated with one pneumatic input and adhesion geometry switching between inflation and deflation phases. By attaching a camera, these robots could be used to navigate and assess hazardous terrain such as nuclear disaster sites or to navigate areas that humans can't fit in. Currently, successful locomotion is only achievable on rough surfaces as mechanical interlocking is required although this could be refined through future research.

This research also has potential applications for devices that assist or enhance human ability. Evidence from the literature shows how soft robots can be beneficial for stroke rehabilitation devices for the hand. Although this research doesn't demonstrate specific human-oriented practical applications, the sixth finger final print shows how complex soft robotic motion could be used to enhance the human body.

CONCLUSION

This research aimed to explore how multi-material 3D printing could be used to fabricate singular channel pneumatically actuated soft robots capable of complex actuation for advanced applications. This has been shown through a series of multi-material 3D printed soft robotic actuators which rely on parametric control of software and biological inspiration to inform the geometry and materiality needed to achieve specific motions through pneumatic actuation. As shown in the final print set, locomotion, gripping, and human interaction can be accomplished in soft robots using only one pneumatic input by fully utilising the geometric freedom and variable materiality of Polyjet printing.

The printable materials on the Stratasys J750 proved to be more prone to tearing and bursting than anticipated, and this limited the possible combinations of segments of actuation in complex soft robots. Although limitations were found in what is possible through one pneumatic input and with the soft printed materials, the actuators in this research demonstrate that complex motion can be achieved through one pneumatic input. The extension and bending sections gave similar deformation results to what had been expected, however, the twisting actuator significantly outperformed what had been anticipated, and the resulting bend angle was much larger than any other that was found in the literature.

Across soft robotic research, a wide range of applications have been identified that take advantage of the inherent compliance of soft actuators. This portfolio demonstrates a method for design and fabrication of soft robots that, with parametric modifications, can be applied to a number of these scenarios.
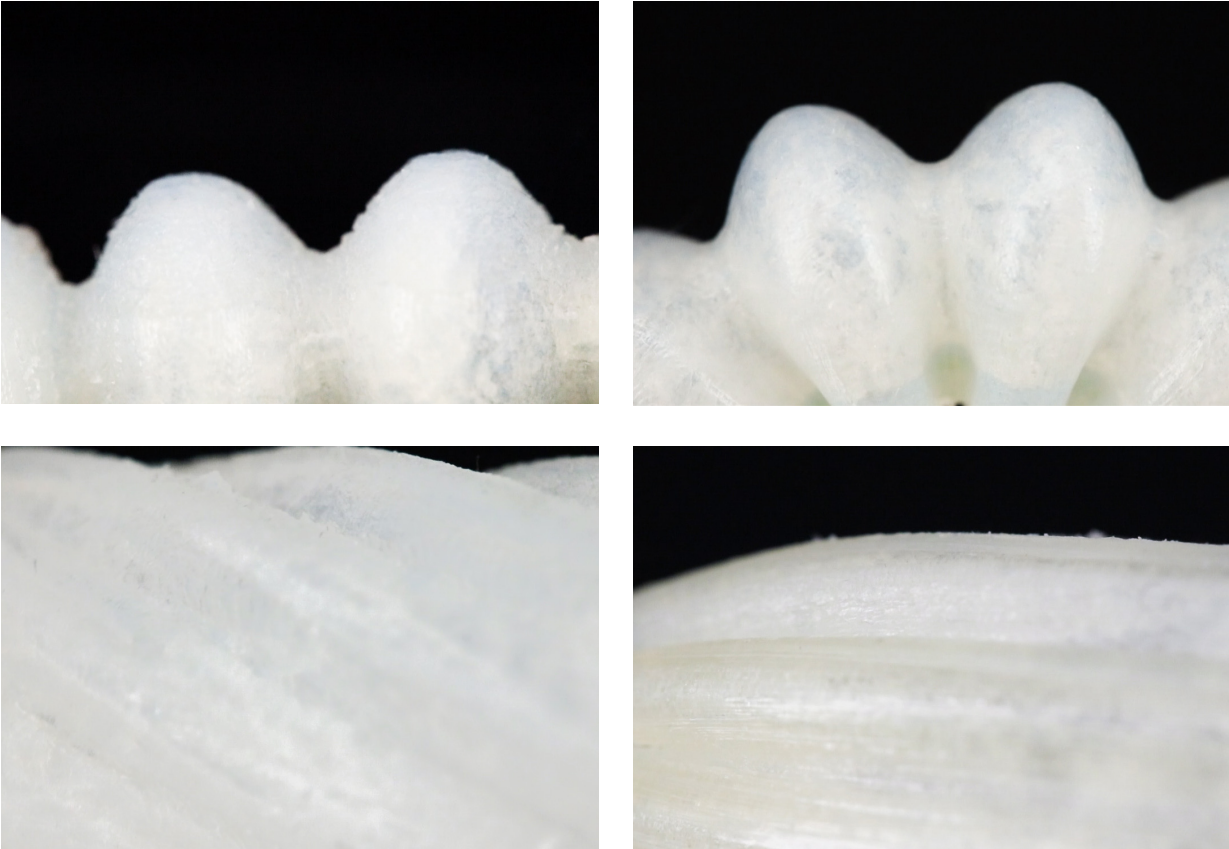

Figure 100. Close-up of the primary motions in their inflated states.

Figure list

All figures not cited have been produced by the author.

Figure 4. Adapted from Heepe, L., & Gorb, S. N.
(2014). Different adehsion mechanisms
resisting the separation of two surfaces.
Annual Review of Materials Research, *44*(1),
173–203. [Diagram]. Retrieved from https://
www.annualreviews.org/doi/10.1146/
annurev-matsci-062910-100458

References

Arzt, E., Gorb, S., & Spolenak, R. (2003). From micro
to nano contacts in biological attachment
devices. *Proceedings of the National Academy
of Sciences*, *100*(19), 10603–10606. https://doi.
org/10.1073/pnas.1534701100

Autumn, K. (2006, March 1). *How gecko toes stick: The
powerful fantastic adhesive used by geckos
is made of nanoscale hairs that engage tiny
forces, inspiring envy among human imitators*.
American Scientist. https://link.galegroup.com/
apps/doc/A143278796/AONE?sid=lms

Autumn, K., Sitti, M., Liang, Y. A., Peattie, A. M., Hansen,
W. R., Sponberg, S., Kenny, T. W., Fearing, R.,
Israelachvili, J. N., & Full, R. J. (2002). Evidence
for van der Waals adhesion in gecko setae.
*Proceedings of the National Academy of
Sciences*, *99*(19), 12252–12256. https://doi.
org/10.1073/pnas.192252799

Barclift, M. W., & Williams, C. B. (2012). *Examining
variability in the mechanical properties of parts
manufactured via polyjet direct 3D printing*. 6–8.

Bartlett, N. W., Tolley, M. T., Overvelde, J. T. B., Weaver, J.
C., Mosadegh, B., Bertoldi, K., Whitesides, G. M.,
& Wood, R. J. (2015). A 3D-printed, functionally
graded soft robot powered by combustion.
Science, *349*(6244), 161–165. https://doi.
org/10.1126/science.aab0129

Benyus, J. M. (1997). *Biomimicry: Innovation inspired by
nature* (1st ed..). Morrow.

Bhushan, B. (2009). Biomimetics: Lessons from nature–
an overview. *Philosophical Transactions of the
Royal Society A: Mathematical, Physical and
Engineering Sciences*, *367*(1893), 1445–1486.
https://doi.org/10.1098/rsta.2009.0011

Cianchetti, M., Laschi, C., Menciassi, A., & Dario, P.
(2018). Biomedical applications of soft robotics.
Nature Reviews Materials, *3*(6), 143–153.
https://doi.org/10.1038/s41578-018-0022-y

Cianchetti, M., Ranzani, T., Gerboni, G., De Falco, I.,
Laschi, C., & Menciassi, A. (2013). STIFF-FLOP
surgical manipulator: Mechanical design and
experimental characterization of the single
module. *2013 IEEE/RSJ International Conference
on Intelligent Robots and Systems*, 3576–3581.
https://doi.org/10.1109/IROS.2013.6696866

Clode, D. (2017). *The Third Thumb Project*
[Portfolio]. Dani Clode Design. https://www.
daniclodedesign.com/thethirdthumb

Connolly, F., Polygerinos, P., Walsh, C. J., & Bertoldi,
K. (2015). Mechanical Programming of
Soft Actuators by Varying Fiber Angle. *Soft
Robotics*, *2*(1), 26–32. https://doi.org/10.1089/
soro.2015.0001

Connolly, F., Walsh, C. J., & Bertoldi, K. (2017). Automatic
design of fiber-reinforced soft actuators for
trajectory matching. *Proceedings of the National
Academy of Sciences*, *114*(1), 51–56. https://doi.
org/10.1073/pnas.1615140114

Darekar, B., Naik, P., Unde, J., & Ohol, S. S. (2019). *Development of Multi-chamber Pneumatic Twist Actuator for Soft robot* [Portfolio]. https://bhushandarekar.com/project/development-of-multi-chamber-pneumatic-twist-actuator-for-soft-robot/

de Mestral, G. (1955). *Velvet type fabric and method of producing same* (United States Patent No. US2717437A). https://patents.google.com/patent/US2717437A/en

Drotman, D., Jadhav, S., Karimi, M., deZonia, P., & Tolley, M. T. (2017). 3D printed soft actuators for a legged robot capable of navigating unstructured terrain. *2017 IEEE International Conference on Robotics and Automation (ICRA)*, 5532–5538. https://doi.org/10.1109/ICRA.2017.7989652

Ecoflex™ 00-30 Product Information. (n.d.). Smooth-On, Inc. Retrieved 13 January 2020, from https://www.smooth-on.com/products/ecoflex-00-30/

Federle, W., Riehle, M., Curtis, A. S. G., & Full, R. J. (2002). An Integrative Study of Insect Adhesion: Mechanics and Wet Adhesion of Pretarsal Pads in Ants. *Integrative and Comparative Biology*, *42*(6), 1100–1106. https://doi.org/10.1093/icb/42.6.1100

Festo. (2012). Bionic handling assistant: Safe human-machine interaction [Company]. *Bionic Learning Network*. https://www.festo.com/group/en/cms/10241.htm

Festo. (2019). Bionic soft arm: Modular pneumatic lightweight robot [Company]. *Bionic Learning Network*. https://www.festo.com/group/en/

cms/13527.htm

Frankel, L., & Racine, M. (2010). *The Complex Field of Research: For Design, through Design, and about Design*. 12.

Frayling, C. (1994). Research in Art and Design. *Royal College of Art Research Papers*, *1*(1). http://researchonline.rca.ac.uk/384/

Galloway, K. C., Becker, K. P., Phillips, B., Kirby, J., Licht, S., Tchernov, D., Wood, R. J., & Gruber, D. F. (2016). Soft Robotic Grippers for Biological Sampling on Deep Reefs. *Soft Robotics*, *3*(1), 23–33. https://doi.org/10.1089/soro.2015.0019

Ge, L., Dong, L., Wang, D., Ge, Q., & Gu, G. (2018). A digital light processing 3D printer for fast and high-precision fabrication of soft pneumatic actuators. *Sensors and Actuators A: Physical*, *273*, 285–292. https://doi.org/10.1016/j.sna.2018.02.041

Glick, P., Suresh, S. A., Ruffatto, D., Cutkosky, M., Tolley, M. T., & Parness, A. (2018). A Soft Robotic Gripper With Gecko-Inspired Adhesive. *IEEE Robotics and Automation Letters*, *3*(2), 903–910. https://doi.org/10.1109/LRA.2018.2792688

Gu, Z., Li, S., Zhang, F., & Wang, S. (2016). Understanding Surface Adhesion in Nature: A Peeling Model. *Advanced Science*, *3*(7), 1500327. https://doi.org/10.1002/advs.201500327

Gul, J. Z., Sajid, M., Rehman, M. M., Siddiqui, G. U., Shah, I., Kim, K.-H., Lee, J.-W., & Choi, K. H. (2018). 3D printing for soft robotics – a review. *Science and Technology of Advanced Materials*, *19*(1), 243–262. https://doi.org/10.1080/14686996.20

18.1431862

Hamidreza, M., & Hu, D. L. (2012). Friction enhancement in concertina locomotion of snakes. *Journal of The Royal Society Interface*, *9*(76), 3067–3080. https://doi.org/10.1098/rsif.2012.0132

Hanington, B. M., & Martin, B. (2012). *Universal methods of design: 100 ways to research complex problems, develop innovative ideas, and design effective solutions* (Digital ed..). Rockport Publishers. https://ebookcentral.proquest.com/lib/vuw/detail.action?docID=3399583

Hanna, G., Jon, W., & Barnes, W. P. J. (1991). Adhesion and Detachment of the Toe Pads of Tree Frogs. *Journal of Experimental Biology*, *155*(1), 103–125.

Heepe, L., & Gorb, S. N. (2014). Biologically Inspired Mushroom-Shaped Adhesive Microstructures. *Annual Review of Materials Research*, *44*(1), 173–203. https://doi.org/10.1146/annurev-matsci-062910-100458

Ilievski, F., Mazzeo, A. D., Shepherd, R. F., Chen, X., & Whitesides, G. M. (2011). Soft Robotics for Chemists. *Angewandte Chemie International Edition*, *50*(8), 1890–1895. https://doi.org/10.1002/anie.201006464

Kier, W. M., & Smith, A. M. (2002). The Structure and Adhesive Mechanism of Octopus Suckers. *Integrative and Comparative Biology*, *42*(6), 1146–1153. https://doi.org/10.1093/icb/42.6.1146

Kier, W. M., & Smith, K. K. (1985). Tongues, tentacles and trunks: The biomechanics of movement in

muscular-hydrostats. *Zoological Journal of the Linnean Society*, *83*(4), 307–324. https://doi.org/10.1111/j.1096-3642.1985.tb01178.x

Krüger, J., Lien, T. K., & Verl, A. (2009). Cooperation of human and machines in assembly lines. *CIRP Annals*, *58*(2), 628–646. https://doi.org/10.1016/j.cirp.2009.09.009

Li, X., Tao, D., Lu, H., Bai, P., Liu, Z., Ma, L., Meng, Y., & Tian, Y. (2019). Recent developments in gecko-inspired dry adhesive surfaces from fabrication to application. *Surface Topography: Metrology and Properties*, *7*(2), 023001. https://doi.org/10.1088/2051-672X/ab1447

Marchese, A. D., Onal, C. D., & Rus, D. (2014). Autonomous Soft Robotic Fish Capable of Escape Maneuvers Using Fluidic Elastomer Actuators. *Soft Robotics*, *1*(1), 75–87. https://doi.org/10.1089/soro.2013.0009

Martinez, R. V., Branch, J. L., Fish, C. R., Jin, L., Shepherd, R. F., Nunes, R. M. D., Suo, Z., & Whitesides, G. M. (2013). Robotic Tentacles with Three-Dimensional Mobility Based on Flexible Elastomers. *Advanced Materials*, *25*(2), 205–212. https://doi.org/10.1002/adma.201203002

MGrip. (n.d.). [Company]. Soft Robotics. Retrieved 18 December 2019, from https://www.softroboticsinc.com/mgrip

Milton, A., & Rodgers, P. (2013). *Research methods for product design*. Laurence King Publishing Ltd.

Ngo, T. D., Kashani, A., Imbalzano, G., Nguyen, K. T. Q., & Hui, D. (2018). Additive manufacturing (3D printing): A review of materials, methods,

applications and challenges. *Composites Part B: Engineering*, *143*, 172–196. https://doi.org/10.1016/j.compositesb.2018.02.012

Patel, D. K., Sakhaei, A. H., Layani, M., Zhang, B., Ge, Q., & Magdassi, S. (2017). Highly Stretchable and UV Curable Elastomers for Digital Light Processing Based 3D Printing. *Advanced Materials*, *29*(15), 1606000. https://doi.org/10.1002/adma.201606000

Peele, B. N., Wallin, T. J., Zhao, H., & Shepherd, R. F. (2015). 3D printing antagonistic systems of artificial muscle using projection stereolithography. *Bioinspiration & Biomimetics*, *10*(5), 055003. https://doi.org/10.1088/1748-3190/10/5/055003

Peressadko, A., & Gorb, S. N. (2004). When Less Is More: Experimental Evidence for Tenacity Enhancement by Division of Contact Area. *The Journal of Adhesion*, *80*(4), 247–261. https://doi.org/10.1080/00218460490430199

Polygerinos, P., Wang, Z., Galloway, K. C., Wood, R. J., & Walsh, C. J. (2015). Soft robotic glove for combined assistance and at-home rehabilitation. *Robotics and Autonomous Systems*, *73*, 135–143. https://doi.org/10.1016/j.robot.2014.08.014

Ranzani, T., Gerboni, G., Cianchetti, M., & Menciassi, A. (2015). A bioinspired soft manipulator for minimally invasive surgery. *Bioinspiration & Biomimetics*, *10*(3), 035008. https://doi.org/10.1088/1748-3190/10/3/035008

Rizzo, N. W., Gardner, K. H., Walls D.J, Keiper-Hrynko,

N. M., Ganzke, T. S., & Hallahan, D. L. (2006). Characterization of the structure and composition of gecko adhesive setae. *Journal of The Royal Society Interface*, *3*(8), 441–451. https://doi.org/10.1098/rsif.2005.0097

Rus, D., & Tolley, M. T. (2015). Design, fabrication and control of soft robots. *Nature*, *521*(7553), 467–475. https://doi.org/10.1038/nature14543

Schaffner, M., Faber, J. A., Pianegonda, L., Rühs, P. A., Coulter, F., & Studart, A. R. (2018). 3D printing of robotic soft actuators with programmable bioinspired architectures. *Nature Communications*, *9*(1), 1–9. https://doi.org/10.1038/s41467-018-03216-w

Shepherd, R. F., Ilievski, F., Choi, W., Morin, S. A., Stokes, A. A., Mazzeo, A. D., Chen, X., Wang, M., & Whitesides, G. M. (2011). Multigait soft robot. *Proceedings of the National Academy of Sciences*, *108*(51), 20400–20403. https://doi.org/10.1073/pnas.1116564108

Shih, B., Christianson, C., Gillespie, K., Lee, S., Mayeda, J., Huo, Z., & Tolley, M. T. (2019). Design Considerations for 3D Printed, Soft, Multimaterial Resistive Sensors for Soft Robotics. *Frontiers in Robotics and AI*, *6*. https://doi.org/10.3389/frobt.2019.00030

SLA vs. DLP: Compare Resin 3D Printers (2020 Guide). (n.d.). Formlabs. Retrieved 13 January 2020, from https://formlabs.com/blog/resin-3d-printer-comparison-sla-vs-dlp/

Tolley, M. T., Shepherd, R. F., Mosadegh, B., Galloway, K. C., Wehner, M., Karpelson, M., Wood, R.

J., & Whitesides, G. M. (2014). A Resilient, Untethered Soft Robot. *Soft Robotics*, *1*(3), 213–223. https://doi.org/10.1089/soro.2014.0008

Trivedi, D., Rahn, C. D., Kier, W. M., & Walker, I. D. (2008). Soft robotics: Biological inspiration, state of the art, and future research. *Applied Bionics and Biomechanics*, *5*(3), 99–117. https://doi.org/10.1080/11762320802557865

Vincent, J. F. V., Bogatyreva, O. A., Bogatyrev, N. R., Bowyer, A., & Pahl, A.-K. (2006). Biomimetics: Its practice and theory. *Journal of The Royal Society Interface*, *3*(9), 471–482. https://doi.org/10.1098/rsif.2006.0127

Vogel, M. J., Steen, P. H., & Probstein, R. F. (2010). Capillarity-based switchable adhesion. *Proceedings of the National Academy of Sciences*, *107*(8), 3377–3381. https://doi.org/10.1073/pnas.0914720107

Whitesides, G. M. (2016, May 26). *Soft Robotics* [Lecture]. H.C. Ørsted Lecture, Denmark. https://youtu.be/6j7FB4pCumU

Yap, H. K., Jeong Hoon Lim, Nasrallah, F., Goh, J. C. H., & Yeow, R. C. H. (2015). A soft exoskeleton for hand assistive and rehabilitation application using pneumatic actuators with variable stiffness. *2015 IEEE International Conference on Robotics and Automation (ICRA)*, 4967–4972. https://doi.org/10.1109/ICRA.2015.7139889

Yap, Hong Kai, Ng, H. Y., & Yeow, C.-H. (2016). High-Force Soft Printable Pneumatics for Soft Robotic Applications. *Soft Robotics*, *3*(3), 144–158. https://doi.org/10.1089/soro.2016.0030

Yirmibesoglu, O. D., Morrow, J., Walker, S., Gosrich, W., Cañizares, R., Kim, H., Daalkhaijav, U., Fleming, C., Branyan, C., & Menguc, Y. (2018). Direct 3D printing of silicone elastomer soft robots and their performance comparison with molded counterparts. *2018 IEEE International Conference on Soft Robotics (RoboSoft)*, 295–302. https://doi.org/10.1109/ROBOSOFT.2018.8404935

Zhang, Y.-F., Zhang, N., Hingorani, H., Ding, N., Wang, D., Yuan, C., Zhang, B., Gu, G., & Ge, Q. (2019). Fast-Response, Stiffness-Tunable Soft Actuator by Hybrid Multimaterial 3D Printing. *Advanced Functional Materials*, *29*(15), 1806698. https://doi.org/10.1002/adfm.201806698

Zhu, M., Mori, Y., Wakayama, T., Wada, A., & Kawamura, S. (2019). A Fully Multi-Material Three-Dimensional Printed Soft Gripper with Variable Stiffness for Robust Grasping. *Soft Robotics*, *6*(4), 507–519. https://doi.org/10.1089/soro.2018.0112

Well, Actuate(ly)...: Parametric Multi-Material 3D Printed Soft Robotics
Patrick Coulson
2020